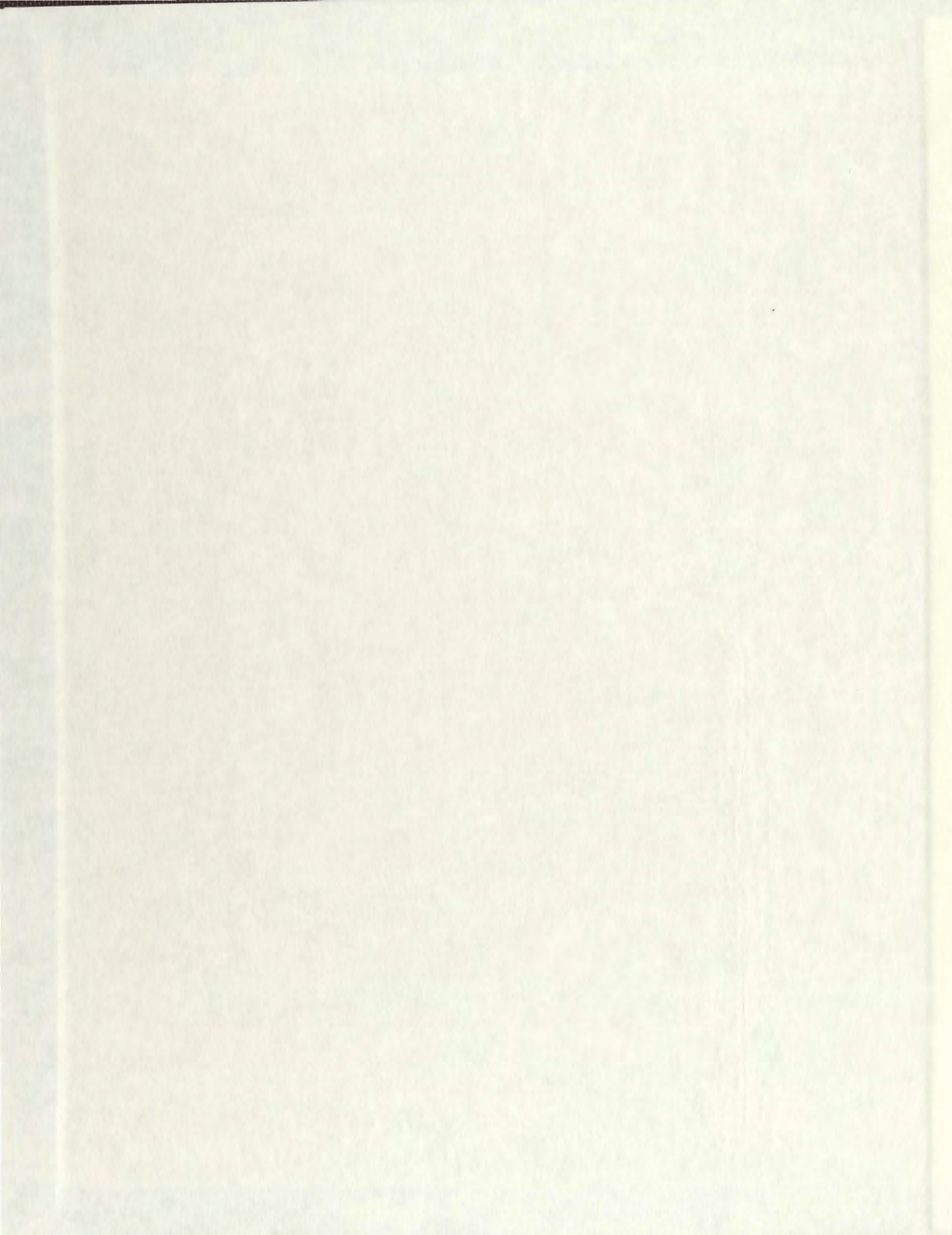


ON FORWARD AND INVERSE MODELLING IN  
SEISMOLOGY: RAYTRACING IN INHOMOGENEOUS MEDIA

PETER M. SMITH



**On forward and inverse modelling  
in seismology: Raytracing in  
inhomogeneous media**

by

© Peter M. Smith

A thesis submitted to the  
School of Graduate Studies  
in partial fulfillment of the  
requirements for the degree of

Master of Science

Dept of Earth Sciences

Memorial University of Newfoundland

July 2006



## Abstract

The first part of this thesis deals with forward modelling. We present a raytracing method based on the concept of simulated annealing: a computational tool based on physical principles used for obtaining optimal solutions of problems of in areas ranging from combinatorics to condensed matter physics. Our method solves for rays that render signal traveltimes stationary, in accordance with Fermat's principle of stationary traveltimes. We test this method for two types of media: layered inhomogeneous media and linearly inhomogeneous media. We show that rays and traveltimes generated from this algorithm for these models quantitatively agree with predicted results.

The second part of the thesis deals with inverse modelling. In this part, we introduce the generalized form of Radon's transform and its adjoint operator. We show that by treating traveltimes as Radon's transform acting on the slowness function along a ray, we can use the adjoint operator to recover qualitative information about a medium from collected traveltimes. This method of backprojection is presented as an application of our raytracing method. We calculate rays and their associated traveltimes between sources and receivers on a square lattice for layered- and linearly-inhomogeneous media and use the backprojection method to construct slowness functions for each set of data.

We show that although the backprojection method does not retain the quantitative properties of the original medium, results indicate that qualitative properties of the medium can be resolved by this method.

## Acknowledgments

I would like to take the opportunity to thank the many people who have directly and indirectly contributed to the completion of this thesis.

First and foremost, I would like to thank my supervisors: Dr. Michael Slawinski and Dr. Andrej Bóna. This work would not have come to fruition without their constant assistance, encouragement, and guidance over the last two years. Their intensity and enthusiasm towards conducting meaningful scientific research has inspired me to work towards becoming a competent physicist in my own right, and their tutelage has taught me to keep focused on the crux of the problem at hand. Michael and Andrej are great people, and I can only hope that we will collaborate again in the future.

One lesson I have learned over the past two years is that the progression of successful scientific research is driven by collaboration. The work in this thesis is no different. I would like to thank the following people for their input in this thesis: Dr. John Whitehead, Dr. Philip Bording, Dr. Ivan Booth, Dr. Nelu Bucataru, Cagri Diner, Aron Murphy, and Justin Pittman. At different stages of my graduate studies, these people have given me advice and direction on topics that led to the completion of this work, and their contributions deserve the proper recognition.

I am a firm believer that if you surround yourself with the right people, you will be inspired to become the best at whatever you do. I could write pages upon pages about my friends who have helped me and been there for me throughout my graduate studies. However, I would like to acknowledge two people with whom I have been very close over the past two years: Natasha Kirby and Noel Strapp. I would like to thank Natasha for being such a good friend over the last few years we have spent together at Memorial, and for the many, *many*, coffee breaks we took together. I wish her the best of luck in her academic career, and I hope our paths will cross again someday. I would like to thank Noel for being one of the best friends a person could have. Your work ethic is nothing short of inspirational, and you deserve all the success that comes to you. I would like to wish him and his fiancée, Jennifer O'Brien, the best of luck in their life together. You guys deserve it.

I can say without hesitation that I have the best and most supportive family any person could ever hope for. I cannot thank them enough for everything they have done for me over the years, but I will try anyways. My brothers, Paul and Mark, are more than just that – they are my role models and my best friends, and they have always pushed me to become the best that I can be at whatever I do. My mother and father are the greatest people on earth. Without their love, encouragement, and support, I do not know how I could have achieved the amount of success I have enjoyed thus far in life. They taught me to never settle for less, and that lesson has resonated well throughout the

ACKNOWLEDGMENTS

v

course of my life. In closing, words cannot do justice to exactly how much my family has contributed to all I have done. Thank you.

Finally, I would like to thank the staff at Tim Horton's located on campus in the Aquarena. Without your coffee, I would still be on Chapter 1. And asleep.

## Contents

Abstract	I
Acknowledgments	III
List of Figures	XIII
List of Tables	XVII
Chapter 1. Forward and Inverse Problems	1
1.1. Forward versus inverse problems	1
1.1.1. Forward problems: Mathematical formulation	2
1.1.2. Inverse problems: Mathematical formulation	3
1.2. Goals and purpose	5
Chapter 2. Raytracing: Theory and application	7
2.1. Rays: Definition	7
2.2. Rays: Physical interpretation in isotropic inhomogeneous media	10
2.3. Ray theory and differential geometry	12
2.3.1. Signal velocity as metric	12
2.3.2. Rays as geodesics	16
2.4. Raytracing	19
2.4.1. Forward modelling: Initial-value versus boundary-value problems	19

2.4.2.	Solutions to boundary-value problems: Current methods	21
2.4.2.1.	Shooting methods	21
2.4.2.2.	Bending methods	23
2.4.2.3.	Comparison of shooting and bending methods	24
2.4.3.	Bending methods based on minimizing traveltime	24
2.4.4.	Simulated annealing raytracing: Alternative formulations	25
Chapter 3. Raytracing: Simulated annealing method		27
3.1.	Introduction: Simulated annealing	28
3.1.1.	Physical context	28
3.1.2.	Definition	28
3.2.	Metropolis algorithm	29
3.2.1.	Background: Equilibrium of a closed system in a heat bath	29
3.2.2.	Role of Metropolis algorithm	32
3.2.3.	Generating states: Importance sampling	33
3.2.3.1.	Markov processes and Markov chains	33
3.2.3.2.	Constraints on Markov processes: Ergodicity and detailed balance	35
3.2.4.	Acceptance probability $A$	36
3.2.5.	Simulated annealing: Implementation of Metropolis algorithm	37
3.3.	Ray theory: Analogies to statistical mechanics	38
3.4.	Discretization of physical model: Technical concerns	39
3.4.1.	Physical Media: Discretized Representation	39
3.4.2.	Rays: Discrete representation	41

CONTENTS	IX
3.4.3. Traveltime: Calculations on a lattice	43
3.4.3.1. Traveltime approximation: Numerical integration	43
3.4.3.2. Weighted slowness function $\bar{p}$	45
3.4.3.3. Traveltime expression	46
3.5. Simulated annealing: Raytracing formulation	47
3.5.1. Initialization	47
3.5.2. Perturbing the ray: Changes in traveltime $T$	47
3.5.2.1. Removal of ray segment	49
3.5.2.2. Addition of ray segment	52
3.5.3. Acceptance scheme: Metropolis criterion	54
3.5.4. Markov chains, equilibration times, and cooling schedules	55
3.6. Summary	56
 Chapter 4. Radon's transform: Application to inverse problems	 59
4.1. History	59
4.2. Classical definition	60
4.2.1. Forward transform	60
4.2.2. Inverse of Radon's transform	62
4.2.3. Adjoint operator $R^*$	62
4.2.4. Inversion formula	63
4.2.5. Calculating the inverse	65
4.3. Inverse problems: Generalized adjoint method	67
4.3.1. Motivation	67
4.3.2. Generalized Radon transform	67
4.3.3. Generalized Adjoint operator $R^*$	68
4.3.4. Backprojection: Application of $R^*$	69

4.4. Seismic inverse modelling: Backprojection method	70
4.4.1. Calculation of backprojection $\Pi$	71
4.5. Notes on application of backprojection method	74
<b>Chapter 5. Results</b>	<b>77</b>
5.1. Methodology	78
5.2. Forward modelling: Simulated annealing method	79
5.2.1. Model 1: Layered medium	79
5.2.1.1. Background	79
5.2.1.2. Results	81
5.2.2. Model 2: Linearly inhomogeneous medium	87
5.2.2.1. Background	87
5.2.2.2. Results	89
5.2.3. Summary	93
5.3. Inverse modelling: Backprojection method	94
5.3.1. Results	94
5.3.1.1. Model 1: Layered inhomogeneous medium	94
5.3.1.2. Model 2: Linearly inhomogeneous medium	99
5.3.2. Summary	104
5.4. Conclusions and Future Considerations	105
5.4.1. Results: Interpretation	105
5.4.2. Future considerations	108
5.4.2.1. Simulated annealing method	108
5.4.2.2. Backprojection method	110
5.5. Final remark	112
<b>Bibliography</b>	<b>115</b>

## CONTENTS

XI

Appendix A. Adjoint Operators	117
A.1. Radon's transform: Operator and adjoint	117
A.2. Scalar products	118
A.3. Proof of adjointness of $R^*$	118
Appendix B. Analytical Solutions	123
B.1. Rays and traveltimes: Homogeneous media	123
B.1.1. Traveltime	123
B.1.2. Rays	124
B.2. Rays and traveltimes: Layered inhomogeneous media	127
B.2.1. Transmitted Signals	127
B.2.2. Reflected signals: Reflection at an interface	130
B.2.3. Reflected signals: Total internal reflection	131
B.3. Rays and traveltimes: Linearly inhomogeneous media	133
Appendix C. Code	137

## List of Figures

- 3.1 Illustration of a perturbation that results in the removal of a segment. Segment 2 is removed from the original (black) path; the new (red) path is formed by connecting segment 1 of the original path to segment 3 of the original path at point  $q$ . Point  $S$  denotes the source and point  $R$  denotes the receiver. 50
- 3.2 Illustration of a perturbation that results in the removal of the segment connected to the source. Segment 1 is removed from the original (black) path; the new (red) path is formed by connecting segment 2 of the original path to the source. Point  $S$  denotes the source and point  $R$  denotes the receiver. 51
- 3.3 Illustration of a perturbation that results in the removal of the segment connected to the receiver. Segment 3 is removed from the original (black) path; the new (red) path is formed by connecting segment 2 of the original path to the receiver. Point  $S$  denotes the source and point  $R$  denotes the receiver. 52
- 3.4 Illustration showing the perturbation to the path resulting in the addition of a segment. Segment 2 of the original (black) path is split into two segments and reconnected at point  $q$ , forming the new (red) path. Point  $S$  denotes the source and point  $R$  denotes the receiver. 53

- 4.1 Plot of function  $f(x, y) = \exp(-(x^2 + y^2))$ . We say that  $f$  has compact support on its domain since function  $f$  tends to zero rapidly as the values of  $x$  and  $y$  increase. 61
- 5.1 Rays constructed for a layered inhomogeneous velocity model; source located at  $(0m, 0m)$ , receivers located at a)  $(1000m, 100m)$ , b)  $(1000m, 600m)$ , and c)  $(1000m, 1000m)$ . 82
- 5.2 Rays constructed for a layered inhomogeneous velocity model; source located at  $(500m, 0m)$ , receivers located at a)  $(1000m, 100m)$ , b)  $(1000m, 600m)$ , and c)  $(1000m, 1000m)$ . 83
- 5.3 Rays constructed for a linearly inhomogeneous velocity model; source located at  $(0m, 0m)$ , receivers located at a)  $(1000m, 100m)$ , b)  $(1000m, 600m)$ , and c)  $(1000m, 1000m)$ . 90
- 5.4 Rays constructed for a layered inhomogeneous velocity model; source located at  $(500m, 0m)$ , receivers located at a)  $(1000m, 100m)$ , b)  $(1000m, 600m)$ , and c)  $(1000m, 1000m)$ . 91
- 5.5 Results of backprojection method applied to layered inhomogeneous medium; lattice spacings a)  $h = 100m$ , b)  $h = 50m$ , and c)  $h = 25m$ . 95
- 5.6 Plot of slowness function  $p(x, z)$  for a layered inhomogeneous medium. 96
- 5.7 Absolute error of results of backprojection method applied to layered inhomogeneous medium; lattice spacings a)  $h = 100m$ , b)  $h = 50m$ , and c)  $h = 25m$ . 97

- 5.8 Results of backprojection method applied to linearly inhomogeneous medium; lattice spacings a)  $h = 100m$ , b)  $h = 50m$ , and c)  $h = 25m$ . 100
- 5.9 Plot of slowness function  $p(x, z) = 1/(2000 + 1.5z)$  for a linearly inhomogeneous medium. 101
- 5.10 Reciprocal of backprojection functions; lattice spacings a)  $h = 100m$ , b)  $h = 50m$ , and c)  $h = 25m$ . 102
- 5.11 Absolute error of backprojection functions in comparison with exact function  $p(x, z)$ ; lattice spacings a)  $h = 100m$ , b)  $h = 50m$ , and c)  $h = 25m$ . 103

## List of Tables

- 1 Table of traveltimes collected for rays corresponding to transmission of signal through the interface: layered inhomogeneous medium. 84
- 2 Table of traveltimes corresponding to signals propagating within the upper layer of the medium. Analytical results are presented for direct arrival and reflected arrival of signal at a receiver located at  $(1000m, 100m)$ . 85
- 3 Traveltimes collected from forward modelling of rays in a linearly inhomogeneous medium with velocity function (5.2) for lattice spacings  $h = 25m, 50m, \text{ and } 100m$ . 92

## CHAPTER 1

### Forward and Inverse Problems

In this chapter, we will formulate forward and inverse problems in the context of seismic ray theory. We define forward problems as the modelling of the traveltime of a signal propagating between source and receiver in a known medium, and we define inverse problems as the recovery of the properties of a medium from traveltimes collected at receivers around the medium. At the end of the chapter, we present an outline of the work presented in this thesis.

#### 1.1. Forward versus inverse problems

In theoretical seismology, there exist two types of problems: forward problems and inverse problems. These problems are closely related to one another in that what is known in one problem is the desired result of the other.

In forward problems, traveltimes of signals between sources and receivers in a medium are modelled. Beginning with the physical properties of a medium – such as signal slowness – one constructs the ray along which a signal travels between two points within this medium. By Fermat's principle, this ray is the path of stationary traveltime within the medium. Letting  $f$  denote slowness,  $\gamma$  denote the ray, and  $ds$  be an arclength element along  $\gamma$ , we solve for the traveltime  $T$  of this signal

using the following expression:

$$(1.1) \quad T = \int_{\gamma} f ds.$$

The success of these studies depends on the knowledge of the medium in which signals propagate. The properties of the medium are often unknown – determining these properties is the focus of inverse problems.

In inverse problems, one uses measurements associated with the medium, such as measured traveltimes between sources and receivers, to determine its internal structure; specifically, to determine properties of the medium by recovering information about signal slowness. This class of problems is the focus of much research in seismology.

**1.1.1. Forward problems: Mathematical formulation.** A forward problem can be formulated as follows. Suppose we are given a function  $f$  on a domain  $\mathcal{D}$ . Physically, this function corresponds to the signal slowness within the medium. From  $f$ , we can infer properties associated with the medium. In our studies, the measurement that is physically meaningful is traveltime of a signal – the integral of  $f$  along a ray. We denote this measurement by  $T$  and its domain  $\mathcal{D}'$ .

Mathematically, traveltime  $T$  is obtained by acting upon  $f$  by an operator denoted by  $\Omega$ ; the result of  $\Omega$  acting on  $f$  is given by

$$(1.2) \quad \begin{aligned} \Omega : \mathcal{C}(\mathcal{D}) &\rightarrow \mathcal{C}(\mathcal{D}'), \\ \Omega : f &\mapsto T. \end{aligned}$$

Operator  $\Omega$  and its actions on functions are typical of a forward problem in seismology. We know the structure and properties of the medium that we are studying, and we are using  $\Omega$  to calculate a result, such as traveltime of a signal through the medium.

In physical studies, we can readily measure traveltime without prior knowledge of the properties of the medium in which these signals propagate. It is those properties that we wish to find, and it is the focus of inverse problems.

**1.1.2. Inverse problems: Mathematical formulation.** In an inverse problem, we are faced with a particular challenge. Formally, we wish to recover  $f$  from known values of  $T$ . To accomplish this, we need to act on  $T$  by another operator  $\omega$ , such that

$$(1.3) \quad \begin{aligned} \omega : \mathcal{C}(\mathcal{D}') &\rightarrow \mathcal{C}(\mathcal{D}), \\ \omega : T &\mapsto f. \end{aligned}$$

In other words,

$$\omega(T) = f$$

Since  $T = \Omega(f)$ , we can formally write

$$(1.4) \quad \omega(T) = \omega(\Omega(f)) = f$$

Thus, by the properties of operators, equation (1.4) implies that

$$\omega(\Omega) = \mathbf{I},$$

and, equivalently,

$$\Omega(\omega) = \mathbf{I},$$

where  $\mathbf{I}$  is the identity operator. It then follows that  $\omega$  is the inverse operator of  $\Omega$ . In other words,

$$(1.5) \quad \omega \equiv (\Omega)^{-1}.$$

In view of equation (1.4),  $\omega$  acting on  $T$  recovers the slowness surface from the traveltimes.

Our wish is to obtain information about a medium through knowledge of the traveltimes of signals propagating through that medium. In this sense, one would expect to know the paths  $\gamma$  along which traveltimes is calculated. If we know the shape of these paths, then we would expect to have some knowledge of the medium described by  $f$ . In an inverse problem, function  $f$  is the desired result – not the given information. In this context, we see the difficulty surrounding the area of inverse problems. In order to find  $f$ , we need to know something about its properties, but knowledge of its properties implies that we already know  $f$ . This is the conundrum surrounding inverse problems in seismology. The goal of these studies is to develop methods that mimic the action of  $\omega$  on traveltimes  $T$  to obtain  $f$  uniquely.

as the forward Radon transform of the slowness function. As we will explain, the construction of an inverse to Radon's transform is hindered by our lack of knowledge of integration paths. By treating rays as the paths of optimal traveltimes, knowledge of the rays implies knowledge of the medium. To recover information from a collection of traveltimes obtained from the forward modelling method, we will introduce the generalized adjoint to Radon's transform. We will illustrate how we will use this adjoint operator to construct a backprojected function onto the space of the original slowness function using a collection of traveltimes. Our goal is to show that the adjoint operator can be used as an approximation to the inverse that recovers qualitative properties about the original slowness function.

In Chapter 5, we will present results obtained from the forward modelling of rays via the simulated annealing method. With these data, we will apply the adjoint operator to test the backprojection method as an approximate inversion scheme to Radon's transform. We conclude by describing the results of our forward and inverse methods, and offer suggestions for their improvement, computational optimization, and extensions in future work.

## CHAPTER 2

### **Raytracing: Theory and application**

In this chapter, we introduce the concept of a ray. Physically, we define a ray as the path along which a signal propagates in a medium; mathematically, we define a ray as the solution to the variational problem where traveltime is to be rendered stationary. In this sense, rays are the solutions one obtains by invoking Fermat's principle of stationary traveltime.

For most types of media, closed-form solutions for rays do not exist. To find rays, one generally employs numerical methods. These methods, referred to as raytracing methods, are the focus of the second half of this chapter. At the end of this discussion, we will introduce the method that we will use in our work: the method of bending rays via the simulated annealing method.

#### **2.1. Rays: Definition**

Rays are important in forward modelling in seismology: they are the mathematical representation of the path of a signal as it propagates through a medium. In this work, a signal corresponds to a disturbance caused by a point source; this disturbance propagates within a medium.

One can calculate the traveltime of a signal as it travels from point to point by integration along the ray over the slowness function of the medium. The shape of a ray depends on the properties of the medium

through which the signal propagates. These properties are given by function  $v(\mathbf{x})$ , which describes the velocity of a signal at any point  $\mathbf{x}$  within the medium. In forward modelling studies, function  $v$  is known. In this work, we consider only two-dimensional media. The space of the medium is  $\mathbb{R}^2$ , and we denote a single point in the medium by coordinates  $\mathbf{x} = (x, z)$ .

Recall traveltime expression (1.1):

$$T = \int_{\gamma} f ds.$$

Let  $f = 1/v(\mathbf{x})$ , where  $v$  is signal velocity. Consider Fermat's principle of stationary traveltime:

**THEOREM 2.1.1.** *Rays are the solutions of the variational problem*

$$(2.1) \quad \delta \int_A^B \frac{ds}{v(\mathbf{x})} = 0,$$

where  $ds$  is an arclength element,  $v(\mathbf{x})$  is the signal velocity at position  $\mathbf{x}$ , and  $A$  and  $B$  are fixed endpoints of this variational problem.

Theorem 2.1.1 can be interpreted as follows: The units of  $v(\mathbf{x})$  are metres per second ( $m/s$ ) and the units of  $ds$  are metres ( $m$ ); hence, the integral in equation (2.1) has the units of seconds – or, units of time – and thus, it is an expression of the time travelled along the ray connecting  $A$  and  $B$ . We can view this integral as a functional that depends on the velocity and the endpoints of the path; namely,

$$(2.2) \quad T(v(\mathbf{x}); A, B) = \int_A^B \frac{ds}{v(\mathbf{x})}.$$

As Truesdell noted in [22, p. 4],

“[functionals] are simpler and much closer to physical experience than are ‘derivative’ and ‘integral’...”

In our studies, we do not measure a signal’s velocity within the medium; we measure a signal’s traveltime from source to receiver. Treating traveltime as a functional of signal velocity gives us more physical insight into the rays obtained from solving equation (2.2).

In view of equation (2.2), we rewrite equation (2.1) as

$$(2.3) \quad \delta T(v(\mathbf{x}); A, B) = 0;$$

it states that an object travelling from point  $A$  to point  $B$  with velocity  $v(\mathbf{x})$  will travel along the path that renders its traveltime stationary.<sup>1</sup>

Operator  $\delta$  is analogous to the derivative operator in single-variable calculus. For example, if one wants to find  $x$  such that  $f(x)$  is at an extremum, one solves the following equation for  $x$ :

$$\frac{df}{dx} = 0.$$

Analogously, when one solves equation (2.3), one obtains the curve which renders the value of the integral in equation (2.2) stationary.

---

<sup>1</sup>In general, one can consider rays as the path that minimizes the traveltime of a signal. However, it is possible to construct rays that also maximize traveltime.

## 2.2. Rays: Physical interpretation in isotropic inhomogeneous media

In this paper, we will consider two-dimensional media that are isotropic and inhomogeneous. This means that the properties of a signal travelling within this type of medium change only with position  $\mathbf{x}$  of the signal. The velocity function of this type of medium is written as  $v = v(\mathbf{x})$ , where  $\mathbf{x} = (x, z)$  is a coordinate in the space of the medium. Isotropy indicates that the velocity of the signal does not depend on the direction of propagation.

Let  $p(\mathbf{x}) = 1/v(\mathbf{x})$ . Function  $p(\mathbf{x})$  is the slowness function: it describes the slowness of a signal propagating in a medium. The smaller the slowness, the faster the signal propagates, and vice versa. In view of function  $p$ , we can rewrite traveltime functional  $T$  in expression (2.2) as

$$(2.4) \quad T(v(\mathbf{x}); A, B) = \int_A^B p(\mathbf{x}) ds.$$

Furthermore, in view of equation (2.4), Fermat's principle in isotropic inhomogeneous media can be rewritten as

$$(2.5) \quad \delta \int_A^B p(\mathbf{x}) ds = 0.$$

In Section 2.1, we mentioned that the concept of a ray is invoked in seismological studies to give one a mathematical description of the path of propagation of a signal within a medium. However, in order to make use of rays – more specifically, ray theory – we must make assumptions about the medium that is being studied. Hence, the motivation to

## 2.2. RAYS: PHYSICAL INTERPRETATION IN ISOTROPIC INHOMOGENEOUS MEDIA

use rays as a mathematical tool for describing signal propagation must have physical meaning within the context of our studies.

By Theorem 2.1.1, a ray is defined as the solution to the variational problem described by equation (2.1). In this problem, we solve for the extremal curves of an integral whose integrand is the reciprocal of signal velocity. These curves correspond to the paths along which signals propagate. What is not given in this formulation is the signal corresponding to the velocity.

There are two types of waves that can propagate within an isotropic<sup>2</sup> medium: *P*-waves, which cause changes in volume within the medium; and *S*-waves, which cause changes in shape within the medium. These waves are generated as a result of disturbances in the medium. In general, these waves are coupled. In view of our definition of rays, this presents a problem: in order to use Fermat's principle as a basis to calculating rays, we assume that we can treat these waves as separate entities; if the waves are coupled, then this is not possible.<sup>3</sup>

In the context of asymptotic ray theory (ART), it is possible to decouple *P* and *S* waves. The foundations of ART are based on high-frequency<sup>4</sup> approximations of the asymptotic series expansion of the

---

<sup>2</sup>We will consider only isotropic media in this thesis. Hence, we will omit the term "isotropic" from all descriptions of media herein.

<sup>3</sup>For further discussion of the properties of *P* and *S* waves in elastic media, the reader is referred to [3, Ch. 6].

<sup>4</sup>As Bleistein states in [20, p.6],

"high frequency" does not refer to absolute values of the frequency content of the waves. What must be considered is the relationship between the wavelengths... and the natural length scales of the medium.

elastodynamic equation: the equation that describes equations of motion of signals propagating within a medium. In the context of ART, rays are solutions to the zeroth-order asymptotic expansion of the elastodynamic equation in the high-frequency limit. Note that even in the high-frequency limit, we can only treat rays of decoupled signals as an approximate solution [2, p.2].

To construct rays connecting a source to a receiver, one needs knowledge of the velocity function that describes the medium. This is the crux of forward modelling in seismology: given a velocity function that describes a particular medium and the locations of sources and receivers, one wishes to solve equation (2.3) for the raypath  $\mathbf{x}$  that optimizes the value of the integral in equation (2.2). This area of study is commonly referred to as raytracing, and is central to problems in forward modelling in seismology.

### 2.3. Ray theory and differential geometry

Before moving into the realm of raytracing, we make connections between the physical concepts of seismology and the underlying mathematical structure of raytracing.

**2.3.1. Signal velocity as metric.** To begin, let us consider traveltime  $T$  along a ray as an integral over infinitesimal traveltime elements  $dT'$  from initial time  $T_0$  to final time  $T_f$ :

$$(2.6) \quad T = \int_{T_0}^{T_f} dT'.$$

We can relate infinitesimal elements of traveltime in equation (2.6) to infinitesimal elements of distance,  $ds$ , by the following equation:

$$(2.7) \quad dT(s)' = \frac{ds}{v(\mathbf{x}(s))},$$

where  $v(\mathbf{x}(s))$  is the velocity of the signal at point  $\mathbf{x}(s)$ , with  $s$  being a parameter along the ray. This equation says that infinitesimally, time is proportional to distance by the instantaneous velocity at that point. In view of expression (2.7), we express traveltime as an integral of function  $1/v(\mathbf{x}(s))$  along the raypath parameterized by  $s$ :

$$T = \int_{s_0}^{s_f} \frac{ds}{v(\mathbf{x}(s))}.$$

Parameters  $s$  and  $T$  give different parameterizations of the ray over the same space  $-\mathbb{R}^2$ . Each parameterization carries a different meaning. When we integrate over  $T$ , we say that the traveltime of a signal is the integral of elapsed time that the signal spends propagating in the medium. However, when we integrate over arclength parameter  $s$ , we say that traveltime is the average of the distance along the path, divided by its velocity at each point.

Although each parameterization can be interpreted in a different way, they both describe the same physical quantity: the traveltime of a signal along a ray. We would like to relate these two representations of the coordinates along a ray in a mathematical context. To do so, we introduce the Riemannian metric:

**DEFINITION 2.3.1.** A *metric* is a non-negative function that describes the “distance” between points  $x$  and  $y$  on a manifold  $M$ . Let

$g$  represent such a function; it is symmetric, satisfies the triangle inequality, and is nonzero for unique points  $x$  and  $y$ . Suppose for every point  $x$  in a manifold  $M$ , an inner product,  $\langle \cdot, \cdot \rangle_x$ , is defined on a tangent space  $T_x M$  at  $x$ . The collection of all these inner products is called the *Riemannian metric*.

The Riemannian metric allows us to calculate distance at all points within a medium defined by a metric. To elucidate this point, consider the following example.

**EXAMPLE 2.3.2.** The Riemannian metric for rectangular Euclidean space is given by

$$g_{ij} = \delta_{ij}.$$

Function  $\delta_{ij}$  is Kroenecker's delta, defined by

$$(2.8) \quad \delta_{ij} = \begin{cases} 1, & i = j \\ 0 & i \neq j \end{cases}.$$

If  $d\xi$  is an element of distance in this space, and  $dx^{(1)} = dx$ ,  $dx^{(2)} = dy$ , and  $dx^{(3)} = dz$  are infinitesimal distances along the  $x$ ,  $y$ , and  $z$  directions respectively, then

$$\begin{aligned} d\xi^2 &= g_{ij} dx^{(i)} dx^{(j)} \\ &= \delta_{ij} dx^{(i)} dx^{(j)} \\ &= dx^2 + dy^2 + dz^2, \end{aligned}$$

where the Einstein summation notation has been invoked.<sup>5</sup> Taking the square root of both sides, we obtain

$$(2.9) \quad d\xi = \sqrt{dx^2 + dy^2 + dz^2},$$

which is just the Pythagorean theorem in Euclidean space. Hence, the distance between two points in Euclidean space can be written in the integral form as

$$\xi = \int_{\xi_0}^{\xi_f} d\xi = \int_{\mathbf{x}_0}^{\mathbf{x}_f} \sqrt{dx^2 + dy^2 + dz^2},$$

where we have made the change of coordinates from a single variable  $\xi$  to variables  $x$ ,  $y$ , and  $z$ . Note that we have made no assumptions about the path of integration; this will be discussed in the next section. For a general metric,  $g_{ij}(\mathbf{x})$ , one can write this result in the following form:

$$(2.10) \quad \xi = \int_{\mathbf{x}_0}^{\mathbf{x}_f} \sqrt{g_{ij}(\mathbf{x}) dx^{(i)} dx^{(j)}}.$$

Here we have assumed the general case of spatial dependence of the metric .

---

<sup>5</sup>Note here the superscripts  $i$  in the  $dx^{(i)}$ s do not correspond to exponential factors; they refer to covariant indices used in Einstein summation convention – also referred to as repeated index summation. For example, the product  $y_i dx^{(i)}$ , where  $i = 1, 2, 3$ , can be written

$$y_i dx^{(i)} = y_1 dx^{(1)} + y_2 dx^{(2)} + y_3 dx^{(3)}.$$

Herein, we will follow the convention that superscript numbers enclosed by parentheses will refer to indices; superscript numbers without parentheses will refer to exponents. For a more complete description of the Einstein summation convention, the reader is referred to [5, p.56].

Returning to equation (2.6), and in view of equation (2.9), we relate the metric of the medium expressed in terms of traveltime to the metric expressed in terms of displacement by equation (2.7). Hence,  $g_{ij}^T = \delta_{ij}$  when we parameterize the ray with respect to traveltime, while  $g_{ij}^S(s) = \delta_{ij}/v(\mathbf{x}(s))^2$  when we parameterize with respect to arclength. When we parameterize the ray with respect to traveltime, the metric is coordinate-independent. In this case, the results of Example 2.3.2 hold. However, when the coordinates along the ray are expressed in arclength, the metric resulting from this choice of parameterization changes with position. As a result, the results of Example 2.3.2 no longer hold.

Recall traveltime expression (2.2). In view of the results of this section, one can view integration over the reciprocal of signal velocity along a ray – that is, the traveltime of the signal from source to receiver – as integration in a Riemannian space defined by the metric  $g_{ij}^S(s) = \delta_{ij}/v(\mathbf{x}(s))^2$ . Hence, the properties of metric  $g_{ij}^S(\mathbf{x})$  are the same as the mathematical properties of the medium described by function  $v$ . If  $g_{ij}^S$  depends on parameter  $s$  – that is,  $\mathbf{x} = \mathbf{x}(s)$  – we are only considering points in the medium that lie on the ray.

**2.3.2. Rays as geodesics.** In inhomogeneous media, rays are, in general, curved. In the special case of homogeneity, rays can be viewed as straight lines. (See Appendix B.1.)

When one changes the coordinates of integration in equation (2.6) from temporal to spatial, the notion of a "straight line" changes meaning. In view of Theorem 2.1.1, one wishes to solve the variational equation (2.3) for the ray  $\mathbf{x}(s)$  that renders traveltime stationary.

Consider the following theorem.

**THEOREM 2.3.3.** *Consider a two-dimensional space, whose coordinates are  $(x, z)$ . Function  $\mathbf{x}(s) = \{x(s), z(s)\}$  with the continuous first derivative on interval  $[A, B]$  yields a stationary value of integral (2.2), namely,*

$$(2.11) \quad I(f(\mathbf{x}(s), \mathbf{x}'(s); s); A, B) = \int_A^B f(\mathbf{x}(s), \mathbf{x}'(s); s) ds,$$

where  $f(\mathbf{x}(s), \mathbf{x}'(s); s) = 1/v(\mathbf{x}(s), \mathbf{x}'(s); s)$ , in the class of functions with boundary conditions  $\mathbf{x}(A) = \{x_A, z_A\}$  and  $\mathbf{x}(B) = \{x_B, z_B\}$ , if the following system of equations are satisfied:

$$\begin{aligned} \frac{\partial f}{\partial x} - \frac{d}{ds} \left( \frac{\partial f}{\partial x'} \right) &= 0 \\ \frac{\partial f}{\partial z} - \frac{d}{ds} \left( \frac{\partial f}{\partial z'} \right) &= 0 \end{aligned}$$

The prime denotes a total derivative taken with respect to variable  $s$

We can generalize this result for  $n$  functions of one variable:

$$(2.12) \quad \frac{\partial f}{\partial x^{(i)}} - \frac{d}{ds} \left( \frac{\partial f}{\partial (x^{(i)})'} \right) = 0, \quad i = 1, 2, \dots, n.$$

Equations (2.12) are referred to as the Euler-Lagrange equations: they are a set of second-order ordinary differential equations, whose solution is the path  $\mathbf{x}(s) = \{x(s), z(s)\}$ .<sup>6</sup>

<sup>6</sup>Upon first viewing, one may be inclined to classify equations (2.12) as a set of partial differential equations. However, note that the solution depends on the

The solution to ordinary differential equations (2.12) is the integration path  $\mathbf{x}(s)$  that renders the integral in equation (2.11) stationary; given initial conditions, they can be solved by known methods. In differential geometry, path  $\mathbf{x}(s)$  is referred to as a geodesic.

To relate geodesics in abstract mathematical spaces to rays in physical media, we invoke the results of Section 2.3.1. Recall that we can express the properties of a given medium by a metric of the form

$$(2.13) \quad g_{ij}(s) = \frac{\delta_{ij}}{v(\mathbf{x}(s))}.$$

Herein, we assume that velocity function  $v$  is a function of spatial coordinates  $x^{(1)} = x$  and  $x^{(2)} = z$ ; then  $v = v(x, z)$ .

Substitution of equation (2.13) into equation (2.10), and letting  $\xi = T$ , we obtain

$$T = \int_{\mathbf{x}_0}^{\mathbf{x}_f} \sqrt{g_{ij}(\mathbf{x}) dx^{(i)} dx^{(j)}} = \int_{s_0}^{s_f} \frac{\sqrt{dx(s)^2 + dz(s)^2}}{v(x(s), z(s))}.$$

Since integration elements  $dx$  and  $dz$  depend on parameter  $s$ , we express the radicand in terms of element  $ds$ ; hence,  $ds = \sqrt{dx(s)^2 + dz(s)^2}$ , and we write

$$T = \int_{s_0}^{s_f} \frac{ds}{v(x(s), z(s))}.$$

To solve for the geodesics, we invoke Theorem 2.3.3: let  $I = T$ ; then

$$f(x(s), z(s), x'(s), z'(s); s) = \frac{1}{v(x(s), z(s))}.$$

---

parameter  $s$ , not the spatial coordinates  $x$  and  $z$ . For a heuristic approach to the derivation of these equations, the reader is referred to [3, pp.271-272]. For a more rigorous approach, the reader is referred to [6, pp. 34-38].

We wish to solve equations (2.12) for geodesic  $\{x(s), z(s)\}$ : setting  $n = 2$ , we solve the following system of ordinary differential equations in variable  $s$ :

$$(2.14) \quad \begin{aligned} \frac{\partial f}{\partial x} - \frac{d}{ds} \left( \frac{\partial f}{\partial x'} \right) &= 0 \\ \frac{\partial f}{\partial z} - \frac{d}{ds} \left( \frac{\partial f}{\partial z'} \right) &= 0 \end{aligned}$$

Equations (2.14) describe the geodesic  $\{x(s), z(s)\}$  in the space defined by metric (2.13). In our studies, this metric describes a particular physical medium. Hence, these geodesics can be used to describe the rays within a particular medium. Thus, by invoking the Euler-Lagrange equations and making the appropriate connections, we have a tool that allows us to describe rays in inhomogeneous media.

## 2.4. Raytracing

**2.4.1. Forward modelling: Initial-value versus boundary-value problems.** Recall from Section 1.1.1 the motivation behind forward modelling: given a velocity function representing a particular medium, one wishes to compute the traveltimes of signals that propagate between sources and receivers. For certain types of velocity functions, one can solve analytically for the shapes of these raypaths; see Appendix B for specific examples. In general, closed-form solutions of rays in inhomogeneous media are not available.

In the cases where analytical solutions are not available, one can solve for rays by either numerical integration of expression (2.2) or numerical differentiation of equations (2.12). The problem of solving

either of these equations numerically can be classified into two categories: initial-value problems and boundary-value problems.

In Section 2.3.2, we introduced the Euler-Lagrange equations of motion. We showed that we could consider the solutions to these ordinary differential equations as rays in a medium described by slowness function  $1/v$ . These equations can be solved by standard methods: given initial ray position  $\mathbf{x}(s = 0) = \mathbf{x}_0$  and initial ray velocity  $\mathbf{x}'(s = 0) = \mathbf{x}'_0$ , one can solve equations (2.12). This type of problem is known as an initial-value problem: given initial conditions pertaining to position and velocity of the desired solution – in this case, the raypath – one can uniquely obtain a solution to these equations.

The problem with initial-value problems and their utility towards raytracing is as follows. In raytracing, one wishes to obtain the ray,  $\mathbf{x}(s)$ , connecting source  $S$  to receiver  $R$  by solving differential equations (2.12). In solving initial-value problems, initial values of position and velocity are used to solve equations (2.12) for  $\mathbf{x}(s)$ . With this method, we do not know if  $\mathbf{x}(s)$  passes through  $R$  using the initial conditions specified until  $\mathbf{x}(s)$  is found. In other words, one cannot predict the accuracy of the specified initial conditions until the ray has been obtained.

Another class of problem associated with solving second-order ordinary differential equations is known as the boundary-value problem. The crux of the boundary-value problem is as follows. Given two unique points in space, one wishes to solve ordinary differential equations, such as those in equation (2.12), for the solution connecting these points.

The setup of this type of problem is fundamentally different from the initial-value problem in that we specify an initial position – the source – and a position located away from the source that the ray is prescribed to pass through – the receiver. However, equations (2.12) are of second order in  $\mathbf{x}(s)$ ; to solve, one must specify an initial velocity along with the initial positions. As a result, specifying the position of the receiver adds extraneous information to the problem. Thus, the procedure of solving boundary-value problems must be modified to differentiate this approach from the approach of solving initial-value problems. In the following section, we will discuss various methods in solving boundary-value problems.

**2.4.2. Solutions to boundary-value problems: Current methods.** A common approach to solving problems in raytracing is to attack the problem from the viewpoint of solving boundary-value problems. Methods used to solve second-order ordinary differential equations as boundary-value problems can be grouped into two categories: shooting methods and bending methods. We will discuss the characteristics of these methods in the following paragraphs, where our basis for comparison is based on [2, pp. 220-227].

**2.4.2.1. Shooting methods.** Given ray  $\mathbf{x}(s)$ , let  $\mathbf{x}'(s) = [x'(s), z'(s)]$  denote its tangent vector at any value of parameter  $s$  along the ray. We can express the angle of the tangent vector at  $s$ ,  $\theta(s)$ , by the following expression:

$$(2.15) \quad \tan(\theta(s)) = \frac{z'(s)}{x'(s)}.$$

We refer to  $\theta(s)$  as the ray angle.

The shooting method for boundary-value problems makes use of ray angle  $\theta(s)$  in the following way. In inhomogeneous media, ray velocity  $x'(s)$  is equal to signal velocity  $v(s)$ ;

$$v(s) = \sqrt{x'(s)^2 + z'(s)^2}.$$

Solving equation (2.15) for  $z'$ , we write the above expression as

$$v(s) = x'(s)\sqrt{1 + \tan(\theta(s))^2} = x'(s) |\sec(\theta(s))|.$$

Velocity function  $v$  is known at all points in the medium. Hence, given source  $S$  at point  $s = 0$  and a guess to initial angle  $\theta_0 = \theta(0)$  – the takeoff angle – we can solve for the  $x$ -component of initial velocity by the following:

$$(2.16) \quad x'(0) = |\cos(\theta_0)| v(0).$$

In view of expression (2.16), we solve equation (2.15) for the  $z$ -component of the initial velocity;

$$(2.17) \quad z'(0) = |\sin(\theta_0)| v(0).$$

With these components of initial ray velocity, we solve equations (2.12) for the ray, and check to see if it passes through  $R$ . If it does, we are done; if not, we iteratively guess values of  $\theta_0$  until we calculate the ray that passes through  $R$  (or by  $R$ , within some fixed distance).

The shooting method works well when one needs to find rays connecting sources to receivers in various configurations within a two-dimensional structure [2, p. 222]. However, this method has its drawbacks. First, one has no control over which regions the rays pass through. These regions – called “shadow zones” – cannot be studied by raytracing methods. Second, there may be regions of multipathing, where two distinct rays from the same source arrive at the same receiver. Third, this method breaks down when modelling rays in complicated media. In this case, trajectories of neighbouring rays with slightly perturbed takeoff angles may differ greatly; hence, there can arise great difficulty in connecting sources to receivers in certain configurations [2, p.220].

*2.4.2.2. Bending methods.* The drawbacks associated with the shooting method are mainly centred around the ability of this method to connect source to receiver. This is a very important problem to address: the motivation of treating second-order ordinary differential equations as boundary-value problems is to obtain solutions that connect specific points within a medium prescribed by function  $v$ . If these points cannot be connected by a particular method, then the method fails.

The bending method addresses this problem as follows. One begins by connecting source  $S$  to receiver  $R$  with a trial path,  $\mathbf{x}_0$ . This trial path is perturbed – or, bent – according to some prescribed method until one obtains the desired ray. Three ways to do this are: to fit trial path  $\mathbf{x}_0$  to ray equations (2.12) until the left-hand side disappears; to use a paraxial ray approximation, where true rays are used to calculate

neighbouring rays; and to perturb the ray not according to shape, but according to traveltime along the path until it is minimized [2, pp. 225-226].

The bending method is desirable to use because the solutions obtained are guaranteed to connect sources to receiver. However, the implementation of these methods is not as straightforward as the shooting method, and some thought must be given to their setup and applicability to the problem at hand.

**2.4.2.3. Comparison of shooting and bending methods.** The shooting method lends itself to problems where the velocity function is simple. However, for more complicated media, its ability to connect sources to receivers greatly decreases. This is where the utility of the bending method overshadows the shooting method: The bending method ensures that the final solution – the ray – connects the source to receiver. In this work, we will implement the bending method for calculating rays; specifically, the bending method based on bending paths according to the minimization of their associated traveltime.

**2.4.3. Bending methods based on minimizing traveltime.** The bending method based on minimizing traveltime fits well within the context of our definition of rays. Fermat's principle states that for all possible paths connecting source to receiver, the signal will always choose to travel along the path that renders its traveltime stationary. The bending method is essentially a numerical formulation of the selection process of the signal. Starting with an initial guess to the ray,

the path is varied until the traveltimes associated with the ray reaches its minimum value.

According to Červený in [2, p.226], “[this] method is very popular in seismic exploration because it is very fast.” We should note that in this method, one calculates the traveltimes with respect to rays corresponding to selected signal velocities obtained from ray theory methods. We can calculate rays for  $P$ -waves or for  $S$ -waves, but we must note that only rays corresponding to  $P$ -wave velocities correspond with first-arrival times.

What is needed now is a way of bending these paths in order to calculate the desired rays. In Chapter 3, we will introduce the method of simulated annealing. We will show how the simulated annealing method lends itself to the bending method, and we will formulate our bending method using these tools.

**2.4.4. Simulated annealing raytracing: Alternative formulations.** The simulated annealing method is a commonly-used technique in areas of mathematics and physics for obtaining an optimal solution to a problem that is subject to particular constraints. As we will show in Chapter 3, the algorithm presented in this work makes heavy use of the simulated annealing technique to calculate rays. However, the author would like to point out that the method presented in this work is not the first raytracing method to implement simulated annealing.

The first implementation of simulated annealing in raytracing methods, [23], was to determine the ray connecting a source to a receiver in

the path is varied until the traveltimes associated with the ray reaches its minimum value.

According to Červený in [2, p.226], “[this] method is very popular in seismic exploration because it is very fast.” We should note that in this method, one calculates the traveltimes with respect to rays corresponding to selected signal velocities obtained from ray theory methods. We can calculate rays for *P*-waves or for *S*-waves, but we must note that only rays corresponding to *P*-wave velocities correspond with first-arrival times.

What is needed now is a way of bending these paths in order to calculate the desired rays. In Chapter 3, we will introduce the method of simulated annealing. We will show how the simulated annealing method lends itself to the bending method, and we will formulate our bending method using these tools.

**2.4.4. Simulated annealing raytracing: Alternative formulations.** The simulated annealing method is a commonly-used technique in areas of mathematics and physics for obtaining an optimal solution to a problem that is subject to particular constraints. As we will show in Chapter 3, the algorithm presented in this work makes heavy use of the simulated annealing technique to calculate rays. However, the author would like to point out that the method presented in this work is not the first raytracing method to implement simulated annealing.

The first implementation of simulated annealing in raytracing methods, [23], was to determine the ray connecting a source to a receiver in

a complex two-dimensional medium using a variation of the shooting method. In this work, the authors develop an algorithm that searches for the optimal takeoff angle of the ray that minimizes traveltime. In [24], the authors extend their raytracing algorithm to calculating rays in complex three-dimensional media.

The key difference between the algorithm presented in [23] for two-dimensional media and the algorithm presented in this work is the difference in formulations. The algorithm developed by Ulrych and Velis varies the takeoff angle of each trial path to find the optimal takeoff angle. The angle is varied according to the change in total traveltime along the path according to the Metropolis criterion, which is discussed in Chapter 3. Our algorithm, however, varies the path itself, and perturbations to the path are accepted according to the Metropolis criterion with respect to the resulting change in signal traveltime. In essence, our formulation is a numerical variational formulation that minimizes the traveltime along the ray by directly perturbing its shape.

Direct comparison between the simulated annealing raytracing method of Ulrych and Velis and the method presented in this work is outside the scope of this thesis.

## CHAPTER 3

### **Raytracing: Simulated annealing method**

In this chapter, we will introduce the method of simulated annealing. We will give a brief tutorial of the concepts that motivate the use of this method in solving problems of optimization – namely, the relation of statistical mechanics to general problems in optimization.

The method of simulated annealing makes extensive use of the Metropolis algorithm, which simulates the process of a system coming to equilibrium with a heat bath at a given temperature. We will present background pertaining to the mathematical formulation of the Metropolis algorithm, and will refer the reader to other works to expand on points that are outside the scope of this work.

To formulate the simulated annealing method in the context of ray tracing, we will relate aspects of ray theory to statistical mechanics. Our formulation treats all possible paths between source and receiver as the possible states of our system, with the ray being the groundstate of this system. We treat the traveltime along each path as the energy of the system, the minimum traveltime corresponding to the energy of the groundstate.

At the end of this chapter, we will outline the technical aspects of implementing the simulated annealing method in raytracing.

### 3.1. Introduction: Simulated annealing

Simulated annealing is a computational tool that is used in solving problems of optimization<sup>1</sup> in areas ranging from condensed matter physics to combinatorics. Its formulation is based on simulating the physical process of annealing solids into optimal configurations.

**3.1.1. Physical context.** In physics, annealing denotes a physical process in which a solid in a heat bath is melted by increasing the temperature of the heat bath to a maximum value at which all particles arrange themselves randomly in the liquid phase, followed by cooling the particles back into the solid phase through slowly lowering the temperature of the heat bath [7, p.7].

In annealing, one must take care when cooling the system. As the liquid is cooled, it must be allowed to reach thermal equilibration with the heat bath at each temperature, to ensure that when the system reaches the freezing point, the particles settle into the groundstate configuration. If the cooling process is carried out too fast, one runs the risk of “freezing” defects into the structure of the solid. In condensed matter physics, the process whereby a solid is melted and then instantaneously cooled is referred to as *quenching*. If the annealing is done properly, the resulting solid should be in its state of minimum energy. This state is referred to as the groundstate [1].

**3.1.2. Definition.** The process of simulated annealing is “based on the analogy between the simulation of the annealing of solids and the problem of solving large combinatorial problems” [7, p. 7]. This

---

<sup>1</sup>By optimization, we mean finding the optimal solution to a particular problem.

method – developed by Kirkpatrick [8] and later independently by Černý [9] – applies statistical mechanical reasoning in its formulation to solve optimization problems.

In simulated annealing, one poses the problem in the framework of statistical mechanics. The goal is to construct the optimal solution (the groundstate) to a particular problem (the system) by varying a trial solution according to a specific protocol (heating, then cooling the system) with respect to a particular parameter (the temperature). To perform this type of calculation, one needs a method of varying the possible trial solutions. One such method is the Metropolis algorithm.

### 3.2. Metropolis algorithm

In 1953, Metropolis et. al [10] proposed an algorithm that simulates the physical process of the evolution of a system as it reaches thermal equilibrium with a heat bath at temperature  $\tau$ . In this section, we will introduce this algorithm, herein referred to as the Metropolis algorithm.

This section is present as a brief tutorial of the method itself – we will not go into detail about thermodynamic properties of systems. For a complete description of the Metropolis algorithm and its application to simulations of statistical mechanical systems, the reader is referred to [11].

**3.2.1. Background: Equilibrium of a closed system in a heat bath.** Consider the physical setup of a system immersed in a heat bath at temperature  $\tau$ . The size of the heat bath is much larger than the system. While there is energy transfer between system and

heat bath, the temperature of the heat bath remains constant. The property of constant temperature is the defining characteristic of a heat bath. In a closed system, there is no loss of energy from the heat bath to the surroundings; hence, the total energy of the combined system is constant.

Let  $\epsilon_i$  represent the energy of a system in a particular state  $i$ ; for  $i = 1, 2, \dots, r, \dots$  there exist states with energy  $\epsilon_1, \epsilon_2, \dots, \epsilon_r, \dots$  such that  $\epsilon_1 \leq \epsilon_2 \leq \dots \leq \epsilon_r \leq \dots$ . Note that we do not require the energy of each state to satisfy a strict inequality. Although our system can configure itself in a countably-infinite number of states, we cannot classify each state uniquely according to energy. There can exist states that possess the same energy yet differ in other characteristics.

Consider a system in thermal equilibrium with a heat bath at temperature  $\tau$ . By equilibrium, we mean that the temperature of the system is equal to that of the heat bath, and so the rate of energy flow between the system and the heat bath is constant. At equilibrium, the probability of the system being in a state having energy  $\epsilon_i$  is given by the Boltzmann distribution:

$$(3.1) \quad P(\epsilon = \epsilon_i) = \frac{1}{Z(\tau)} \exp\left(-\frac{\epsilon_i}{k_B \tau}\right),$$

where  $k_B$  is Boltzmann's constant, which has units of energy per temperature. The product  $k_B \tau$  in equation (3.1) is the thermal energy of the heat bath in which the system is placed; it is a measure of how

much energy the system has to extract from the heat bath at that temperature. Note that the thermal energy of the heat bath is independent of the system immersed in it.

At equilibrium, the temperature of the system is equal to that of the heat bath; however, its energy is not. Fluctuations in the system's energy are a result of the system being in contact with the heat bath. At equilibrium, the system does not assume a stationary value of energy – transitions between states occur at a constant rate, and each state occurs with probability (3.1).

Function  $Z(\tau)$  in equation (3.1) is known as the partition function: it is the sum of all Boltzmann probabilities over all states  $\epsilon_j$  of the system at temperature  $\tau$ ; that is,

$$(3.2) \quad Z(\tau) = \sum_j \exp\left(-\frac{\epsilon_j}{k_B\tau}\right).$$

Function  $Z(\tau)$  acts as a normalization factor to the Boltzmann probability of the system at temperature  $\tau$ , to ensure that  $\sum_i P(\epsilon = \epsilon_i) = 1$ .<sup>2</sup>

As the temperature of the heat bath decreases, so does the amount of energy that the system can draw from it. As a result, the probability of the system configuring into states of high energy decreases exponentially with decreasing temperature; as temperature approaches zero, the number of states that the system can assume according to

---

<sup>2</sup>In statistical mechanics, the partition function allows one to describe all measured quantities of a system at a given temperature – such as energy, number of states, and so on. Hence, the partition function is crucial for studies of systems in the realm of statistical mechanics. The reader is referred to [21] for further discussion and explanation of the physical significance and importance of the partition function.

the Boltzmann distribution decreases. In the limit of zero temperature, there is no energy flow between system and heat bath; hence, the system must configure itself into its state of minimum energy to reach thermal equilibrium. This state is the groundstate of the system.

**3.2.2. Role of Metropolis algorithm.** The purpose of the Metropolis algorithm is to model the process whereby a system reaches thermal equilibrium with a heat bath at a given temperature. Starting from an initial configuration,  $\sigma_0$ , we perform perturbations on the system until it reaches a configuration that is in thermal equilibrium with the heat bath. These perturbations are performed randomly – the mechanism used to perform the perturbations is dependent on the structure of the problem.

Let  $\sigma_i$  denote the initial configuration of the system at temperature  $\tau$  having energy  $E_i$ . We perturb  $\sigma_i$  to random state  $\sigma_j$ ; the energy of this system is denoted  $E_j$ , which can differ from  $E_i$ . We denote the change in the energy of the system by  $\Delta E$ .

To decide whether or not to accept this new state, we invoke the Metropolis criterion for accepted perturbations: if the perturbation lowers the energy of the system, it is automatically accepted; if the perturbation increases the energy of the system, we choose to accept this change with probability

$$(3.3) \quad p(\sigma_i \rightarrow \sigma_j) = \exp\left(-\frac{\Delta E}{k_B \tau}\right).$$

By assigning a nonzero probability to perturbations that raise the system's energy, we ensure that the system does not settle at a local minimum rather than the true minimum energy. If the system does enter into a state whose energy is a local minimum, then with a sufficient number of perturbations, it is possible for the system to accept perturbations that allow it to exit this state and find the global minimum. This property is crucial to the simulated annealing process.

**3.2.3. Generating states: Importance sampling.** At low temperatures, there are very few states whose energy contributes to the Boltzmann distribution. If the phase space of the system is large, then there are many states whose energy makes a negligible contribution to the distribution at this temperature. We would like to avoid sampling these states in our simulation.

Importance sampling gives us a way around sampling these low-probability states. It is defined as a process that samples only regions of phase space with significant contribution to the probability distribution. In order to sample these states, we need a method of generating states from initial configurations of the system with a probability in accordance with the Boltzmann distribution.

**3.2.3.1. Markov processes and Markov chains.** Let  $\sigma_i$  be a given system configuration. A Markov process is a mechanism that generates a new configuration from  $\sigma_i$  at random; that is, it does not generate the same new state from  $\sigma_i$  every time [11, p.35]. The Metropolis algorithm is designed to mimic this process to generate new configurations.

Let  $\zeta(\sigma_i \rightarrow \sigma_j)$  denote the transition probability of moving to a randomly chosen configuration  $\sigma_j$  from an initial configuration  $\sigma_i$ . The transition probability should satisfy two properties: it should not vary over time, and it should depend only on the states  $\sigma_i$  and  $\sigma_j$ . Furthermore, for all possible states, the transition probability should satisfy the following constraint:

$$(3.4) \quad \sum_j \zeta(\sigma_i \rightarrow \sigma_j) = 1.$$

Equation (3.4) states that the sum of all probabilities of moving from configuration  $\sigma_i$  to every possible configuration  $\sigma_j$  equals one; starting from  $\sigma_i$ , we must move to another state. Note that the transition probability  $\zeta(\sigma_i \rightarrow \sigma_i)$  need not be zero. This means that we are not restricted to move to a new configuration at each step of the algorithm; it is possible to randomly choose to stay put.

A Markov process allows one to construct a Markov chain: a sequence of states chosen from the phase space of the system, where each state is generated from the previous one with transition probability  $\zeta(\sigma_i \rightarrow \sigma_j)$ . In view of the Metropolis algorithm as a Markov process, the probability of moving to a randomly chosen state depends on the energetic properties of the current state and the change in energy resulting from a move to the new state.

In a sufficiently long time, the Markov process generates a Markov chain of states in which each state appears in the chain with a probability according to the Boltzmann distribution. At this point, we say

that the system is in equilibrium with the heat bath at temperature  $\tau$  [11, p.35].

3.2.3.2. *Constraints on Markov processes: Ergodicity and detailed balance.* In addition to constraint (3.4), we impose the following two constraints: ergodicity and detailed balance.

Ergodicity implies that there are no restraints on the possible states that we can generate. For initial state  $\sigma_i$ , we should be able to generate a Markov chain where we reach any other possible state  $\sigma_j$ . Ergodicity dictates that all transition probabilities  $\zeta$  be nonzero.

Detailed balance ensures that at equilibrium we are generating states according to the Boltzmann distribution, rather than some other probability distribution. According to Newman [11, p.36], the fundamental defining property of a system at equilibrium is that the transition rates of a system moving in and out of any state must be equal to each other. Mathematically, we say that the probability of accepting a perturbation in configuration from  $\sigma_i$  to  $\sigma_j$  is equal to the probability of the system being in configuration  $\sigma_i$  times the probability of transition from  $\sigma_i$  to  $\sigma_j$ . Letting  $E_i$  denote the energy of the system in configuration  $\sigma_i$ , and in view of the Boltzmann distribution in equation (3.1), we express the condition of detailed balance as

$$(3.5) \quad P(E_i)\zeta(\sigma_i \rightarrow \sigma_j) = P(E_j)\zeta(\sigma_j \rightarrow \sigma_i).$$

Solving equation (3.5) for the Boltzmann probabilities on the right-hand side and the transition probabilities on the left-hand side, we

write

$$\frac{\zeta(\sigma_i \rightarrow \sigma_j)}{\zeta(\sigma_j \rightarrow \sigma_i)} = \frac{P(E_j)}{P(E_i)}.$$

In view of equation (3.1), and letting  $\Delta E = E_j - E_i$ , we write

$$(3.6) \quad \frac{\zeta(\sigma_i \rightarrow \sigma_j)}{\zeta(\sigma_j \rightarrow \sigma_i)} = \exp\left(-\frac{\Delta E}{k_B \tau}\right).$$

Equation (3.6) is the second mathematical constraint on a Markov process. It says that our choice of transition probability must satisfy this equation to ensure that we sample states according to the Boltzmann distribution at thermal equilibrium.

**3.2.4. Acceptance probability  $A$ .** Let us define the transition probability  $\zeta(\sigma_i, \rightarrow \sigma_j)$  by the following expression:

$$(3.7) \quad \zeta(\sigma_i \rightarrow \sigma_j) = \kappa(\sigma_j)A(\sigma_i \rightarrow \sigma_j).$$

Function  $\kappa(\sigma_j)$  is the probability of choosing state  $\sigma_j$ , and function  $A(\sigma_i \rightarrow \sigma_j)$  is the probability of accepting the transition from  $\sigma_i$  to  $\sigma_j$ .

For  $N$  possible moves from  $\sigma_i$ , we define

$$(3.8) \quad \kappa(\sigma_j) = 1/N, \quad j = 1, 2, \dots, N.$$

Hence, we can randomly choose to move to any one of the  $N$  possible states with equal probability. Substituting expression (3.7) into equation (3.6), and in view of equation (3.8), we obtain

$$(3.9) \quad \frac{A(\sigma_i \rightarrow \sigma_j)}{A(\sigma_j \rightarrow \sigma_i)} = \exp\left(-\frac{\Delta E}{k_B \tau}\right).$$

Equation (3.9) is the constraint of detailed balance written in terms of acceptance probability  $A$ . The final step is to choose  $A$  such that equation (3.9) is satisfied. One function that satisfies this constraint is

$$(3.10) \quad A(\sigma_i \rightarrow \sigma_j) = \begin{cases} 1, & \Delta E \leq 0 \\ \exp\left(-\frac{\Delta E}{k_B \tau}\right), & \Delta E > 0 \end{cases}.$$

Equation (3.10) is precisely the Metropolis criterion for acceptance of perturbations to the system.

**3.2.5. Simulated annealing: Implementation of Metropolis algorithm.** The mechanism of the Metropolis algorithm is simple. Starting with an initial configuration at a given temperature, we perturb the system randomly to reach a new configuration, and accept or reject this perturbation according to equation (3.10). We repeatedly perturb this system at this temperature for a sufficiently long period of time until the system has equilibrated – that is, until we are sampling states according to the Boltzmann distribution.

The simulated annealing algorithm can be viewed as the repeated use of the Metropolis algorithm to simulate the process of a system reaching thermal equilibrium for a succession of decreasing temperatures. Starting in the high-temperature range, we perturb the system using the Metropolis algorithm until the system reaches thermal equilibrium with the heat bath and lower the temperature. Repeating this process, we slowly cool the system until we reach a near-zero temperature, at which point the system accepts little to no perturbations. If we have cooled the system properly, we will have reached the groundstate.

An important characteristic of the simulated annealing algorithm is its applicability to optimization problems in a broad range of fields in mathematics and physics. Kirkpatrick [8] and Černý [9] both showed how the method of simulated annealing can be used to solve optimization problems by making analogies between the quantities that defined their problems and quantities in statistical mechanics. We wish to implement the simulated annealing algorithm as an alternative method of raytracing. To do so, we make analogies between ray theory and statistical mechanics.

### 3.3. Ray theory: Analogies to statistical mechanics

The goal of the simulated annealing method is to find the system configuration whose energy is minimal – the groundstate. We will associate system configurations with rays connecting sources and receivers. Let  $\gamma_i(S, R)$  represent the configuration of a particular path connecting source  $S$  to receiver  $R$ , and let  $T(\gamma_i(S, R))$  denote the traveltime associated with this path. Our goal is to find the ray that minimizes the traveltime between source and receiver. In this context, it is natural to associate system energy with traveltime along a path. As a result, the groundstate corresponds to the path that minimizes traveltime. Hence, the ray is the groundstate.

The relation of thermal energy  $k_B\tau$  to ray theory is not as straightforward. The finite-temperature properties of rays have no immediate application in the context of our formulation – at least, none that the author is aware of at the time of writing – since our main concern is to find the ray. To represent the role of heat bath in raytracing, we

employ the parameter  $T_c$ , which has units of time; we refer to this parameter as the temporal energy. In the annealing process, we will lower the value of this parameter in the same way that one would lower the temperature of the heat bath in annealing of solids.

In view of these analogies, we write the transition probability of moving from path  $\gamma_i$  to  $\gamma_j$  at temporal energy  $T_c$  as

$$(3.11) \quad A(\gamma_i \rightarrow \gamma_j) = \begin{cases} 1, & \Delta T \leq 0 \\ \exp\left(-\frac{\Delta T(\gamma_j)}{T_c}\right), & \Delta T > 0 \end{cases},$$

where  $\Delta T = T(\gamma_j) - T(\gamma_i)$  is the change in traveltime of the signal associated with the perturbation of the path. In applying this algorithm to raytracing, we impose on it the same conditions as per Section 3.2.3.2.

### 3.4. Discretization of physical model: Technical concerns

In this section, we will detail how we discretize media and the effects of discretization on the physical interpretation of results obtained from the algorithm.

**3.4.1. Physical Media: Discretized Representation.** In our model, we approximate a two-dimensional medium by a square lattice of  $N = L_x \times L_z$  points, where parameters  $L_x$  and  $L_z$  denote the number of lattice points along the  $x$  and  $z$  directions respectively. Let  $\mathcal{D}$  denote the lattice model of the medium. At each node  $(x, z) \in \mathcal{D}$ , where

$x, z \in \mathbb{Z}$ , we discretize the slowness function<sup>3</sup>; that is,

$$(3.12) \quad p(x, z) = \frac{1}{v(h_x(x-1), h_z(z-1))}.$$

Constants  $h_x$  and  $h_z$  scale the distance between points on the lattice to represent the actual spacing between the corresponding points in the medium. Function  $p(x, z)$  is defined on lattice  $\mathcal{D}$ ; it is the representation of the magnitude of signal slowness within the medium at each point  $(x, z)$ , calculated from the reciprocal of velocity function  $v(x, z)$ . Note that in equation (3.12), we have shifted the origin in physical space to the point  $(1, 1)$  on the lattice. This is done for computational purposes, and has no bearing on the physical interpretation of our model. For the scope of this work, we will work with square lattices having equidistant nodes. To reflect this imposition on our model, we let  $L_x = L_z = L$ , and  $h_x = h_z = h$ .

Recall that the objective of this calculation is to calculate the rays that connect sources to receivers. On the lattice, the sources and receivers are located along the edge of the lattice at equidistant nodes; let  $\bar{h}$  represent the spacing between sources and receivers along the side of a lattice. Note that parameters  $h$  and  $\bar{h}$  need not be equal; however,

---

<sup>3</sup>The choice to represent the medium in terms of signal slowness has both physical and computational motivation. Computationally, it is faster and easier to deal with functions such as signal slowness  $p(x, z)$  rather than calculating reciprocals of a function at each iteration. Physically, we consider rays as the path of a signal travelling between points on a surface described by function  $p$  that minimizes both its slowness and traveltime. This is equivalent to saying that a signal travels along the path that maximizes its velocity while minimizing its traveltime. Both formulations are equivalent; invoking the concept of signal slowness over signal velocity just happens to be more convenient to our studies.

they are related by the following relation:

$$\bar{h} = n h, n \in \mathbb{Z}.$$

In other words, the spacing between sources and receivers is fixed, but we are allowed to decrease the spacing between nodes. This allows us to increase the resolution of the medium we are studying to obtain better approximations to the rays.

**3.4.2. Rays: Discrete representation.** A consequence of representing the physical medium by a lattice model is that we cannot calculate smooth rays. As such, we represent rays in continuous media by a spline of straight lines that approximates the shape of the rays.

Let  $S$  be a source,  $R$  a receiver, and  $\gamma(s; S, R)$  be the ray connecting these points; arclength parameter  $s$  traces the shape of the ray within the medium. Let  $\bar{\gamma}(\xi; S, R)$  be a spline of  $M$  piecewise-continuous straight line segments that approximates  $\gamma(s; S, R)$  by the following:

$$\begin{aligned} \gamma(s; S, R) &\approx \bar{\gamma}(\xi; S, R), \\ (3.13) \qquad &= \bigcup_{k=1}^M \bar{\gamma}_k(\xi), \end{aligned}$$

Term  $\bar{\gamma}_k(\xi)$  in equation (3.13) represents the  $k$ th segment of splined ray  $\bar{\gamma}$ : it is a linear function defined on interval  $\mathcal{I}_k = [\xi^0, \xi^f]$  according to the rule

$$(3.14) \qquad \bar{\gamma}_k(\xi) = m_k \xi + b_k.$$

In a two-dimensional medium, with coordinates  $(x, z)$ , parameter  $\xi$  in equation (3.14) is allowed to take the value of either  $x$  or  $z$ . Its slope with respect to the  $x$ -axis,  $m_k^x$ , determines the choice of parameterization of a line segment. If  $m_k^x \leq 1$ , we parameterize  $\bar{\gamma}_k$  by  $x$ , and let  $m_k = m_k^x$ . If the slope is greater than one, we parameterize  $\bar{\gamma}_k$  with respect to  $z$ , and let  $m_k = 1/m_k^x$ . Parameter  $b_k$  is the point corresponding to  $\xi = 0$  on segment  $\bar{\gamma}_k$ : if  $\xi = x$ , then  $b_k = z_k^0 - m_k x_k^0$ ; if  $\xi = z$ , then  $b_k = x_k^0 - (1/m_k) z_k^0$ . To elucidate this process, consider the following example.

**EXAMPLE 3.4.1.** Consider the case where the slope of the  $k$ th line segment with endpoints  $(x_k^0, z_k^0)$  and  $(x_k^f, z_k^f)$  in approximated ray  $\bar{\gamma}$  is less than one; let  $m_k = (z_k^f - z_k^0)/(x_k^f - x_k^0)$  be the slope of this line. By equation (3.14), the equation of this line segment is

$$(3.15) \quad \bar{\gamma}_k(x) = m_k x + b_x,$$

where  $b_k = z_k^0 - m_k x_k^0$ . In view of parameterization by  $x$ , we can parameterize  $z$  by  $x$ ;  $z = z(x)$ . In view of equation (3.15), and by the properties of equations for straight lines, we can say that  $z(x)$  and  $\bar{\gamma}_k(x)$  are equal, and so

$$z(x) = m_k x + b_x.$$

The decision to use either  $x$  or  $z$  in the formulation of the discretized rays, rather than a single parameter such as arclength  $s$  for  $\gamma(s)$ , was made for two reasons. The first reason is that by allowing flexibility in the choice of parameter, we avoid situations where the slope of the

line segments are undefined with respect to  $x$  i.e.  $m_k^x \rightarrow \infty$ . With this formulation, we parameterize the segment with respect to  $z$ , and the slope of this line segment is zero. The second reason is related to the computation of traveltimes along the discretized ray, which will be discussed in Section 3.4.3.

**3.4.3. Traveltime: Calculations on a lattice.** Recall travel-time expression (2.4):

$$T(p(\mathbf{x}); A, B) = \int_A^B p(\mathbf{x}) ds.$$

This expression is valid for signals travelling along smooth rays. We wish to rewrite equation (2.4) for the traveltime of a signal along rays of the form (3.13). Let  $A = S$  be the source,  $B = R$  be the receiver; in view of approximating continuous rays by equation (3.13), we approximate traveltime as the sum traveltimes over each segment of the splined ray; that is,

$$\begin{aligned} T(p(\mathbf{x}); S, R) &\approx \sum_{k=1}^M T(p(\mathbf{x}); \bar{\gamma}_k) \\ (3.16) \qquad \qquad &= \sum_{k=1}^M T_k(p(\mathbf{x})), \end{aligned}$$

where  $T(p(\mathbf{x}); \bar{\gamma}_k) = T_k(p(\mathbf{x}))$  in equation (3.16) denotes the traveltime of a signal along the  $k$ th segment of the ray.

**3.4.3.1. Traveltime approximation: Numerical integration.** Consider the traveltime of a signal propagating along straight line  $\bar{\gamma}_k$ :

$$(3.17) \quad T(\bar{\gamma}_k) = \int_{\bar{\gamma}_k} p(\mathbf{x}) \, ds.$$

We will consider parameterization of  $\bar{\gamma}_k$  with respect to  $x$  for demonstration purposes – parameterization with respect to  $z$  follows the same methods. We write equation (3.17) as

$$(3.18) \quad T(\bar{\gamma}_k) = \int_{x_k^0}^{x_k^f} p(x, z(x)) \sqrt{1 + m_k^2} \, dx.$$

Note that the integral operator in equation (3.18) is an abuse of notation: function  $p(x, z(x))$  is defined at points on the lattice – it is a discrete function. In this case, one cannot integrate over  $p$  in the traditional sense. However, we can numerically integrate expression (3.18). We do so using the composite trapezoidal rule.

**DEFINITION 3.4.2.** Let  $f$  be a function to be integrated over an interval  $[a, b]$ ; denote the value of this integral by  $I = \int_a^b f(x) dx$ . To numerically integrate  $I$  by the composite trapezoidal rule, divide the interval of integration into  $n$  subintervals of length  $h = \frac{b-a}{n}$ . Let  $x_i = a + i h$ , and at each point  $x_i \in (a, b)$ , let  $f(x_i) = f_i$ ; at the endpoints,  $f(a) = f_0$  and  $f(b) = f_n$ . Integral  $I$  can then be approximated by the composite trapezoidal rule using the following numerical scheme:

$$I = \sum_{i=0}^{n-1} h \left( \frac{f_i + f_{i+1}}{2} \right) - \frac{h^3}{12} f''(\zeta).$$

The term  $\frac{h^3}{12} f''(\zeta)$  give the upper bound on the error of the approximation. The parameter  $\zeta$  is the value of  $x$  on the interval of integration that maximizes  $f''(x)$ .

In view of Definition 3.4.2, we write expression (3.18) as follows:

$$(3.19) \quad T(\bar{\gamma}_k) \approx \sum_{x=x_k^0}^{x_k^f-h_x} \frac{h_x \sqrt{1+m_x^2}}{2} \times (p(x, z(x)) + p(x+h_x, z(x+h_x))).$$

We omit the error term in the approximation since discrete slowness function  $p$  is not differentiable. Also, the distance between adjacent nodes on the lattice is set equal to the value of the physical spacing between nodes; in this case,  $\Delta x = h_x$ . However, one must note that each line segment  $\bar{\gamma}_k$  connects two points on the lattice over an interval  $\mathcal{I}_k$ . In general, the length of this interval is greater than one. To gain an accurate approximation to the traveltime along this segment, we would like to sum over all values of  $x$  in the interval  $\mathcal{I}_k^x = [x_k^0, x_k^f]$ . However, since function  $p$  is defined on a discrete domain, we cannot evaluate  $p$  at  $(x, z(x))$  if  $z(x)$  is not an integer.

3.4.3.2. *Weighted slowness function  $\bar{p}$ .* We approach the problem of evaluating  $z(x)$  at both nodal and non-nodal points within interval  $[x_k^0, x_k^f]$  by defining a new function  $\bar{p}(x)$ , which we refer to as the weighted slowness function. It is defined by the following expression:

$$(3.20) \quad \bar{p}(x) = \frac{|z(x) - z^+(x)| p(x, z^-(x)) + |z(x) - z^-(x)| p(x, z^+(x))}{h_z}.$$

Here,  $z^+$  indicates that  $z$  is rounded up to the next highest integer, while  $z^-$  indicates that it is rounded down to the next lowest integer.

Function  $\bar{p}$  evaluates  $p$  exactly if  $z(x)$  is an integer; if  $z(x)$  is not an integer, we take a weighted average of the velocities at  $(x, z^+(x))$  and  $(x, z^-(x))$ . Thus, function  $\bar{p}$  gives us an approximation to discrete slowness function  $p$  that allows us to evaluate slowness at all  $x \in [x_k^0, x_k^f]$ . Again, we express  $\bar{p}$  in terms of  $x$  only to reflect the parameterization of the line segment for the purposes of this example. The same formulation applies for parameterization with respect to  $z$ .

3.4.3.3. *Traveltime expression.* We simplify equation (3.19) by bringing the radicand outside the summation – since it does not depend on  $x$  – and replacing  $p$  with  $\bar{p}$ . The following expression allows us to numerically find the traveltime of a signal along a straight line segment:

$$(3.21) \quad T(\mathcal{I}_k^x) = \frac{h_x \sqrt{1 + m_k^2}}{2} \times \sum_{x \in \mathcal{I}_k^x} (\bar{p}(x, z(x)) + \bar{p}(x + 1, z(x + 1))).$$

Note that expression (??) can be expressed in terms of  $z$  by following the exact same procedure, but with  $x$  and  $z$  reversed. With this expression, we rewrite expression (3.16) for general coordinates: let  $\xi$  be the variable of parameterization of the  $k$ th segment,  $\bar{p}(\xi)$  be defined by expression (3.20),  $h_x = h_z = h$ , and  $\mathcal{I}_k$  be the interval over which the contribution of segment  $k$  is summed. The traveltime of a signal propagating along a ray defined by expression (3.13) having  $M$  segments

is

$$(3.22) \quad T(\bar{\gamma}) = \sum_{k=1}^M T(\mathcal{I}_k^\xi).$$

Expression (3.22) allows us to calculate traveltime along a ray by summing over discrete values of slowness.

### 3.5. Simulated annealing: Raytracing formulation

In Section 3.4, we presented details on how we represent physical quantities in our method of raytracing by simulated annealing. In this section, we will formulate the Metropolis algorithm in the context of raytracing via bending rays.

**3.5.1. Initialization.** For source  $S = (x_s, z_s)$  and receiver  $R = (x_R, z_R)$ , we begin with the initial guess of a ray being a straight-line connecting these two points. Let  $\bar{\gamma}^0(\xi; S, R)$  be the initial configuration of a path connecting  $S$  and  $R$  having  $M$  segments. This trial path is a single segment connecting the source to the receiver; hence,  $M = 1$ . The parameterization is determined by expression (3.14) and its traveltime is calculated by expression (3.22).

**3.5.2. Perturbing the ray: Changes in traveltime  $T$ .** At each iteration, we will randomly choose a segment  $\bar{\gamma}_k^0 \in \bar{\gamma}^0$  on this path and a point  $q = (x_q, z_q) \in \mathcal{D}$ . With these, we will randomly choose one of two possible perturbations: the change in traveltime with respect to the removal of a segment and the change in traveltime with respect to the addition of a segment. The role of  $q$  depends on the perturbation: if we choose to remove the chosen segment, we connect the segments adjacent

to the chosen segment at point  $q$ ; if we choose to add a segment, we split the chosen segment into two new segments connected at  $q$ .

For the benefit of the reader, we interject to outline the specific roles of adding and removing segments in the context of the algorithm. The purpose of adding line segments is straightforward: if we are to construct curved rays, we will need to change the length of the initial straight-line approximation to the ray. Since a straight line is the shortest distance between any two points in rectangular coordinates, any perturbation to the initial guess will increase the length of the path. Hence, adding segments allows us to construct accurate discrete representations of the actual rays.

The probability of accepting perturbations to the path that increase the traveltime of a signal increases with increasing temporal energy. If we have no way to decrease the length of a path, then we may end up constructing a ray whose shape in no way resembles that of the true ray and whose associated traveltime is much larger than the minimal traveltime. By allowing the removal of segments at any iteration, the algorithm is able to search the space of all possible paths freely. In a similar respect, the removal of segments allows the algorithm to construct rays whose traveltimes are locally minimal without the risk of being stuck in an extremal configuration.

Let  $\Delta T^-$  be the change in traveltime with respect to the removal of a segment and  $\Delta T^+$  be the change with respect to adding a segment. We will now consider the processes used to calculate these changes in traveltime.

3.5.2.1. *Removal of ray segment.* Let  $\bar{\gamma}^-$  denote the path resulting from the removal of segment  $\bar{\gamma}_k^0$  from  $\bar{\gamma}^0$ . We calculate the change in traveltime due to the removal of this segment by

$$(3.23) \quad \Delta T^- = T(\bar{\gamma}^-) - T(\bar{\gamma}^0).$$

In view of expression (3.22), the traveltime along perturbed path  $\bar{\gamma}^-$  is

$$T(\bar{\gamma}^-) = \sum_{k=1}^{M-1} T(\bar{\gamma}_k^-).$$

and the traveltime along initial path  $\bar{\gamma}^0$  is

$$T(\bar{\gamma}^0; S, R) = \sum_{k=1}^M T(\bar{\gamma}_k^0).$$

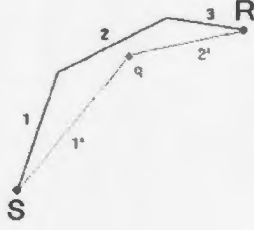
Recall that upon removing segment  $\bar{\gamma}_k^0$ , we stretch segments  $\bar{\gamma}_{k-1}^0$  and  $\bar{\gamma}_{k+1}^0$  to meet at  $q$ . Hence, segments  $\bar{\gamma}_{k-1}^-$  and  $\bar{\gamma}_k^-$  in  $\bar{\gamma}^-$  correspond to the stretching of segments  $\bar{\gamma}_{k-1}^0$  and  $\bar{\gamma}_{k+1}^0$  to  $q$ . The remaining segments of  $\bar{\gamma}^-$  are related to  $\bar{\gamma}^0$  by the following expression:

$$(3.24) \quad \bar{\gamma}_l^- = \begin{cases} \bar{\gamma}_l^0, & l < k - 1 \\ \bar{\gamma}_{l+1}^0, & l > k \end{cases}.$$

By expression (3.13), we know the expressions describing paths  $\bar{\gamma}^0$  and  $\bar{\gamma}^-$  are

$$(3.25) \quad \begin{aligned} \bar{\gamma}^0(\xi; S, R) &= \bigcup_{k=1}^M \bar{\gamma}_k^0(\xi), \\ \bar{\gamma}^-(\xi; S, R) &= \bigcup_{k=1}^{M-1} \bar{\gamma}_k^-(\xi). \end{aligned}$$

FIGURE 3.1. Illustration of a perturbation that results in the removal of a segment. Segment 2 is removed from the original (black) path; the new (red) path is formed by connecting segment 1 of the original path to segment 3 of the original path at point  $q$ . Point  $S$  denotes the source and point  $R$  denotes the receiver.



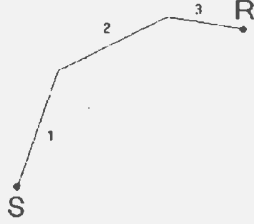
There are five segments that appear only once between expressions (3.25) and (3.24): segments  $\bar{\gamma}_{k-1}^-$  and  $\bar{\gamma}_k^-$  in  $\bar{\gamma}'(\xi; S, R)$ , and segments  $\bar{\gamma}_{k-1}^0$ ,  $\bar{\gamma}_k^0$  and  $\bar{\gamma}_{k+1}^0$  in  $\bar{\gamma}^0(\xi; S, R)$ . We calculate the change in traveltime by evaluating traveltime along each of these segments, and then taking the difference between traveltime along the perturbed path and the initial path; we write this as

$$(3.26) \quad \begin{aligned} \Delta T^- &= (T(\bar{\gamma}'_{k-1}) + T(\bar{\gamma}'_k)) \\ &\quad - (T(\bar{\gamma}_{k-1}^0) + T(\bar{\gamma}_k^0) + T(\bar{\gamma}_{k+1}^0)). \end{aligned}$$

Expression (3.26) is the change in traveltime associated with the removal of a segment from the original path. Figure 3.1 is a visual example of a typical perturbation resulting in the removal of a segment.

If we choose the segment connected to the source,  $\bar{\gamma}_1^0$ , we alter expression (3.26) to account for the non-existence of a segment before

FIGURE 3.2. Illustration of a perturbation that results in the removal of the segment connected to the source. Segment 1 is removed from the original (black) path; the new (red) path is formed by connecting segment 2 of the original path to the source. Point  $S$  denotes the source and point  $R$  denotes the receiver.



$\bar{\gamma}_1^0$ . In this case, expression (3.26) becomes

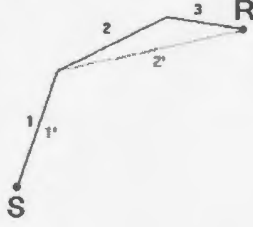
$$\Delta T^- = (T(\bar{\gamma}'_1)) - (T(\bar{\gamma}_1^0) + T(\bar{\gamma}_2^0)).$$

That is, we connect segment  $\bar{\gamma}_2^0$  to the source to create segment  $\bar{\gamma}'_1$ . If we choose the segment connected to the receiver,  $\bar{\gamma}_M^0$ , we alter expression (3.26) to account for the non-existence of segment  $\bar{\gamma}_{M+1}^0$ ; in this case,

$$\Delta T^- = (T(\bar{\gamma}'_{M-1})) - (T(\bar{\gamma}_{M-1}^0) + T(\bar{\gamma}_M^0)).$$

Thus, we create segment  $\bar{\gamma}'_M$  by connecting segment  $\bar{\gamma}_{M-1}^0$  to the receiver. Figure 3.2 is a visual example of a typical perturbation resulting in the removal of the segment connected to the source, while Figure 3.3 is a visual example of a typical perturbation resulting in the removal of the segment connected to the receiver.

FIGURE 3.3. Illustration of a perturbation that results in the removal of the segment connected to the receiver. Segment 3 is removed from the original (black) path; the new (red) path is formed by connecting segment 2 of the original path to the receiver. Point  $S$  denotes the source and point  $R$  denotes the receiver.



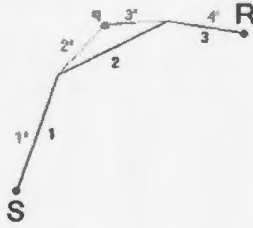
For conciseness, we write  $\Delta T^-$  in terms of the three possible cases for the perturbation of segment  $\bar{\gamma}_k^0$ :

$$(3.27) \Delta T^- = \begin{cases} T(\bar{\gamma}'_1) - (T(\bar{\gamma}_1^0) + T(\bar{\gamma}_2^0)), & k = 1 \\ (T(\bar{\gamma}'_{k-1}) + T(\bar{\gamma}'_k)) \\ - (T(\bar{\gamma}_{k-1}^0) + T(\bar{\gamma}_k^0) + T(\bar{\gamma}_{k+1}^0)), & 1 < k < M \\ T(\bar{\gamma}'_{M-1}) - (T(\bar{\gamma}_{M-1}^0) + T(\bar{\gamma}_M^0)), & k = M \end{cases}$$

When removing segments, one must note that when  $M = 1$  we cannot remove a segment. Otherwise, we could remove the entire path. To remove a segment, we require  $M > 1$ .

3.5.2.2. *Addition of ray segment.* The other perturbation we consider is the addition of a new segment to path  $\bar{\gamma}^0$ . Using randomly chosen segment  $\bar{\gamma}_k^0$  and point  $q$ , we split segment  $\bar{\gamma}_k^0$  into two new segments,  $\bar{\gamma}_k^+$  and  $\bar{\gamma}_{k+1}^+$ . Let this new path be denoted  $\bar{\gamma}^+(\zeta; S, R)$ . We relate the remaining  $M - 1$  segments in this perturbed path to the original path

FIGURE 3.4. Illustration showing the perturbation to the path resulting in the addition of a segment. Segment 2 of the original (black) path is split into two segments and reconnected at point  $q$ , forming the new (red) path. Point  $S$  denotes the source and point  $R$  denotes the receiver.



by

$$\bar{\gamma}_l^+ = \begin{cases} \bar{\gamma}_l^0, & l < k \\ \bar{\gamma}_{l-2}^0, & l > k+1 \end{cases}.$$

Following the procedure of Section 3.5.2.1, we calculate the change in traveltime with respect to the addition of a segment by

$$(3.28) \quad \Delta T^+ = (T(\bar{\gamma}'_k) + T(\bar{\gamma}'_{k+1})) - (T(\bar{\gamma}_k^0)).$$

Note that we do not have to consider special cases of this perturbation. For  $M = 1$ , the only perturbation that we can perform is the splitting of the line segment. Furthermore, the segments connected to the source and receiver can be split according to this method, since we do not detach the segments connected to these points. Figure 3.1 is a visual example of a typical perturbation resulting in the addition of a segment.

**3.5.3. Acceptance scheme: Metropolis criterion.** In Section 3.5.2, we outlined the two possible perturbations to the path at each iteration: the changes in traveltime with respect to removing a segment and with respect to splitting a segment. However, at each iteration, we can only choose to perturb the path according to one of these methods. In view of this, we will randomly choose between adding and removing segments to the path at each iteration.

Let  $\Delta T'$  denote the change in traveltime corresponding to the chosen perturbation. We choose whether or not to accept this perturbation according to the Metropolis acceptance criterion for change in traveltime  $\Delta T'$  at temporal energy  $T_C$ :

$$A(\bar{\gamma}^0 \rightarrow \bar{\gamma}') = \begin{cases} 1, & \Delta T' \leq 0 \\ \exp\left(-\frac{\Delta T'}{T_C}\right), & \Delta T' > 0 \end{cases}.$$

If  $\Delta T' \leq 0$ , then the perturbation results in a traveltime that is lower than the traveltime of the initial path; we automatically accept this perturbation. If  $\Delta T' > 0$ , then the perturbation results in a path with larger traveltime. The probability of accepting this perturbation is equal to  $\exp(-\Delta T'/T_C)$ . To choose whether or not to accept this perturbation according to the Boltzmann factor, we generate a random number  $Z \in [0, 1)$ . If  $Z < \exp(-\Delta T'/T_C)$ , we accept the perturbation; otherwise, we reject.

**3.5.4. Markov chains, equilibration times, and cooling schedules.** Section 3.5.3 outlines the process of perturbing a path at a randomly chosen segment. This corresponds to a single iteration of the Metropolis algorithm, which is the mechanism used to generate a Markov process.

In order to properly equilibrate the path with respect to  $T_C$ , we need to generate enough paths at this temporal energy such that the paths generated occur with a probability according to the Boltzmann distribution. For our studies, we let  $\mathcal{L} = 50N$  be the number of Markov processes that we generate at each temporal energy, where  $N$  is the number of nodes on the lattice.

To simulate the cooling process in the annealing method, we will implement a cooling schedule. We develop this schedule to lower temporal energy  $T_C$  as a function of the number of generated Markov chains. Let  $T_C^0$  denote the initial temporal energy of the system. Nourani and Andersen [12] investigated the properties of several cooling schemes that have been implemented in various simulated annealing studies. The schedules considered in this paper are: constant thermodynamic speed, exponential, logarithmic, and linear cooling schedules. Comparisons were made based on the amount of entropy – or disorder – produced during the annealing process for given initial and final states and a fixed number of iterations. The cooling scheme that yielded the least amount of entropy was then deemed the best. They found that the constant thermodynamic speed schedule performed the best: it always

managed to find the global minimum of the system in the prescribed amount of iterations.

For our simulations, we choose to employ the fixed exponential cooling schedule. Although this schedule was shown to not yield the rapid convergence of the constant thermodynamic speed schedule, it was shown to yield the best results of all the fixed-rate cooling schedules considered. Furthermore, its simplicity in implementation makes it appealing since we are currently concerned only with the accuracy of the results – not with algorithm optimization or benchmark times. Adaptive schedules such as the constant thermodynamic speed schedule can be implemented at a later date when the algorithm has been shown to provide accurate results. The fixed exponential cooling schedule is

$$(3.29) \quad T_C(i) = T_C^0 \exp(-(i-1)).$$

Parameter  $i$  denotes the  $i$ th temperature in the annealing process; we let  $i = 1, 2, \dots, 25$ , and  $T_C^0 = 0.25$ .

### 3.6. Summary

We have presented a large amount of material in this chapter. In this section, we will summarize key points as they pertain to this work.

In Section 3.1, we introduced the concept of simulated annealing. We presented the physical motivation that led to the development of the simulated annealing method, and how it could be used in other problems of optimization.

In Section 3.2, we introduced the Metropolis algorithm. We presented background pertaining to this algorithm, and made references to literature that illustrates the effectiveness of this algorithm and guarantees its convergence to the desired solution – the groundstate configuration of the system. At the end of this section, we outlined how this algorithm could be applied to the process of raytracing.

In Section 3.3, we discussed analogies between elements of ray theory and statistical mechanics. With these analogies, we described how we would implement the simulated annealing algorithm to calculate rays in inhomogeneous media.

In Section 3.4, we described the effects of representing media by discrete methods. We presented discrete models describing physical media and rays and described how we will treat rays within the framework of a discrete model. In view of the discrete models for media and rays, we illustrated how to calculate traveltime along rays in discrete media.

Finally, in Section 3.5, we presented the general outline of how we will use the simulated annealing method to calculate rays within inhomogeneous media. Methods for perturbing rays, calculating the ensuing change in traveltime due to a perturbation, calculating the probability of accepting a perturbation, generating Markov chains, and cooling the system were all outlined.

The simulated annealing method is a commonly-used tool in areas of mathematics and physics; specifically, in problems where one wishes

to obtain the optimal solution, subject to the constraints imposed by the problem. The algorithm presented in this chapter

In Chapter 5, we present results obtained from this algorithm for modelling rays in two specific types of media: layered media and linearly inhomogeneous media. We compare rays and traveltimes calculated from this algorithm to exact results available from the analytical solutions of rays within these media, and the associated errors that arise from the approximation of the media and the rays.

## CHAPTER 4

# Radon's transform: Application to inverse problems

The focus of this chapter switches from forward problems to inverse problems. We will introduce the generalized forms of Radon's transform and its adjoint operator, and discuss their applications to inverse problems. We will show that by treating the traveltimes of a signal as Radon's transform acting on the slowness function along a ray, we can use the adjoint to Radon's transform to recover the slowness function from a collection of these traveltimes.

We will propose a method that uses the adjoint to Radon's transform to recover the quantitative properties of a medium described by its slowness function from a collection of traveltimes treated as the generalized Radon transform of the slowness function along curved rays. We will discuss this method and the technical concerns associated with its implementation at the end of this chapter.

### 4.1. History

The Radon transform was first introduced by Johann Radon in 1917<sup>1</sup>. The results of this paper have inspired much mathematical research in recent years. The interest in this area has not been grounded in the

---

<sup>1</sup>For a translation of this paper, the reader is referred to [13, Appendix B].

transform itself, but the development of techniques for calculating its inverse.

In his paper, Radon discussed the following questions.

- For any function  $f$  in  $\mathbb{R}^2$  integrated along a line  $\gamma$ , can the line integral  $F(\gamma)$  always be determined?
- If so, can  $f$  be uniquely determined from  $F(\gamma)$ ?

We will study these questions in this chapter. The first question deals with the forward problem while the second question deals with the inverse one.

## 4.2. Classical definition

**4.2.1. Forward transform .** The Radon transform is an integral operator. We denote it by  $R$  and define it as follows.

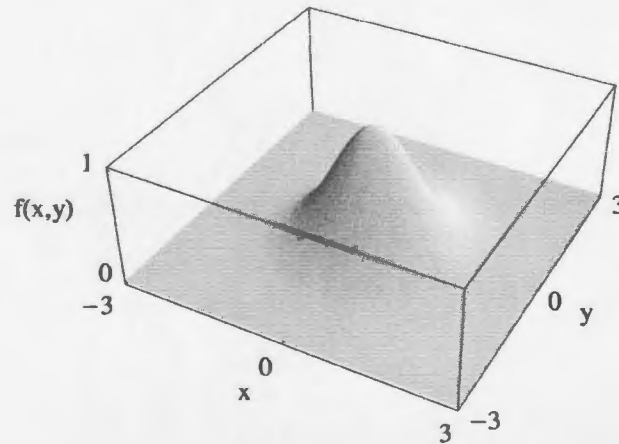
**DEFINITION 4.2.1.** In two dimensions, Radon's transform  $R$  is an operator that integrates a two-dimensional function  $f$  along a path in the space of  $f$  to produce a number. Mathematically, we state

$$(4.1) \quad R(f)(\gamma) = \int_{\gamma} f(x(t), y(t)) dt.$$

Here,  $t$  denotes the parameterization of the path  $\gamma$  over  $\mathbb{R}^2$ , and  $(x(t), y(t))$  are coordinates of  $\mathbb{R}^2$  that lie on  $\gamma$ .

Radon stated that one can determine the value of the line integral in equation (4.1) provided that  $f$  is a smooth function that has compact support on its domain; that is,  $f$  is zero outside of some boundary on its domain; we denote by  $f \in C_0^\infty(\mathbb{R}^2)$ . An example of a function having

FIGURE 4.1. Plot of function  $f(x, y) = \exp(-(x^2 + y^2))$ . We say that  $f$  has compact support on its domain since function  $f$  tends to zero rapidly as the values of  $x$  and  $y$  increase.



compact support is shown in Figure 4.1. The Radon transform fails to produce a result over an infinite domain for functions not having compact support, since the value of the integral diverges. An example of this is the Radon transform of  $f(x, y) = \alpha$ , where  $\alpha$  is a constant, integrated over any line passing through  $\mathbb{R}^2$ .

For any  $\gamma$ , let  $\mathbf{p}$  be a vector perpendicular to  $\gamma$  that passes through the origin. Hence,  $\|\mathbf{p}\| = p$  is the shortest distance between  $\gamma$  and the origin. Let  $\alpha$  be the angle between  $\mathbf{p}$  and the  $x$ -axis. As per Definition 4.2.1, let  $t$  parameterize each point in  $\mathbb{R}^2$  along  $\gamma$ . We express each point  $(x, y)$  that lies on  $\gamma$  by making the following change of coordinates:

$$(4.2) \quad \begin{aligned} x &= p \cos \alpha - t \sin \alpha \\ y &= p \sin \alpha + t \cos \alpha \end{aligned}$$

Equations (4.2) allow us to rewrite equation (4.2.1) as

$$\begin{aligned} R(f)(\gamma) &= \int_{\gamma} f(p \cos \alpha - t \sin \alpha, p \sin \alpha + t \cos \alpha) dt \\ &= F(p, \alpha) \end{aligned}$$

The quantity  $F$  is a function of the new variables  $p$  and  $\alpha$ , and represents the value of Radon's transform of  $f$  along  $\gamma$ .

**4.2.2. Inverse of Radon's transform.** Radon's second question deals with the uniqueness of the recovered function  $f$  from the values of  $F(\gamma)$ . That is, given a collection of measurements along a set of lines passing through a point, can one construct the original function uniquely? In his paper, he showed that it is possible to recover  $f$  from values of  $F(\gamma)$  uniquely, so long as  $f$  satisfies certain conditions. Uniqueness of solutions is very important in the realm of inverse problems. If we cannot guarantee the uniqueness of solutions, then we cannot place any confidence in solutions obtained from inverse problems.

Many approaches have been developed to calculate the inverse to Radon's transform. One such method involves using the adjoint operator to Radon's transform  $R$ , denoted  $R^*$ , to calculate the inverse. Our work in the context of inverse problems will revolve mainly around the use of adjoint operator  $R^*$ .

**4.2.3. Adjoint operator  $R^*$ .** In Appendix A, we give the proof showing  $R^*$  is adjoint to  $R$ ; we prove that

$$\langle Rf, F \rangle_{\mathcal{L}} = \langle f, R^*F \rangle_{\mathcal{M}},$$

where  $\langle \cdot, \cdot \rangle_S$  denotes the scalar product of two functions over the domain of the space  $S$ , where space  $\mathcal{M}$  represents the medium and space  $\mathcal{L}$  represents the space of lines. To define  $R^*$  for straight lines, consider the following theorem.

**THEOREM 4.2.2.** *The adjoint operator,  $R^*$ , takes any integrable function  $G$  of  $p$  and  $\alpha$  and defines a new function of  $x$  and  $y$  by the following expression:*

$$(4.3) \quad R^*(G)(x, y) = \frac{1}{\pi} \int_0^\pi G(x \cos \alpha + y \sin \alpha, \alpha) |d\alpha|,$$

where  $\alpha$  is the variable that gives the angle of the vector  $\mathbf{p}$  with respect to the  $x$ -axis and the absolute value of  $d\alpha$  indicates that the value of the integral is independent of the orientation.

The proof showing that  $R^*$  is adjoint to  $R$  is shown in [4].

In view of Theorem 4.2.2, we set  $G = F_\gamma$  and rewrite equation (4.3) as

$$(4.4) \quad R^*(F)(x, y) = \frac{1}{\pi} \int_0^\pi F(x \cos \alpha + y \sin \alpha, \alpha) d\alpha.$$

Equation (4.3) states that the adjoint operating on  $F$  is the average of all values of  $F_\gamma$  for each  $\gamma$  that passes through  $(x, y)$  and is integrated over  $\alpha$ .

**4.2.4. Inversion formula.** In this section, we will use the adjoint operator  $R^*$  to calculate the inverse to  $R$  following the results of Niev-ergelt, [4].

The scalar product of two functions is the integral of the product of two functions integrated over the entire domain of these functions. Let us consider the case where one of these functions is Dirac's delta. In such a case,  $f = f(x, y)$  and  $g = \delta(x - x_0, y - y_0)$ ; the scalar product of these two functions is

$$\begin{aligned} \langle f, g \rangle &= \langle f, \delta(x - x_0, y - y_0) \rangle \\ &= \int_{\mathbf{R}^2} f(x, y) \delta(x - x_0, y - y_0) dx dy \\ &= f(x_0, y_0). \end{aligned}$$

In the realm of Radon's transform, our goal is to find some function  $g = R^*G$  of  $p$  and  $\alpha$  that behaves like Dirac's Delta. If such a function were to exist, we could write  $f(x_0, y_0)$  as the scalar product of  $f$  and  $g$  as follows:

$$(4.5) \quad f(x_0, y_0) = \langle f, g \rangle = \langle f, R^*G \rangle .$$

By the adjoint property of  $R^*$ , equation (4.5) would become

$$\langle f, R^*G \rangle = \langle Rf, G \rangle$$

and we would obtain

$$f(x_0, y_0) = \langle Rf, G \rangle .$$

One example of such a function was shown by Nievergelt [4]. He showed that the following function recovers  $f$  from  $Rf$ :

$$(4.6) \quad G_c(p, \alpha) = \begin{cases} \frac{1}{\pi c^2}, & \text{if } -c \leq p \leq c \\ \frac{1}{\pi c^2} \left( 1 - \frac{1}{\sqrt{1-c^2/p^2}} \right), & \text{if } \|p\| > c \end{cases}.$$

In the limit  $c \rightarrow 0$ , function  $G_c$  calculates the inverse of  $R$  in the sense of distributions. That is,

$$(4.7) \quad \begin{aligned} f(x, y) &= \lim_{c \rightarrow 0} \langle f_X, g_c \rangle \\ &= \lim_{c \rightarrow 0} \langle Rf_X, G_c \rangle \end{aligned}$$

The proof showing  $G_c = R^* g_c$  is shown in [4, pp.82-83]. By definition of the scalar product in  $L$ -space, we can rewrite this equation in terms of the limit of a double integral as follows:

$$(4.8) \quad f(x, y) = \lim_{c \rightarrow 0} \frac{1}{\pi} \int_0^\pi \int_{-\infty}^{\infty} Rf(p, \alpha) G_c(p, \alpha) dp d\alpha.$$

This inversion formula uniquely recovers any integrable function  $f$  from its Radon transform.

**4.2.5. Calculating the inverse.** While  $G_c$  gives us a readily available expression for inversion of the Radon transform, there are many limitations in applying it to physical situations.

First, expression (4.8) involves the calculation of both an improper integral over  $p$  and the limit of parameter  $c$  tending to zero. Although

numerical schemes do exist for performing these calculations, implementing such a scheme for calculating the inverse of  $R$  would be computationally intensive. That we would be calculating this for an infinite range also adds to the difficulty of this matter.

Next, in practice, we would not be given a continuous form of  $Rf$ ; rather, we would be supplied with a collection of profiles calculated for a finite number of paths over the domain. Furthermore, the domain over which these profiles are collected is a finite subdomain of  $\mathbb{R}^2$ , not the infinite domain assumed in Definition 4.2.1. At the first glance, it would seem that we have eliminated one of the problems previously mentioned - the calculation of the improper integral over  $p$ -space. However, any method for inverting the Radon transform based on methods outlined thus far will need to be modified from a continuous, infinite domain to a finite sublattice of points.

Most importantly, however, for any medium described by function  $f$ , integration paths correspond to geodesics within the space defined by that function, as a result of invoking Fermat's principle in our study. Hence, these paths are governed by the properties of  $f$ . Since  $f$  is an unknown function, we are unable to make *a priori* assumptions about these paths. However, this method assumes that all integration paths are straight, regardless of the properties of the medium described by  $f$ . In a seismological context, this argument is valid only in the case of homogeneous media. For inhomogeneous media, the assumption that integration paths are straight lines is invalid, was shown in Chapter 2.

Our goal is to develop a new method of recovering  $f$  from  $Rf$  where we make no assumptions about the shapes of the integration paths.

### 4.3. Inverse problems: Generalized adjoint method

**4.3.1. Motivation.** By invoking Fermat's principle, it is incorrect to assume that integration paths over a medium described by function  $f$  are always straight. As a result, methods introduced in Section 4.2.4 for calculating the inverse of Radon's transform are, in general, invalid. Unless we know that rays are straight in the medium, we cannot justify using these methods.

We wish to formulate an expression for  $R^*$  that accounts for curved rays. To do so, we will use a variation of the method used to formulate the adjoint operator to the standard Radon transform.

**4.3.2. Generalized Radon transform.** Recall Radon's transform acting on a function  $f$  along path  $\gamma$  parameterized by parameter  $t$ :

$$R(f)(\gamma) = \int_{\gamma} f(x, y) dt.$$

In Section 4.2.1 we assumed that integration path  $\gamma$  was a straight line over the space defined by  $f$ . In view of Fermat's principle, we know that, in general, this assumption is invalid. Herein, we will make no assumptions on the shape of path  $\gamma$ . The general formulation of Radon's transform for curved rays behaves similarly to the standard Radon transform. The key difference is that the generalized Radon transform acts along a ray, whose shape is governed by function  $f$ .

Herein, operator  $R$  refers to the generalized Radon transform. In cases where the rays are straight lines, the generalized Radon Transform reduces to the standard Radon transform, and inversion techniques developed for straight lines can be applied.

**4.3.3. Generalized Adjoint operator  $R^*$ .** In Section 4.2.3, we defined adjoint operator  $R^*$  operating at point  $X = (x, y)$  as the average of all values of  $F_\gamma = Rf(p, \alpha)$  at  $X$ , integrated over all geodesics passing through  $X$  at angle  $\alpha$ . Expressing parameter  $p$  in terms of angle  $\alpha$  and coordinate  $X$ , we wrote  $Rf(p, \alpha) = Rf(x \cos \alpha + y \sin \alpha, \alpha)$  and expressed adjoint operator  $R^*$  acting on all values of  $Rf$  at  $X$  as

$$R^*(Rf)(x, y) = \frac{1}{\pi} \int_0^\pi (Rf)(x \cos \alpha + y \sin \alpha, \alpha) d\alpha.$$

The development of the adjoint operator was facilitated by the fact that  $\gamma$  was assumed to be a straight line. Hence, the angle of the tangent vector to  $\gamma$  is constant along the path.

In the case of curved paths, the angle of the tangent to  $\gamma$  varies along the path. Applying the adjoint operator  $R^*$  formulated for straight lines on values of  $Rf$  calculated by the generalized Radon transform would mean that we are integrating over incorrect paths.

In Appendix A, we construct the adjoint to generalized Radon transform  $R$ ,  $R^*$ , using a procedure similar to [4]. We define  $R^*$  as the average of all values of  $Rf(\gamma)$  at  $X$  integrated over the tangent space of all geodesics passing through  $M$ . Let  $\alpha$  denote the angle of the tangent vector  $v^\alpha$  to path  $\gamma_X^\alpha$  passing through point  $X$ . Let  $\exp_X(v^\alpha)$  be the projection of tangent vector  $v^\alpha$  onto the space of the medium; on space

$\mathcal{M}$ ,  $\gamma_X^\alpha = \exp_X(v^\alpha)$ . The effect of  $R^*$  acting on  $Rf$  at  $X$  is given by

$$(4.9) \quad R^*(Rf)(x, y) = \frac{1}{\pi} \int_0^\pi (Rf)(\exp_X(v^\alpha)) \frac{d\alpha}{|\exp_X(v^\alpha)|}.$$

Note the inclusion of the  $1/|\exp_X(v^\alpha)|$  term in equation (4.9). In this work, we will be working with compact domains. Hence, we divide by the length of each line corresponding to the value of  $F$  when applying the adjoint. Furthermore, in view of  $F$  corresponding to values of traveltime, dividing by line lengths ensures that results obtained from  $R^*$  acting on  $F$  has units of slowness ( $s/m$ ).

Using the generalized formulations of Radon's transform and its adjoint, we propose a method for recovering function  $f$  from a collection of measurements  $Rf$  as treated in the context of the generalized Radon transform.

**4.3.4. Backprojection: Application of  $R^*$ .** A consequence of applying the generalized form of adjoint operator  $R^*$  to measurements  $Rf$  is that we are not carrying out a true inversion of the measured data. Mathematically, we describe the operation of  $R^*$  on  $F = Rf$  at  $X$  by the following:

$$R^*(F)(x, y) = \frac{1}{\pi} \int_0^\pi F(\exp_X(v^\alpha)) \frac{d\alpha}{|\exp_X(v^\alpha)|}$$

Let  $\Pi = R^*(F)$ . Function  $\Pi(x, y)$  is called the backprojection of  $F$ . This function is defined on the same space as function  $f$ ; that is,  $\Pi$  maps traveltimes in the space of rays,  $\mathcal{L}$ , to the space of slowness,  $\mathcal{M}$ . As stated in [13, p. 134], backprojection  $\Pi$  does not recover  $f$  exactly – in general, the adjoint is not the inverse to Radon's transform; hence,

$R^*$  is not the inverse operator to  $R$ . However, the adjoint does yield a blurred image of the original function when acted on the data. Our hope is that  $\Pi$  will provide enough qualitative information about the medium to be considered as a good approximation to the slowness function describing the medium.

Various reconstruction techniques have been developed in recent years that use backprojection techniques to facilitate the inversion process, see [18, Ch. V], [13, Ch. 6]; However, these techniques have been developed under the assumption of straight line integration paths. In this work, we will employ the backprojection method to recover information about function  $f$ . Our hope is that  $\Pi$  will recover qualitative properties of function  $f$ . In the next section, we will propose a method for recovering details about a medium described by slowness function  $f = p$  given a collection of traveltime measurements  $T = Rf$ .

#### 4.4. Seismic inverse modelling: Backprojection method

To recover information about slowness function  $p$  at point  $X^2$ , we apply  $R^*$  to traveltimes from all rays passing through that point. Mathematically, we calculate

$$(4.10) \quad \Pi(x, z) = \frac{1}{\pi} \int_0^\pi T(\exp_X(v^\alpha)) \frac{d\alpha}{|\exp_X(v^\alpha)|}.$$

To facilitate the process of testing this method, we will need to calculate rays and their associated traveltimes. We will do so by employing the simulated annealing method presented in Chapter 3.

---

<sup>2</sup>We change coordinates in this section from  $(x, y)$  to  $(x, z)$  to reflect the fact that we are now discussing backprojection methods as they relate to geophysical studies.

**4.4.1. Calculation of backprojection  $\Pi$ .** In view of discrete media, we will make approximations to the backprojection function  $\Pi$ . Recall expression (4.10):

$$\Pi(x, z) = \frac{1}{\pi} \int_0^\pi T(\exp_X(v^\alpha)) \frac{d\alpha}{|\exp_X(v^\alpha)|}.$$

This expression says that we integrate over the entire tangent space of point  $X$  – in practice, this is not the case. For a fixed number of sources and receiver, only a finite number of rays will pass through any point within the medium. Hence, we will need to approximate  $\Pi(x, z)$  to account for the limited data.

We calculate the integral of  $\Pi(x, z)$  by invoking the composite trapezoid rule, Definition 3.4.2. For  $M$  values of traveltime collected at point  $(x, z)$ , we numerically evaluate backprojection  $\Pi(x, z)$  at  $X$  as

$$\begin{aligned} \Pi(x, z) &= \frac{1}{\pi} \int_0^\pi T(\exp_X(v^\alpha)) \frac{d\alpha}{|\exp_X(v^\alpha)|} \\ (4.11) \quad &= \frac{1}{\pi} \sum_{k=2}^M \frac{\Delta\alpha_k}{2} \left( \frac{\bar{T}(P; \alpha_{k-1})}{|\bar{\gamma}_X^{k-1}|} + \frac{\bar{T}(P; \alpha_k)}{|\bar{\gamma}_X^k|} \right). \end{aligned}$$

In view of a discrete set of traveltimes, we omit the error term. In equation (4.11),  $\Delta\alpha_k$  corresponds to the difference in tangent angles at  $X$  between rays  $\bar{\gamma}_X^{k-1}$  and  $\bar{\gamma}_X^k$ , and  $|\bar{\gamma}_X^k|$  corresponds to the length of ray  $\bar{\gamma}_X^k$ . Function  $\bar{T}(X; \alpha_k)$  corresponds to the  $k$ th traveltime associated with ray  $\bar{\gamma}_X^k$  stored at  $X$ , whose tangent angle is  $\alpha_k$  at  $X$ .

Consider the quantity  $\bar{T}(X; \alpha_{k-1})/|\bar{\gamma}_X^{k-1}|$ : the traveltime of a signal divided by the length of its corresponding ray  $\bar{\gamma}_X^{k-1}$ . This quantity is the

average slowness of a signal traveling along ray  $\bar{\gamma}_X^k$ . We let

$$\tilde{p}(X; \bar{\gamma}_X^k) = \frac{\bar{T}(X; \alpha_X)}{|\bar{\gamma}_X^k|}.$$

Thus, instead of storing the traveltimes of a ray passing through point  $X$ , we store its average slowness. We rewrite expression (4.11) as

$$(4.12) \quad \Pi(X) = \frac{1}{\pi} \sum_{k=2}^M \frac{\Delta\alpha_k}{2} (\tilde{p}(X; \alpha_{k-1}) + \tilde{p}(X; \alpha_k))$$

Expression (4.12) gives us a readily calculable expression for  $\Pi(X)$ . Before continuing, we must address one more problem: the calculation of tangent angles  $\alpha_k$ ; moreover, the calculation of measure of integration  $\Delta\alpha_k$ .

Remember that rays calculated in a discretized medium are not smooth curves – they are a spline of linear functions defined on subintervals within the interval of integration. As a result, the concept of differentiability only applies to the line segments of the ray. That is, unless segments sharing a common endpoint have the same slope, the ray is not differentiable at this point.

We suggest the following resolution: for neighbouring rays  $\bar{\gamma}_{k-1}$  and  $\bar{\gamma}_k$ , let  $\Delta S_k$  denote the distance between the sources of these rays, and  $\Delta R_k$  the difference between their receivers. For all rays passing through or near point  $(x, z)$ , it can be shown that

$$\sum_{k=2}^M (\Delta S_k + \Delta R_k) = 8L,$$

where  $L$  is the length of one side of the lattice. Let  $\mathcal{P}$  denote the perimeter of the lattice;  $\mathcal{P} = 4L$ . Then

$$(4.13) \quad \sum_{k=2}^M (\Delta S_k + \Delta R_k) = 2\mathcal{P}.$$

Let  $\Delta\gamma_k = \Delta S_k + \Delta R_k$  denote the spacing between adjacent rays passing through  $P$ . We propose to replace measure  $\Delta\alpha_k$  by a new measure,  $\Delta\gamma_k$ . Our reasoning is that since the backprojection formula is physically defined as the average of all traveltimes of signals passing through a point  $X$  integrated over all geodesics that passing through that point, we view averaging over the spacing between adjacent rays as the equivalent process of averaging over the tangent space of point  $X$ .

Before replacing  $\Delta\alpha_k$  by this measure  $\Delta\gamma_k$ , we must note that this new measure will change the units of expression (4.12). In view of this, we replace the normalizing constant  $\frac{1}{\pi}$  by  $\frac{1}{2\mathcal{P}}$ . Expression (4.12) then becomes

$$(4.14) \quad \Pi(X) \approx \frac{1}{2\mathcal{P}} \sum_{k=2}^M \frac{\Delta\gamma_k}{2} (\tilde{p}(X; \alpha_{k-1}) + \tilde{p}(X; \alpha_k)).$$

We will use expression (4.14) to calculate backprojection  $\Pi$  at each point  $X$  from values of average slowness.

To store these data, we define matrix  $\zeta$  as the  $L \times L$  matrix in which we store data recovered in the calculation: for each node  $\zeta(x, z)$  that ray  $\tilde{\gamma}_k$  passes through, we store the location of the source and receiver connected by the ray, and the average slowness associated with this ray.

#### 4.5. Notes on application of backprojection method

The next step in this work is to apply expression (4.14) to travel-time data collected between sources and receivers on a square lattice, as calculated from the simulated annealing method presented in Chapter 3. Our goal is to construct backprojected function  $\Pi(x, z)$  using a collection of traveltimes to show that this function recovers the qualitative properties of the original slowness function  $p(x, z)$ . Starting with slowness function  $p$ , we will solve for rays connecting sources to receivers and their associated traveltimes by the method of simulated annealing. We will then apply expression (4.14) to the traveltimes collected to obtain the value of the backprojected function  $\Pi(x, z)$  at each point  $X$  on the lattice.

At this point, the reader may ask: why develop a method that requires prior knowledge of a function whose properties we are trying to obtain, but can only recover the function's properties qualitatively? Moreover, why go through the process of obtaining function  $\Pi$  when we already have  $p$ ?

We have noted that backprojection expression (4.14) is not a true inverse operator; the image one constructs from data measured on the medium is blurry at best. If the medium is not too complicated, one can hope to obtain an image that closely resembles slowness function  $p$ . Hence, if the results of this method are qualitatively bad even when we know the rays, one can expect that any modification of this method will not increase its applicability.

Evaluation of expression (4.14) requires values of average slowness along each ray passing through point  $X$ . To calculate average slowness, one needs to know the length of the associated ray. In physical situations, one can only measure traveltimes, as the ray itself is unknown. The simulated annealing method presented in this thesis calculates traveltimes from rays – not vice versa – and we use these rays in the calculation of  $\Pi(X)$  at each  $X \in \mathcal{D}$ . In view of this, how can one apply the backprojection operator to real physical data? At the time of writing, the answer to this question is unknown to the author.

In this thesis, we are concerned only with testing the accuracy of the backprojection operator to collected traveltimes. In Section (5.4), we will introduce a method that uses the backprojection procedure but makes no assumptions about the rays.

## CHAPTER 5

### Results

In this chapter, we will present results collected from the implementation of our proposed methods for forward and inverse modelling for two velocity models: layered inhomogeneous media and linearly inhomogeneous media. We chose these models for the availability of analytical solutions that can be used to test the accuracy of the results obtained.

We will first present the results obtained from the simulated annealing method. Our basis for comparison between analytical and numerical results focuses on the shapes of the rays obtained for specific source/receiver configurations and the traveltimes associated with these rays. Results are gathered for different values of physical node spacing.

Next, we will use the simulated annealing method to calculate rays and associated traveltimes connecting all sources to all receivers for both velocity models. We will apply the backprojection method to these data and compare our results to the original slowness function.

At the end of this chapter, we will discuss the errors in the results obtained in the forward and inverse modelling methods with respect to quantitative and qualitative accuracy.

### 5.1. Methodology

To test the accuracy of the simulated annealing method, we use a vertical seismic profile configuration – a common setup in geophysical exploration studies. We will construct rays connecting sources at  $(0m, 0m)$  and  $(500m, 0m)$  to receivers located at  $(1000m, 100m)$ ,  $(1000m, 600m)$ , and  $(1000m, 1000m)$  using node spacings  $h = 25m$ ,  $50m$ , and  $100m$ .<sup>1</sup> We will conclude by discussing the accuracy of results obtained for each model.

We will use the simulated annealing method to generate data to be used in the testing of the backprojection method. We will construct rays between sources and receivers at all nodes along the edges of the lattice for node spacings  $h = 25m$ ,  $50m$ , and  $100m$ . This setup is an idealized source/receiver configuration – in seismological studies, the placement of sources and receivers all around a cross-section of a medium to collect such data is, in general, physically impossible. At this stage, our goal is to test the efficiency of the backprojection method using a complete data set<sup>2</sup> generated from the simulated annealing method. Considerations involving incomplete data sets are outside the scope of this work.

---

<sup>1</sup>In forward modelling studies, the choice of node spacing depends on the frequency of the signal. In this work, we will use arbitrary node spacings to test the efficiency of results obtained from the method. However, future applications of this method will require that the choice of  $h$  be consistent with signal frequency.

<sup>2</sup>By complete data set, we mean that data is collected from all possible rays passing through the compact domain of the lattice.

The results presented in this chapter for the simulated annealing method and the backprojection method were generated from code written in *Fortran 90* and run on an SGI Onyx 3400 processor. Computational optimization concerns were not considered in the work presented in this thesis, as the speed at which the code produced results was sufficient for the scope of this thesis. The code used to implement these methods and produce results are included on a compact disc in Appendix C.

## 5.2. Forward modelling: Simulated annealing method

We will now present the results obtained from the forward modelling of rays in two types of media. The first medium considered is a horizontally-layered inhomogeneous medium and the second medium considered is a linearly inhomogeneous medium. Results are discussed in the contexts of the shapes of rays and traveltimes associated with these rays.

### 5.2.1. Model 1: Layered medium.

5.2.1.1. *Background.* Consider a horizontally-layered medium consisting of two distinct layers whose interface lies along the line  $z = z_I$ . Such a medium can be described by a function of the form

$$(5.1) \quad v(x, z) = \begin{cases} v_1, & z < z_I \\ v_2 & z \geq z_I \end{cases}.$$

This function describes a medium whose properties change at the interface  $z = z_I$ . We will test the accuracy of the raytracing algorithm

with the following velocity model:

$$v(x, z) = \begin{cases} 1000m/s, & z < 200m \\ 2000m/s, & z \geq 200m \end{cases} .$$

In Appendix B.1, we derive expressions for rays and traveltimes of signals in homogeneous media, and in Appendix B.2, we derive expressions for calculating rays and traveltimes of signals propagating within layered media.

Depending on the source-receiver configuration, we can have four types of signals. For configurations where the source is located within one layer and the receiver is located within the other, the results of Appendix B.2.1 apply, as the signal must transmit through the interface. For configurations where the source and receiver are located within the same layer, three types of signals exist. The first type is the direct arrival of the signal at the receiver. In this case, the results of Appendix B.1 apply, since the signal is propagating in a medium that is locally homogenous.

The second type of signal that can propagate within a single layer of a layered medium is a reflected signal. A reflected signal arrives at the interface of the layer at an angle  $\vartheta_i$  and is reflected at an angle  $\vartheta_r$ , where both angles are measured with respect to the interface. These angles are subject to the constraint

$$\vartheta_i = \vartheta_r.$$

That is, the angle of incidence is equal to the angle of reflection. Expressions for calculating the point of reflection on an interface and the traveltime associated with a reflected signal are shown in Appendix B.2.2.

The third type occurs when the signal meets the interface at a critical angle, and propagates along the interface and reflects at the same angle towards the receiver. This type of signal, known as a head wave, is caused by total internal reflection of the signal within the layer. For this type of source-receiver configuration, the traveltimes associated with the direct arrival and the reflected arrival correspond to local minima. Note that for each simulation, we start with an initial guess of a straight line; hence, we start each simulation already in a local minimum. If this configuration corresponds to the global minimum of traveltime, then we should end up with the same configuration; else, we should end up with a ray corresponding to a reflected signal. Exact expressions for rays and their corresponding traveltimes of signals undergoing total internal reflection are discussed in Appendix B.2.3.

5.2.1.2. *Results.* As we can see in Figures 5.1 and 5.2, the qualitative accuracy of rays constructed by this method was very high and increased with increased resolution. For example, consider the source-receiver configuration shown in Figure 5.2(c). The ray constructed at  $h = 100m$  bends below the interface while rays constructed at lattice spacings  $h = 25m$  and  $h = 50m$  show transmission of the signal directly through the interface. We say that this is a by-product of constructing

FIGURE 5.1. Rays constructed for a layered inhomogeneous velocity model; source located at  $(0m, 0m)$ , receivers located at a)  $(1000m, 100m)$ , b)  $(1000m, 600m)$ , and c)  $(1000m, 1000m)$ .

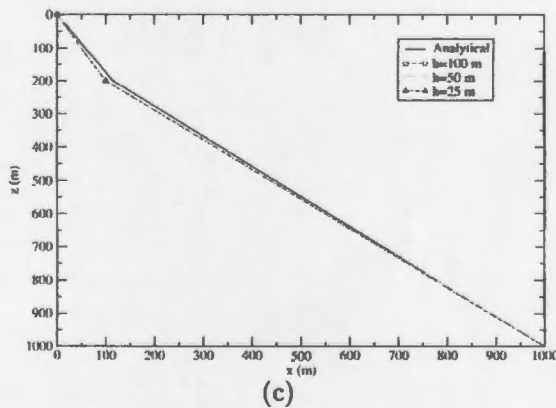
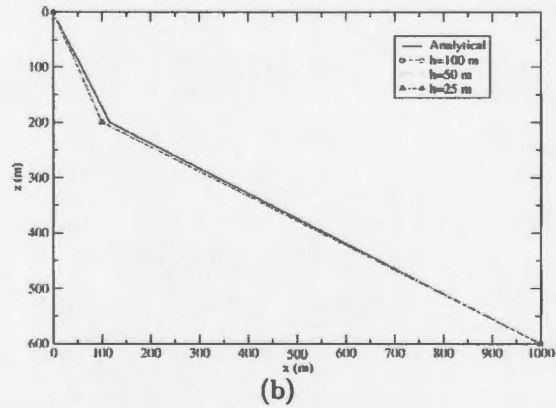
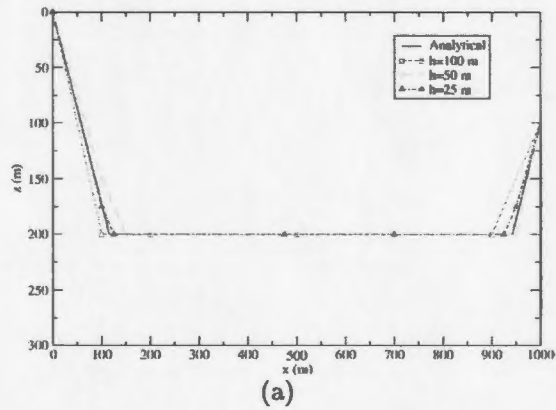


FIGURE 5.2. Rays constructed for a layered inhomogeneous velocity model; source located at  $(500m, 0m)$ , receivers located at a)  $(1000m, 100m)$ , b)  $(1000m, 600m)$ , and c)  $(1000m, 1000m)$ .

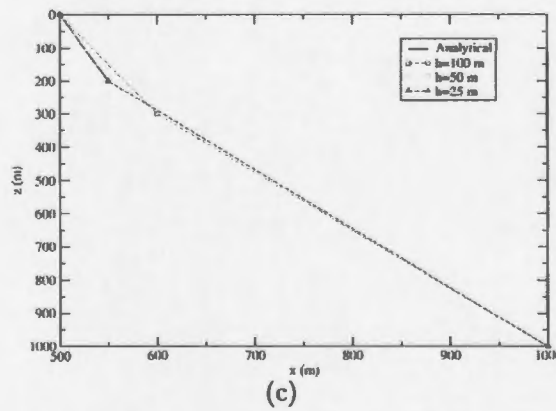
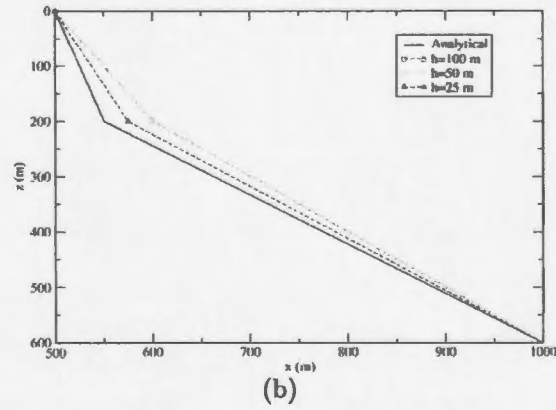
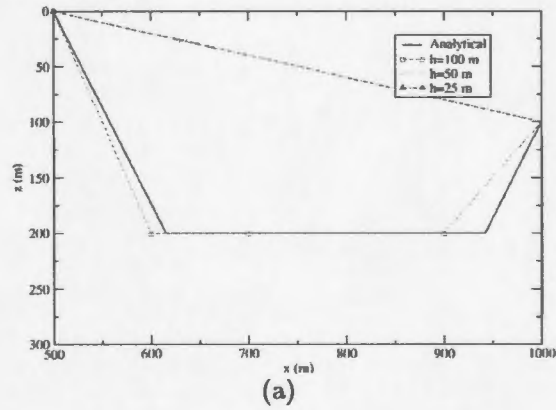


TABLE 1. Table of traveltimes collected for rays corresponding to transmission of signal through the interface: layered inhomogeneous medium.

Source	Receiver	Analytic	$h = 100m$	$h = 50m$	$h = 25m$
$(0m, 0m)$	$(1000m, 600m)$	$0.716037s$	$0.688099s$	$0.702074s$	$0.709062s$
$(0m, 0m)$	$(1000m, 1000m)$	$0.824992s$	$0.797736$	$0.811711s$	$0.818699s$
$(500m, 0m)$	$(1000m, 600m)$	$0.505397s$	$0.478499s$	$0.492474s$	$0.498701s$
$(500m, 0m)$	$(1000m, 1000m)$	$0.665094s$	$0.640284s$	$0.652210s$	$0.658652s$

rays at low resolution. Note that the rays shown in Figures 5.1 b) and c) were the same for all values of resolution considered.

As shown in Table 1, the traveltimes associated with rays corresponding to transmitted signals are in close qualitative agreement with expected results. However, in experimental situations, errors in traveltime are roughly two milliseconds. Hence, these traveltimes are not on the level of accuracy of an experimental situation.

Notice that as the resolution increased, so did the traveltime of the constructed rays. We can show that this is a result of increasing the number of nodes in the summation of traveltime along the segment. For instance, consider the segment extending from a source at  $(0m, 0m)$  to the interface at  $(100m, 200m)$  in the rays plotted in Figure 5.1(a). By the composite trapezoidal rule, the traveltime along this segment for  $h = 100m$  is

$$T(h = 100m) = 100\sqrt{5} \left( \frac{3}{2v_1} + \frac{1}{2v_2} \right) = 0.195656s.$$

For  $h = 50m$ , the traveltime along the same segment is

$$T(h = 50m) = 50\sqrt{5} \left( \frac{7}{2v_1} + \frac{1}{2v_2} \right) = 0.209631s,$$

TABLE 2. Table of traveltimes corresponding to signals propagating within the upper layer of the medium. Analytical results are presented for direct arrival and reflected arrival of signal at a receiver located at  $(1000m, 100m)$ .

Source	Direct	Reflected	$h = 100m$	$h = 50m$	$h = 25m$
$(0m, 0m)$	1.00499s	0.759808s	0.701722s	0.731139s	0.744728s
$(0m, 500m)$	0.509902s	0.509808s	0.451722s	0.509902s	0.509902s

and for  $h = 25m$ ,

$$T(h = 25m) = 25\sqrt{5} \left( \frac{15}{2v_1} + \frac{1}{2v_2} \right) = 0.216619s,$$

Thus, we see that by decreasing the spacing between nodes by a factor of two, traveltime increases by roughly two hundredths of a second just for this segment. In this case, it is reasonable to expect traveltime to increase with decreasing lattice spacing.

The results were not as straightforward for rays constructed within the upper layer,  $z \in [0m, 200m]$ . For the source-receiver configuration shown in Figure 5.1(a), the constructed rays indicated total internal reflection of the signal at the interface. However, for the source-receiver configuration shown in Figure 5.2(a), constructed rays corresponded to both direct arrival and reflected arrival of the signal, with the signal corresponding to total internal reflection occurring for  $h = 100m$ .

As shown in Table 2, the difference in predicted traveltimes between reflected and direct signals is large for the source-receiver configuration of Figure 5.1(a); hence, we would expect that our method would have no trouble in calculating the rays associated with reflected signals. However, for the configuration of Figure 5.2(a), the difference in expected

traveltimes between the direct signal and the reflected signal differ by roughly one ten-thousandth of a second. To explain why our method has such difficulty in constructing the ray corresponding to minimum traveltime in this case, we offer the following explanation.

First, given the numerical errors associated with numerical integration, it is not unreasonable to expect that this method would have trouble calculating the ray corresponding to the global minimum for such a small difference in values of traveltime of direct and reflected signals. Since the number of points over which we integrate increases with resolution, we would expect errors associated with addition to increase along with it.

Second, notice in Figure 5.1(a) that the ray shows signs of bending near the interface. Specifically, the segments of the ray within the upper layer of the medium indicate that the signal bends toward the interface – rather than hitting it directly – before traveling along the interface. Although the slowness function describing the physical model is discontinuous at the interface, the weighted slowness function is continuous – at least in the discrete sense. Within the sublayer  $(200m - h, 200m)$ , the traveltime along the ray is calculated according to weighted slowness function  $\bar{p}$  – expression (3.20):

$$\bar{p}(x) = \frac{|z(x) - z^+(x)|p(x, z^-(x)) + |z(x) - z^-(x)|p(x, z^+(x))}{h_z}.$$

For values of  $z(x)$  not passing through a node, the value of  $\bar{p}$  is the average of values of slowness between adjacent nodes. For segments parameterized by  $x$  within this range  $\bar{p}$  behaves like a smooth function

whose slowness ranges from  $1/1000 \text{ s m}^{-1}$  to  $1/2000 \text{ s m}^{-1}$ , implying that signals will travel within this sublayer travel at faster speeds than predicted in the continuous model. As a result, traveltimes of signals propagating through or within this sublayer will be lower than expected. Since the width of this sublayer decreases with increased resolution, the traveltimes of signals passing through it will increase.

By considering this example, we have identified three limitations of our approximation of signal slowness by a weighted function. First, the approximation of the slowness function as a weighted average causes the shapes of the rays corresponding to reflected signals to bend near the interface in the sublayer  $[200m - h, 200m]$ . Second, traveltimes associated with each ray passing through or near the interface tend to increase with increased resolution. By decreasing the width of this sublayer, we decrease the area on the lattice where slowness decreases continuously with position. Third, we see that for local minima whose values differ slightly from each other, the method had trouble constructing the ray corresponding to global traveltime.

### 5.2.2. Model 2: Linearly inhomogeneous medium.

5.2.2.1. *Background.* A linearly inhomogeneous medium can be described as a medium whose properties vary linearly along one axis. Let  $z$  be the axis along which the properties of the medium vary; along the  $x$ -axis, the properties remain constant with respect to  $z$ . Such a medium can be described in general by a function of the form

$$(5.2) \quad v(z) = a + b z.$$

Parameter  $a$  corresponds to the velocity of the signal at the free-surface,  $z = 0$ , and parameter  $b$  corresponds to the gradient of velocity. We will construct rays within a medium described velocity function (5.2) with parameters

$$(5.3) \quad \begin{aligned} a &= 2000 \frac{m}{s} \\ b &= 15 s^{-1} \end{aligned} .$$

Parameters (5.3) describe a medium in which a signal's velocity increases sharply with depth. At  $z = 1000m$ , signal velocity is 75% faster than at the free surface.

A linearly inhomogeneous medium can also be viewed as a layered inhomogeneous medium having an infinite number of layers of width  $\delta z \ll 1$ , where the velocity of signals within each layer increases with depth. In the limit of an infinite number of layers having infinitesimal width, the velocity function for such a medium reduces to expression (5.2). In a discrete medium, these layers have a finite width  $h$  that is not necessarily on the scale of  $\delta z$ .

Let  $(x, z)$  be coordinates in a discrete medium. For  $N$  layers of width  $h$ , we write the discrete velocity function describing the medium in a form similar to expression (5.2):

$$v(x, z) = a + b h z, \quad z \in \mathcal{Z}.$$

Hence, the problem of solving for rays in linearly inhomogeneous media in the discrete case is tantamount to solving the problem of a multiply-layered medium – a generalization of the layered-inhomogeneous medium example presented earlier in this work.

In [15], the authors derived the following inequality:

$$(5.4) \quad X > \sqrt{2Z \left( \frac{a}{b} + \frac{Z}{2} \right)},$$

where  $X$  denotes the horizontal offset between source and receiver and  $Z$  denotes the vertical offset. This inequality describes the tendency for a signal to reach a receiver from either above or below. If inequality (5.4) is satisfied, then “the signal reaches the receiver on the way up i.e. after it has reached the deepest point on its trajectory” [15, p.2]. Otherwise, the signal reaches the receiver on its way down. With parameters (5.3), and given the scaled dimensions of our lattice, we should be able to construct rays that bend either upwards or downwards, depending on the offset of the receiver to the source.

5.2.2.2. *Results.* Rays constructed via the simulated annealing algorithm for each source-receiver configuration are presented in Figures 5.3 and 5.4, along with the expected shapes of rays for each configuration. For  $h = 100m$ , we see that our method had trouble calculating rays whose shape were consistent with predicted results. However, the constructed rays were observed to converge towards the shape of the predicted ray with increased resolution.

The discrete model of this medium resembles a multiply-layered medium with increasing velocity. However, in spite of the results for

FIGURE 5.3. Rays constructed for a linearly inhomogeneous velocity model; source located at  $(0m, 0m)$ , receivers located at a)  $(1000m, 100m)$ , b)  $(1000m, 600m)$ , and c)  $(1000m, 1000m)$ .

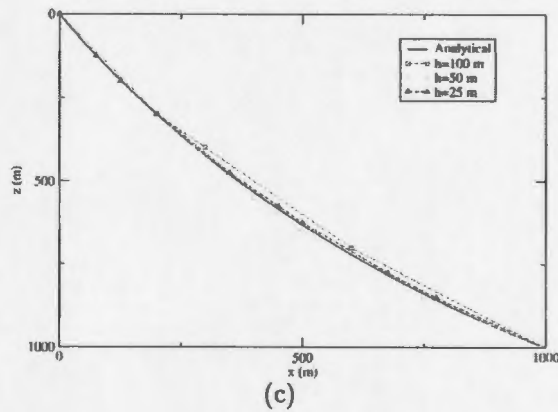
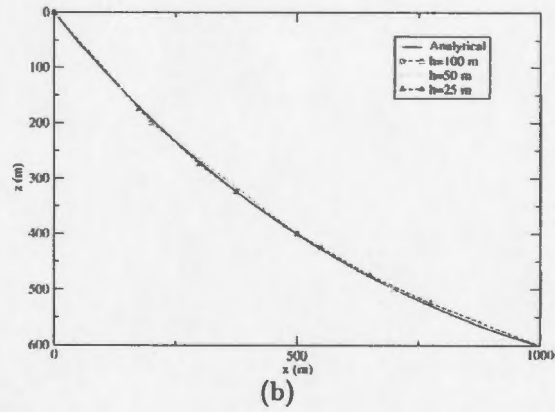
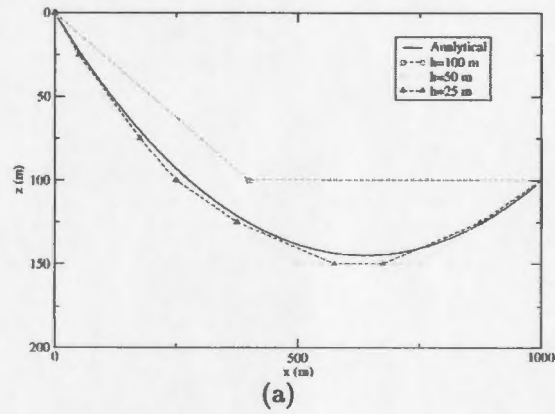


FIGURE 5.4. Rays constructed for a layered inhomogeneous velocity model; source located at  $(500m, 0m)$ , receivers located at a)  $(1000m, 100m)$ , b)  $(1000m, 600m)$ , and c)  $(1000m, 1000m)$ .

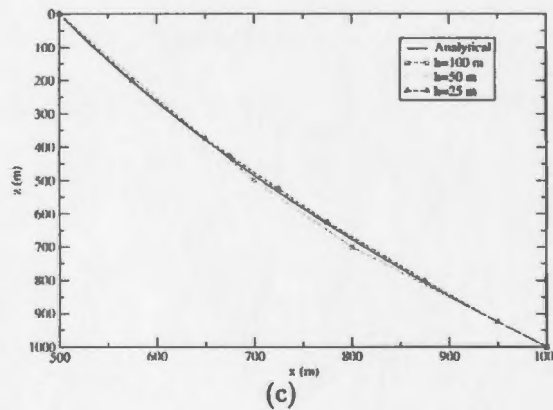
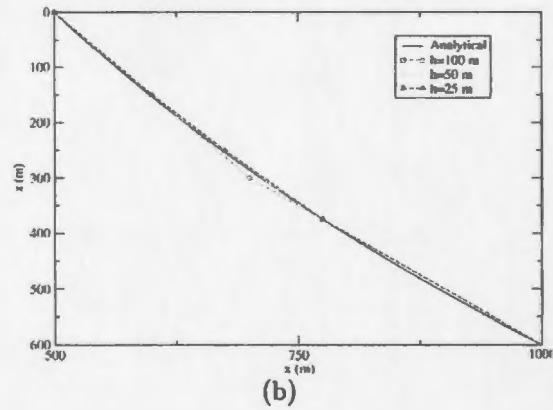
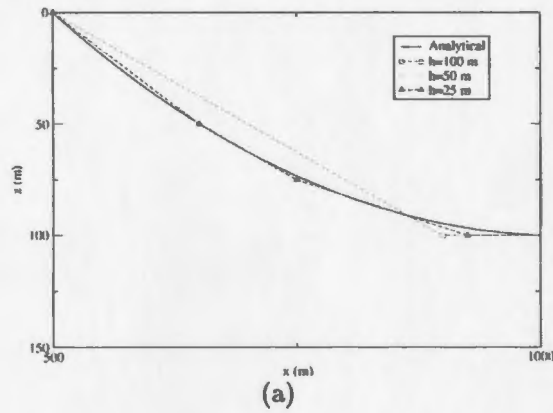


TABLE 3. Traveltimes collected from forward modelling of rays in a linearly inhomogeneous medium with velocity function (5.2) for lattice spacings  $h = 25m, 50m, \text{ and } 100m$ .

Source	Receiver	Exact	$h = 25m$	$h = 50m$	$h = 100m$
(0,0)	(1000,100)	0.474565s	0.474919s	0.475288s	0.478034s
(0,0)	(1000,600)	0.474176s	0.474424s	0.474631s	0.475025s
(0,0)	(1000,1000)	0.521151s	0.521322s	0.521676s	0.522352s
(500,0)	(1000,100)	0.244542s	0.244685s	0.244865s	0.245475s
(500,0)	(1000,600)	0.321188s	0.321324s	0.321426s	0.321791s
(500,0)	(1000,1000)	0.415805s	0.415877s	0.415986s	0.416330s

layered media, we see in Figures 5.3 and 5.4 that the constructed rays did not bend at every interface. We explain this by noting that the slowness function increased smoothly with depth. Although the gradient was comparatively large in this particular model, it is small in comparison with the layered-inhomogeneous model previously considered. Furthermore, by not bending at every interface that the segment passes through, we obtain a better fit to the predicted ray.

For a source at  $(0m, 0m)$  and a receiver at  $(1000m, 100m)$ , inequality (5.4) predicts that the shape of the ray will bend upwards towards the receiver. In Figure 5.3(a), we see that the accuracy of the constructed rays with respect to the predicted ray increased as resolution increased. For example, the ray constructed with lattice spacing  $h = 100m$  indicated the signal was reflected along an interface at  $z = 100m$ . The shape of the ray as compared to the predicted solution fitted better as resolution increased.

As shown in Table 3, traveltimes calculated along the rays decreased with increased resolution. This is in contrast to the results of the layered model, where traveltime increased with increasing resolution. The accuracy of the traveltimes collected from this simulation was much better than that of the traveltimes collected from the layered model simulation. For example, at  $h = 25m$  predicted traveltimes and collected traveltimes differ in value by roughly ten-thousandths of seconds – well within the bounds of what one would measure in an experimental situation.

In view of the high accuracy of the results collected from this model, the reader may wonder why the results in the layered-inhomogeneous medium example never fared as well. Recall that the approximation to the slowness function of the layered model exhibited properties of linearly-decreasing slowness within a finite sublayer located between the layers – a characteristic not shared with the physical model. Since the slowness function of the linearly inhomogeneous model is much smoother than the linearly inhomogeneous model, the weighted slowness function is very good in approximating slowness in the case of the linearly-inhomogeneous medium. As such, the accuracy of the results in this model was higher as compared to the results of the layered model due to the accuracy of the approximation to the slowness function.

**5.2.3. Summary.** The simulated annealing method was able to accurately construct rays and associated traveltimes for both models. Qualitatively, the shapes of the rays and their associated traveltimes were in close agreement with expected values. Quantitatively, the

method was observed to perform better for the linearly-inhomogeneous medium. In the case of the layered medium, the results were skewed from predicted values due to the behaviour of  $\bar{p}$  around the interface. The accuracy of our method seems to depend more on the accuracy of  $\bar{p}$  rather than the algorithm itself. While this is good news for our method, we may have to look into better approximations of slowness in later work. Despite the behaviour of  $\bar{p}$ , we believe that results produced by this method can be viewed with a high degree of confidence.

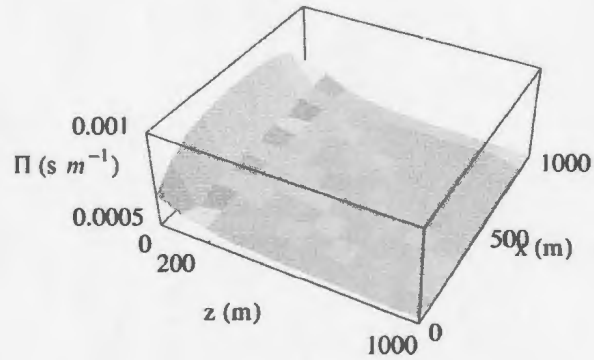
### 5.3. Inverse modelling: Backprojection method

In this section, we use the simulated annealing method to calculate rays and associated traveltimes for all source-receiver configurations around the perimeter of a square lattice. We use these data to test the applicability and accuracy of the backprojection method presented in Chapter 4 to inverse modelling problems in seismology.

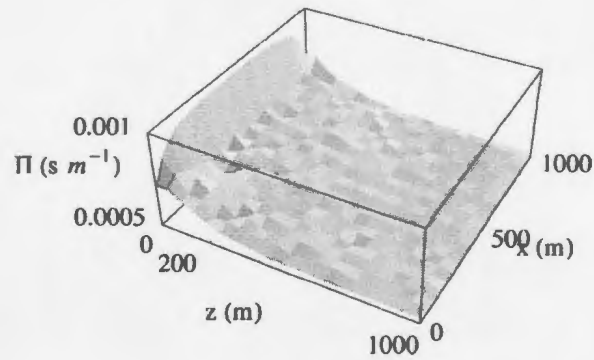
#### 5.3.1. Results.

5.3.1.1. *Model 1: Layered inhomogeneous medium.* Figure 5.5 shows the results of applying the backprojection method to data collected from the layered-inhomogeneous model as compared to the original slowness function, shown in Figure 5.9. In these graphs, we notice three things. First, the backprojection method was very accurate in resolving the lower layer of the model,  $200m \leq z \leq 1000m$ , where signal velocity is highest. However, we see from the plots of relative error  $|\Pi(\mathbf{x}) - p(\mathbf{x})|/p(\mathbf{x})$  shown in Figure 5.7 that the discrepancy between analytical and obtained results in around the interface reaches

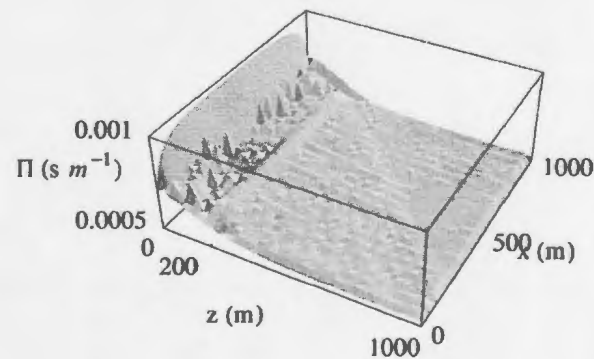
FIGURE 5.5. Results of backprojection method applied to layered inhomogeneous medium; lattice spacings a)  $h = 100m$ , b)  $h = 50m$ , and c)  $h = 25m$ .



(a)  $h=100m$

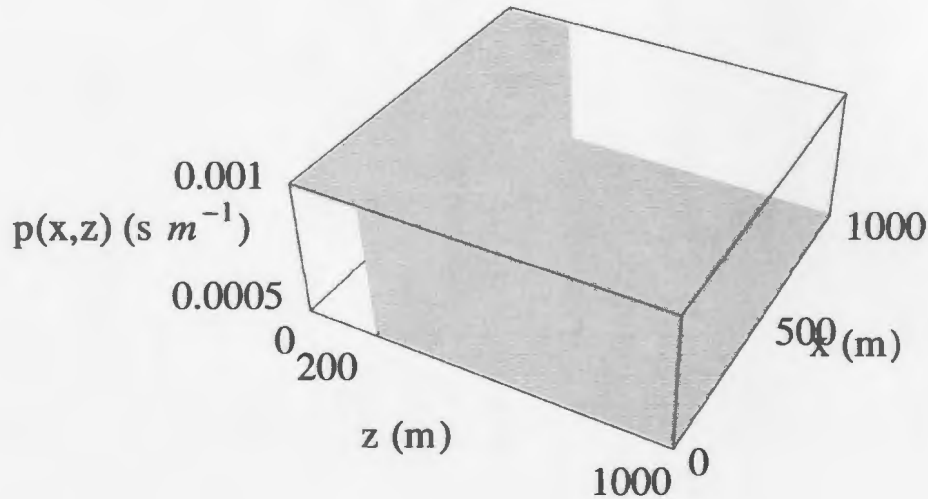


(b)  $h=50m$



(c)  $h=25m$

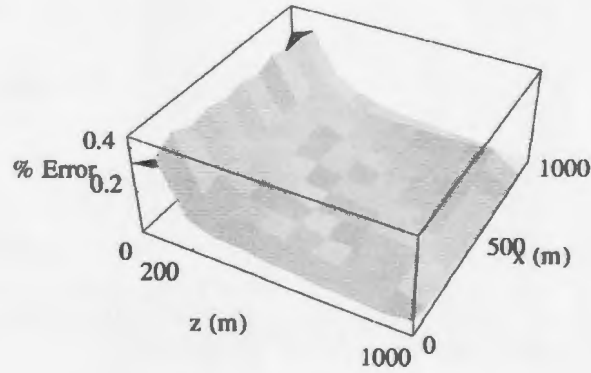
FIGURE 5.6. Plot of slowness function  $p(x, z)$  for a layered inhomogeneous medium.



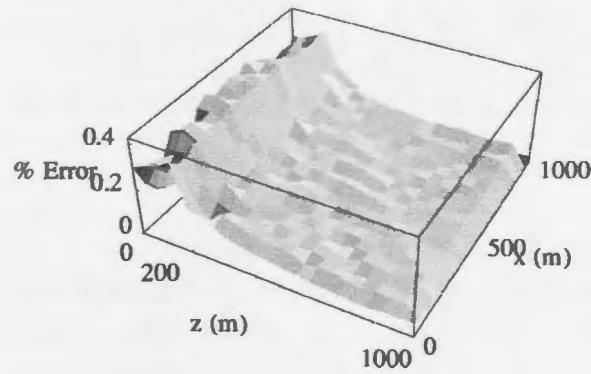
close to 40%. Even as resolution increased, the ability of the back-projection method to resolve this area was very poor. Furthermore, values of  $\Pi$  were much lower than the values of  $p$  in the upper layer  $0m \leq z < 200m$ .

The backprojected data is a weighted average of slowness for all rays passing through each point on the lattice. For rays passing through both layers, the values of slowness stored will generally be small. Hence, points within the upper layer will average over values of slowness that are much smaller than predicted by the original model. Furthermore, rays passing from the upper layer to the lower layer tend to optimize their length by spending the majority of time within the layer

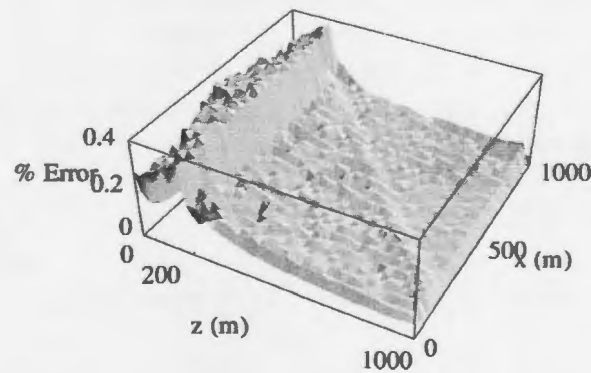
FIGURE 5.7. Absolute error of results of backprojection method applied to layered inhomogeneous medium; lattice spacings a)  $h = 100m$ , b)  $h = 50m$ , and c)  $h = 25m$ .



(a)  $h=100m$



(b)  $h=50m$



(c)  $h=25m$

of higher velocity to minimize traveltime – as predicted by Fermat’s principle. Hence, points within the upper layer will have fewer rays passing through as compared to points within the lower layer. Also, the simulated annealing method calculates rays according to the minimization of first-arrival traveltime. If the majority of rays constructed correspond to reflected arrivals as opposed to direct arrivals, we would expect that the ability to resolve the upper layer would decrease, since the rays will optimize their traveltime by travelling along the interface.

The values of  $\Pi(\mathbf{x})$  along the top and bottom edges of the lattice seem to converge towards expected values as one moves toward the middle of the edge. This is a result of allowing signals to pass along the edge of the lattice. By allowing signal propagation along the edge of the lattice – oftentimes, through other receivers – more rays pass through points towards the middle of the edge as compared to the outer parts. Hence, more data is collected at these points, allowing these points to be resolved much better. For example, consider the edge along  $z = 0$ . In view of Figure 5.7, we see the error in  $\Pi$  decreases along this edge as we move towards the centre. Along the edge  $z = 1000m$ , we obtain the best qualitative results using the backprojection method. However, we do not observe this behaviour along the sides of the lattice. One reason for this is that velocity remains constant along lines parallel to the interface. For lines perpendicular to this interface – such as the sides of the lattice at  $x = 0m$  and  $x = 1000m$  – velocity is not constant. Hence, the averages along these sides will decrease with depth. Also, values of  $\Pi$  corresponding to the corners of the lattice deviate with

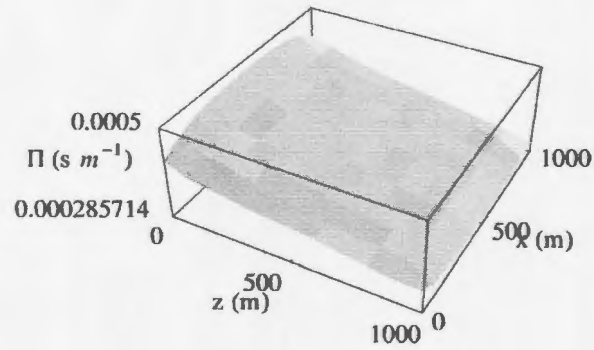
respect to neighbouring data points. This is because the only rays passing through the corners are those arriving at receiver located here. Hence, the amount of data used to calculate  $\Pi$  at these points is lower than points within the edge of the lattice.

The most important result we see in each graph of  $\Pi(\mathbf{x})$  in Figure 5.9 is that the properties of an interface along  $z = 200m$  are seen. This is a very encouraging result: although the numerical results of the backprojection method were not as accurate as we would hope, we can still resolve the location of an interface in a medium described by  $\Pi$ .

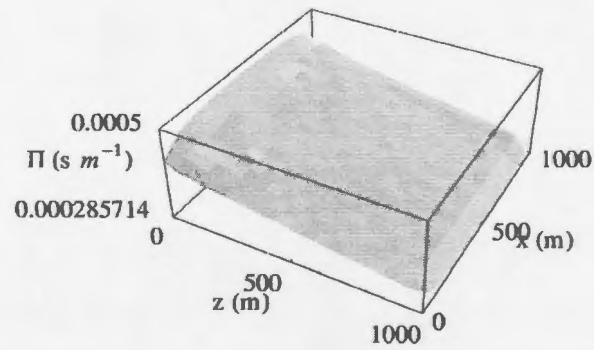
Our goal in applying this method was to test the accuracy of the backprojection method as a means of recovering qualitative aspects of the medium being considered. In this case, the ability to resolve the location of the interface means that the backprojection method is able to retain important qualitative aspects of the original slowness function.

5.3.1.2. *Model 2: Linearly inhomogeneous medium.* In Figure 5.8 we present backprojections generated from data collected by the simulated annealing method for lattice spacings  $h = 25m, 50m,$  and  $100m$ . Compared to the original slowness function in Figure 5.9, we see that as we increased resolution, the accuracy of  $\Pi(\mathbf{x})$  also increased. The shape of  $\Pi(\mathbf{x})$  is in qualitative agreement with the original slowness function  $p(\mathbf{x})$  of the linearly inhomogeneous medium: as depth increases, signal slowness decreases. Furthermore, recall that the original slowness function decreases with depth like  $1/z$ . As shown in Figure 5.10, the reciprocal of  $\Pi(\mathbf{x})$  behaves like a function whose values are observed to also decrease linearly with depth.

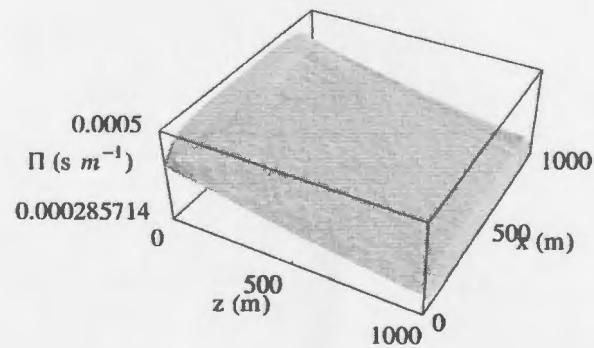
FIGURE 5.8. Results of backprojection method applied to linearly inhomogeneous medium; lattice spacings a)  $h = 100m$ , b)  $h = 50m$ , and c)  $h = 25m$ .



(a)  $h=100m$

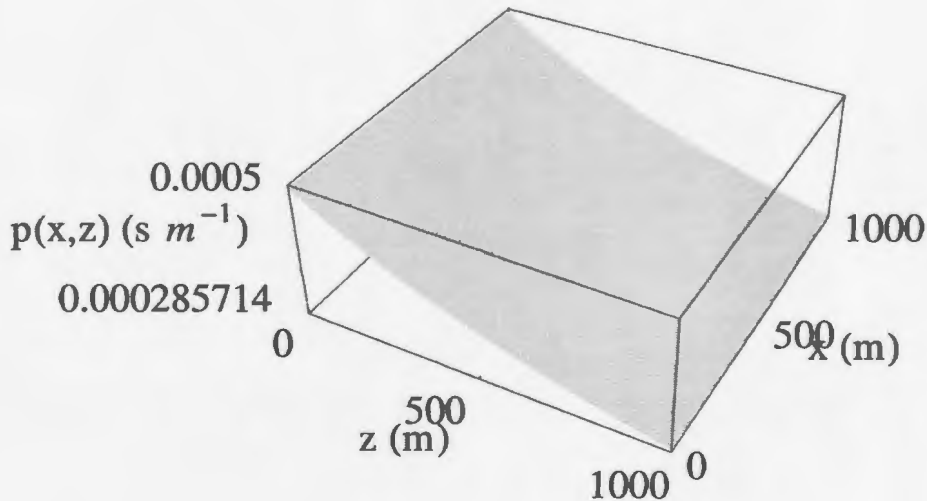


(b)  $h=50m$



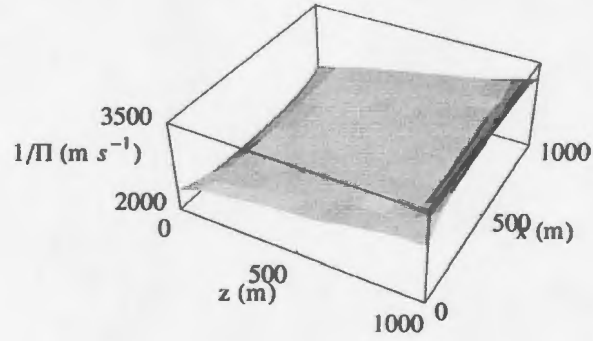
(c)  $h=25m$

FIGURE 5.9. Plot of slowness function  $p(x, z) = 1/(2000 + 1.5z)$  for a linearly inhomogeneous medium.

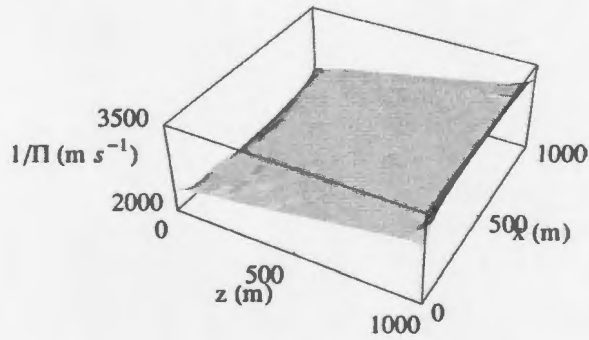


In Figure 5.11, we plot the relative error  $|\Pi(\mathbf{x}) - p(\mathbf{x})|/p(\mathbf{x})$  for each value of  $h$ . As expected, the maximum absolute error for each value of  $h$  decreased with  $h$ . For  $h = 25m$ , the maximum relative error was roughly 14%, located at the corner  $(0m, 0m)$ . As seen in the layered medium model, the relative error of slowness  $\Pi(\mathbf{x})$  along the top and bottom edges of the lattice is low in comparison with the rest of the data and tends to decrease as one moves towards the centre of the edge. For the edge along  $z = 1000m$ , absolute error is very close to zero, while the absolute errors of the data along  $z = 0m$  are much larger. We explain this by noting that rays in linearly-inhomogeneous media bend toward the gradient of velocity. Rays constructed for source-receiver

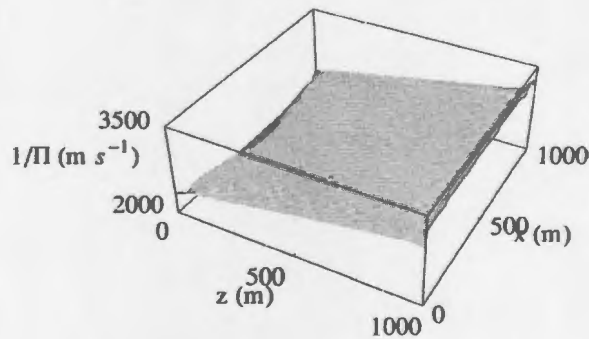
FIGURE 5.10. Reciprocal of backprojection functions; lattice spacings a)  $h = 100m$ , b)  $h = 50m$ , and c)  $h = 25m$ .



(a)  $h=100m$

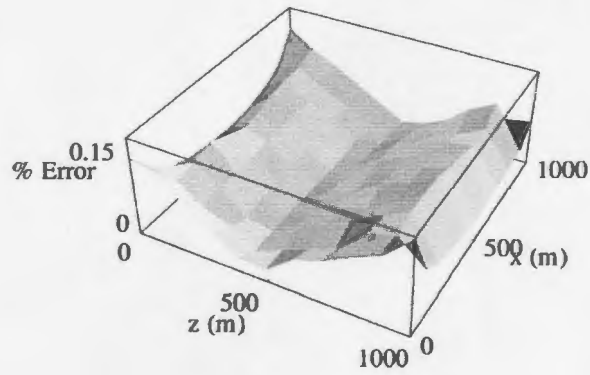


(b)  $h=50m$

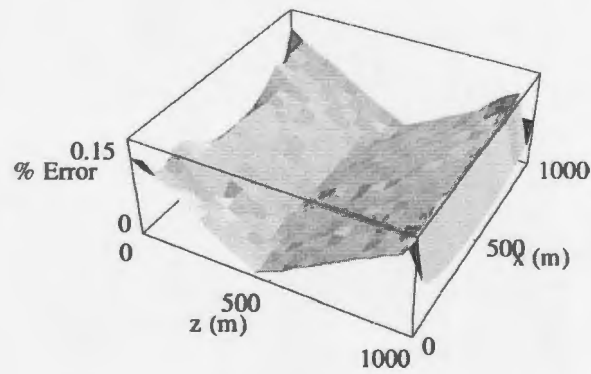


(c)  $h=25m$

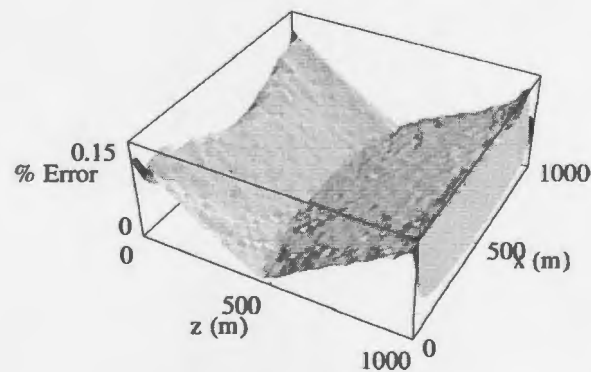
FIGURE 5.11. Absolute error of backprojection functions in comparison with exact function  $p(x, z)$ ; lattice spacings a)  $h = 100m$ , b)  $h = 50m$ , and c)  $h = 25m$ .



(a)  $h=100m$



(b)  $h=50m$



(c)  $h=25m$

configurations along the edge at  $z = 1000m$  cannot bend toward this gradient, since this would require signals to pass outside the lattice. Hence, rays along this edge are straight lines. Rays constructed for source-receiver configurations along the edge at  $z = 0m$  do not have this problem, and so rays constructed in this case can bend away from the edge. As a result, this edge will be less resolved in comparison to the upper edge.

Excluding the top and bottom edges, we see for each value of  $h$  that the error of the reconstructed function increases as we move away from the middle of the medium. The region of medium where absolute error tends to zero corresponds to the intersection of  $\Pi$  with  $p$ . We see that the maximum absolute error in this region is roughly 14%. Given that reconstructed functions  $\Pi(\mathbf{x})$  for each  $h$  each show behaviour that is in qualitative agreement with the original slowness function – that is, function  $\Pi(\mathbf{x})$  describes a linearly-inhomogeneous medium – we say that the backprojection method was able to construct a slowness function whose properties are in qualitative agreement with the original function. As such, we can regard  $\Pi$  as a reasonable approximation to the inverse of Radon's transform in this particular case.

**5.3.2. Summary.** The backprojection method was able to recover qualitative properties of the medium studied in each case. In the layered medium case, we were able to use the backprojection method to construct a slowness function whose properties were observed to change sharply along what could be viewed as an interface. However, the method was unable to accurately resolve the numerical values of

slowness within the layer  $[0m, 200m]$ . We noted that given the nature of the signals travelling within such a medium in relation to the simulated annealing method used to calculate the rays, we would expect difficulty in resolving this area of the medium.

The results were much better in the case of the linearly inhomogeneous medium. Quantitatively, the results still left much to be desired, as the accuracy of  $\Pi$  as compared to  $p$  decreased as one moved further from the centre of the medium. However, the structure of the backprojected function indicated that the data was collected from a medium whose velocity seemed to decrease with depth. Thus, the backprojection method was able to at least qualitatively predict the medium being studied.

#### 5.4. Conclusions and Future Considerations

In this section, we will interpret the results obtained from the forward and inverse modelling methods, and discuss their applicability to problems in seismology. We will then propose ideas for future applications and improvements for each of the methods that have been developed in this work.

**5.4.1. Results: Interpretation.** With the simulated annealing method, we were able to construct rays whose shapes were in quantitative agreement with expected results. In the layered-inhomogeneous model, we were able to calculate rays that corresponded to transmission, reflection, and direct arrival of signals. Rays calculated in the context of linearly inhomogeneous media showed properties of bending

in the direction of the velocity gradient as predicted from analytical solutions.

Traveltimes along constructed rays were shown to be in close agreement with expected values as calculated from analytical solutions. We observed that the minimum traveltime calculated for the layered model tended to increase with increasing resolution, while minimum traveltime decreased with increasing resolution for the linear model. In view of this, we say that rays and associated traveltimes constructed from the simulated annealing method can be considered as very accurate estimations for experimental situations. Our raytracing method is accurate, and results from it can be viewed with a high degree of confidence.

For calculating rays in two-dimensional smooth media, there is no major advantage in choosing the simulated annealing method over the shooting method. However, the shooting method would have had trouble in constructing rays for media such as the layered-inhomogeneous medium considered in this thesis. For example, consider the rays constructed between a source at  $(0m, 0m)$  and receivers at  $(1000m, 600m)$  and  $(1000m, 1000m)$ . For each resolution, the simulated annealing method predicted that the signal transmitted through the interface at an angle of incidence of  $60^\circ$  at  $(100m, 200m)$ . At this angle, the shooting method would only be able to construct one ray, since the solution of the shooting method is unique for each set of initial conditions. The simulated annealing method has the advantage of ensuring

that the constructed ray connects the source to the receiver, and does so by minimizing traveltime along the path.

We predict that the true advantage of the simulated annealing approach to raytracing will occur in the forward modelling of rays in three-dimensional media. The shooting method for three-dimensional media would require the variation of two takeoff angles to construct the ray. For complicated three-dimensional media, one would expect great difficulty in using the shooting method. However, the simulated annealing method requires only the locations of the source and the receiver, regardless of the dimensions of the medium. The construction of a three-dimensional simulated annealing method would be very useful in the context of raytracing in three-dimensional media.

We considered the backprojection method as an application of the simulated annealing method. We found that the application of the backprojection function on data generated by the simulated annealing method managed to resolve the qualitative characteristics of each medium considered. In the case of the layered medium, close inspection of the backprojected data shows evidence of an interface around  $z = 200m$ . In the case of the linearly-inhomogeneous medium we were able to reconstruct a backprojected function whose values decreased along the  $z$ -axis and whose reciprocal values increased linearly with depth. The numerical results were much better in the case of linearly-inhomogeneous media as compared to the results of the layered medium. In the example of the layered medium, values of  $\Pi$  differed from the original function by errors as large as 40 %, while the

maximum absolute error in the linearly inhomogeneous medium was roughly 14%. With these results, we have shown that this method provides a basis for the development of an inversion algorithm based on the generalization of Radon's transform.

#### 5.4.2. Future considerations.

5.4.2.1. *Simulated annealing method.* There are many directions that one can take to develop this algorithm further. First, the implementation of an adaptive cooling schedule in the algorithm must be addressed if one wishes to construct rays within large complicated media at high resolution. Since this type of simulation will require very lengthy times, one would want to implement a schedule such as the constant thermodynamic cooling method [12] to increase the rate of convergence of the annealed paths to the desired ray.

Second, the simulated annealing scheme lends itself to various computational optimization techniques – most of which were not considered in the construction of the current algorithm. For instance, one would expect that this method would be well-suited for construction of a parallelized version to be run on high-performance computers. A proposed parallelization scheme could be as follows. Starting with an initial lattice spacing  $h$ , one constructs a ray of  $M$  segments between the source and receiver. From this initial construction, each processor takes a segment, decreases spacing  $h$ , and varies this segment within the bounds of the Fresnel zone along this segment.<sup>3</sup> This process is continued until the program reaches a prescribed final lattice spacing.

---

<sup>3</sup>This suggestion was first mentioned by Červený [2]

maximum absolute error in the linearly inhomogeneous medium was roughly 14%. With these results, we have shown that this method provides a basis for the development of an inversion algorithm based on the generalization of Radon's transform.

#### 5.4.2. Future considerations.

5.4.2.1. *Simulated annealing method.* There are many directions that one can take to develop this algorithm further. First, the implementation of an adaptive cooling schedule in the algorithm must be addressed if one wishes to construct rays within large complicated media at high resolution. Since this type of simulation will require very lengthy times, one would want to implement a schedule such as the constant thermodynamic cooling method [12] to increase the rate of convergence of the annealed paths to the desired ray.

Second, the simulated annealing scheme lends itself to various computational optimization techniques – most of which were not considered in the construction of the current algorithm. For instance, one would expect that this method would be well-suited for construction of a parallelized version to be run on high-performance computers. A proposed parallelization scheme could be as follows. Starting with an initial lattice spacing  $h$ , one constructs a ray of  $M$  segments between the source and receiver. From this initial construction, each processor takes a segment, decreases spacing  $h$ , and varies this segment within the bounds of the Fresnel zone along this segment.<sup>3</sup> This process is continued until the program reaches a prescribed final lattice spacing.

---

<sup>3</sup>This suggestion was first mentioned by Červený [2]

Third, the development of a code that calculates rays within three-dimensional media would prove to be very beneficial. A three-dimensional version would be able to construct rays between sources and receivers in complicated media where other methods, such as the shooting method, would fail. However, note that increasing the resolution in a three-dimensional model by a factor of two would increase the number of nodes within the medium by a factor of eight. Given that the number of iterations at each temporal energy is dependent on the number of nodes, we see that simulation time increases by a factor of 64. The formulation of the three-dimensional simulated annealing method would inevitably require heavy optimization of the algorithm in order to allow us to construct rays in a sensible amount of time.

From the standpoint of the algorithm itself, the accuracy of our results seemed to be bounded by the accuracy in the approximation of slowness by weighted slowness function  $\bar{p}$ . We showed that this function seemed to introduce errors into the results obtained in the layered inhomogeneous medium – a simple case of a complicated medium. However, for smooth media such as the linearly inhomogeneous medium,  $\bar{p}$  was seen to be an effective approximation to the original slowness function. Further consideration will need to be given to this particular approximation in order to judge its effectiveness in the calculations of rays and traveltimes.

From a theoretical standpoint, the development of a statistical mechanical formulation of seismic ray theory seems to be the next logical

step. As per our method, one can treat rays at the groundstate configuration of the path that connects the source to a receiver. By treating traveltime as energy, one can derive expressions for the partition function describing all possible paths on the lattice. Furthermore, one can study the properties of rays at a finite temporal energy, and try to extract physical insights into the behaviour of rays in a specified medium. These are just a few of the many possibilities that can be considered with such a formulation.

5.4.2.2. *Backprojection method.* While unable to produce a function that quantitatively resembled the original slowness function, the backprojection method produced results that gave a qualitative description of the properties of the original slowness function. However, there is much work to be done on this method before it can be considered as a viable reconstruction method in seismology.

The construction of an inversion scheme based on the backprojection method for generalized curves must be addressed. Many inversion and reconstruction schemes for straight line integration paths, such as the ones introduced in [13, Ch. 5] and [18, Ch. 5], are facilitated by the concept of a backprojection operator acting on data treated as the application of Radon's transform on function  $f$  that is to be recovered. While we could have applied these methods, we would be doing so with full knowledge that we would be incorrectly treating the shapes of the rays, and in effect, violating Fermat's principle – the very principle that provides the basis for the work presented in this paper.

In the calculation of the backprojection function, we divide by the lengths of the rays that pass through each point. That we can do this exactly is facilitated by the fact that we know the paths – these are calculated by the simulated annealing method using a known slowness function. In general, we will not know the shapes of these paths. One scheme that has been proposed deals with this dilemma as follows: given traveltimes between all sources and receivers, one begins by assuming that all paths are straight lines. Using the backprojection method, we obtain an approximate shape to the slowness function. From this first approximation, we apply the simulated annealing method to calculate rays according to this function. Using these rays and the initial traveltimes, we then obtain a second approximation. We iteratively apply the backprojection method to recover approximations to the slowness function, and construct rays from each approximation. For a sufficient number of iterations, we hope to recover a backprojected function that corresponds to the solution we would obtain if we had started with knowledge of the rays. The success of this scheme could be further improved by applying filtering techniques for results obtained in the case of general curves.

Upon the construction of a viable inversion scheme for the generalized Radon transform, one can then look at the effects of incomplete data sets in our studies. The results obtained from this work would be of great interest in the context of industry: if one can show that an inversion scheme based in the context of the generalized Radon transform can yield qualitative results in close agreement with experimental

data, one would then have another mathematical tool at their disposal that can be used in seismic inverse problems.

### 5.5. Final remark

In this thesis, we have laid the groundwork for the development of new tools for forward and inverse modelling in the context of exploration seismology. The methods presented in this work yielded qualitatively good results in comparison with analytical results. Although the results were produced from an idealized model of inhomogeneity within the media, extensions to other models, such as those that include anisotropy and anelasticity, are still possible.

The development of methods presented in this work have applications that reach far beyond the context of seismology. For instance, the simulated annealing method for raytracing is essentially an iterative process of solving the variational problem of Fermat's principle. Hence, we can apply this algorithm not only to the solution of rays, but also to solutions of integrals to be extremized. In essence, we have developed a computational method for solving boundary-value problems. The development of techniques that refine the results obtained from the backprojection method to give better agreement with expected values would have applications in numerous areas where the refinement of images produced from experimental data are of great importance – such as optics, X-ray computed tomography, and ultrasound CT imaging.

The results presented in this work show that the methods of raytracing via simulated annealing and the backprojection of traveltimes

via the generalized adjoint to Radon's transform represent the groundwork for the development of new tools that will be very beneficial in the context of forward and inverse modelling, respectively, in theoretical seismology.

## Bibliography

- [1] Chaikin, P.M., and T.C. Lubensky (1995) *Principles of Condensed Matter Physics*: Cambridge University Press.
- [2] Červený, V.A., (2001). *Seismic Ray Theory*: Cambridge University Press.
- [3] Slawinski, M. A., (2003). *Seismic Waves and Rays in Elastic Continua*: Pergamon.
- [4] Nievergelt, Y., (1986). *Elementary Inversion of Radon's Transform*: SIAM Review, Vol. 28, No. 1, pp. 79-84.
- [5] Schutz, B., (1980). *Geometrical Methods of Mathematical Physics*: Cambridge University Press.
- [6] Goldstein, H., (1950/1980/2000) *Classical Mechanics*: Addison-Wesley Publishing Co.
- [7] van Laarhoven, P.J.M., and E.H. Aarts, (1987) *Simulated Annealing: Theory and Applications*: D. Reidel Publishing Company.
- [8] Kirkpatrick, S., C.D. Gelatt Jr. and M.P. Vecchi, (1982). *Optimization by Simulated Annealing*: IBM Research Report RC 9355.
- [9] Černý, V., (1985) *Thermodynamical Approach to the Traveling Salesman Problem: An Efficient Simulation Algorithm*: J. Opt. Theory Appl., **45**, pp.41-51.
- [10] Metropolis, N.A., A. Rosenbluth, M. Rosenbluth, A. Teller, and E. Teller, (1953) *Equation of State Calculations by Fast Computing Machines*: J. of Chem. Physics, **21**, pp. 1087-1092.
- [11] Newman, M. and G.T. Barkema, (1999/2002) *Monte Carlo Methods in Statistical Physics*: Oxford University Press.

- [12] Nourani, Y. and Bjarne Andersen (1998) A Comparison of Simulated Annealing Strategies: *J. Phys. A: Math. Gen.*, **31**, pp. 8373-8385.
- [13] Deans, S.R., (1983) *The Radon Transform and Some of its Applications*: John Wiley and Sons Inc.
- [14] Slawinski, R.A., and M.A. Slawinski, (1999) On Raytracing In Constant Velocity-Gradient Media: Calculus Approach: *C. J. Exp. Geophys.*, **35**, pp.24-27.
- [15] Epstein, M., and M.A. Slawinski (1999) On Raytracing In Constant Velocity-Gradient Media: Geometrical Approach: *C. J. Exp. Geophys.*, **35**, pp.1-6.
- [16] Slotnick, M.M., (1959) *Lessons in Seismic Computing*: The Society of Exploration Geophysicists.
- [17] Wheaton, C.J. (2004) *Tomographic Traveltime Inversion for Linear Inhomogeneity and Elliptical Anisotropy*: M.Sc. Dissertation: Memorial University of Newfoundland.
- [18] Natterer, F. (2001) *The Mathematics of Computerized Tomography: Classics in Applied Mathematics*: SIAM.
- [19] Bona, A. (2005) *Generalized Radon Transform and its Inverse*: Lecture notes.
- [20] Bleistein, N., J.K. Cohen, and J. Stockwell (2000) *Mathematics of Multidimensional Seismic Imaging, Migration, and Inversion: Interdisciplinary Applied Mathematics, V. 13*: Springer.
- [21] Mandl, F (2001) *Statistical Physics*.
- [22] Truesdell, C. (1966) *Six Lectures on Modern Natural Philosophy*: Springer-Verlag
- [23] Velis, D. R., and T. J. Ulrych (1996) Simulated annealing two-point ray tracing: *Geophysical Research Letters*, **23**, pp. 201-204.
- [24] Velis, D. R., and T. J. Ulrych (2001) Simulated annealing ray tracing in complex three-dimensional media: *Geophys. J. Int.*, **145**, pp. 447-459.

## APPENDIX A

### Adjoint Operators

In this appendix, we prove that operator  $R^*$  is adjoint to generalized Radon transform operator  $R$ . To prove adjointness of an operator, we will define scalar products of functions on the spaces of the medium and the rays; respectively, spaces  $\mathcal{M}$  and  $\mathcal{L}$ . For a rigorous treatment of the definition of these spaces, the reader is referred to [19].

#### A.1. Radon's transform: Operator and adjoint

We define the action of generalized Radon transform operator  $R$  on function  $f \in C_0^\infty(\mathcal{M})$  at point  $\gamma \in \mathcal{L}$  by

$$R(f)(\gamma) = \int_{\gamma} f(\exp_{X(p,\xi)}(t\xi)) dt.$$

Coordinates  $p$  and  $\xi$  uniquely determine  $\gamma$ . Parameter  $p$  is the minimum distance of  $\gamma$  from a central point in space  $\mathcal{M}$  and vector  $\xi$  is the tangent vector to  $\gamma$  at point  $X = X(p, \xi)$ . Function  $\exp_{X(p,\xi)}(t\xi)$  map points along  $\gamma$  parameterized by  $t$  to points in  $\mathcal{M}$ ;  $\gamma(t) = \exp_{X(p,\xi)}(t\xi)$ .

We will prove that operator  $R^*$ , whose action on a function  $F \in C_0^\infty$  at a point  $(x, y) \in \mathcal{M}$  is defined

$$R^*(F)(x, y) = \frac{1}{\pi} \int_0^\pi F(p(x, y), \xi) \frac{d\xi}{|\gamma|},$$

is adjoint to Radon's transform,  $R$ .

### A.2. Scalar products

Let  $C_0^\infty(\mathfrak{S})$  denote the space of functions defined on domain  $\mathfrak{S}$  that are infinitely differentiable and have compact support. For a function to have compact support, we require that it be zero outside a subdomain on space  $\mathfrak{S}$ . This implies that for functions  $f(x) \in C_0^\infty(\mathfrak{S})$  on  $\mathfrak{S}$

$$\lim_{x \rightarrow \infty} |f(x)| = 0.$$

For functions  $f, g \in C_0^\infty(\mathcal{M})$ , we define the scalar products of functions on domain  $\mathcal{M}$  by the following:

$$(A.1) \quad \langle f, g \rangle_{\mathcal{M}} = \int_{\mathbb{R}^2} f(x, y)g(x, y) dx,$$

where  $dx = dx dy$  is the element of integration over  $\mathcal{M}$ . For functions  $F, G \in C_0^\infty(\mathcal{L})$ , we define the scalar products of functions on domain  $\mathcal{L}$  by the following:

$$(A.2) \quad \langle F, G \rangle_{\mathcal{L}} = \int_0^\infty \int_0^\pi F(p, \xi)G(p, \xi) \frac{dp d\xi}{|\gamma(p, \xi)|},$$

where  $dp d\xi / |\gamma(p, \xi)|$  is the element of integration over  $\mathcal{L}$ .

### A.3. Proof of adjointness of $R^*$

In this section we will prove that operator  $R^*$  is adjoint to Radon transform operator  $R$ . To facilitate this process, we invoke the following definition.

DEFINITION A.3.1. Let  $A$  be an operator that maps functions on space  $C_0^\infty(\mathfrak{S})$  to space  $C_0^\infty(\mathfrak{I})$ . Let  $B$  be an operator that maps functions on space  $C_0^\infty(\mathfrak{I})$  to space  $C_0^\infty(\mathfrak{S})$ . Denote scalar products on domains  $\mathfrak{S}$  and  $\mathfrak{I}$  by  $\langle \cdot, \cdot \rangle_{\mathfrak{S}}$  and  $\langle \cdot, \cdot \rangle_{\mathfrak{I}}$ . Let  $f \in C_0^\infty(\mathfrak{S})$  and  $\mathfrak{F} \in C_0^\infty(\mathfrak{I})$ . We say that  $B$  is adjoint to  $A$  if the following equality holds:

$$\langle f, B\mathfrak{F} \rangle_{\mathfrak{S}} = \langle Af, \mathfrak{F} \rangle_{\mathfrak{I}}.$$

We will use Definition A.3.1 to prove that  $R^*$  is adjoint to  $R$ .

PROPOSITION A.3.2. Consider functions  $f \in C_0^\infty(\mathcal{M})$  and  $F \in C_0^\infty(\mathcal{L})$ . Then,

$$\langle Rf, F \rangle_{\mathcal{L}} = \langle f, R^*F \rangle_{\mathcal{M}}.$$

PROOF. Consider scalar product of functions  $R(f), F \in C_0^\infty(\mathcal{L})$ . By equation (A.2), we have

$$\langle Rf, F \rangle_{\mathcal{L}} = \frac{1}{\pi} \int_0^\infty \int_0^\pi R(f)(p, \xi) F(p, \xi) \frac{dp d\xi}{|\gamma(p, \xi)|}.$$

We invoke the definition of Radon's transform acting on function  $f$  along path  $\gamma$  and rearrange terms within the integral to write

$$\langle Rf, F \rangle_{\mathcal{L}} = \frac{1}{\pi} \int_0^\pi \int_0^\infty F(p, \xi) \left[ \int_{-\infty}^\infty f(\exp_{X(p, \xi)} t \xi) dt \right] \frac{dp d\xi}{|\gamma(p, \xi)|}.$$

To express (A.3) as a scalar product over space  $\mathcal{M}$ , we wish to express integration element  $dt dp$  in terms of element  $dx dy$ . This is just the Jacobian transformation of coordinates  $(p, t)$  to coordinates  $(x, y)$ .

Let  $\mathcal{J}(x, y; p, t)$  denote the Jacobian transformation matrix of coordinates  $(x, y)$  with respect to  $(p, t)$ . Given the following relation between element  $dx dy$  and element  $dt d\alpha$ ,

$$dx dy = \det(\mathcal{J}(x, y; p, t)) dt d\alpha,$$

we solve for  $dp dt$  by the following expression:

$$(A.4) \quad dp dt = [\det(\mathcal{J}(x, y; p, t))]^{-1} dx dy.$$

The transformation between  $(p, t)$  and  $(x, y)$  is orthogonal; hence,  $\det(\mathcal{J}(x, y; p, t)) = 1$ . and equation (A.4) becomes

$$(A.5) \quad dp dt = dx dy.$$

We rearrange the terms in equation (A.3) by the following method: we change coordinates from  $p$  and  $t$  to  $x$  and  $y$ , and rearrange the limits of integration by integrating function  $F$  over  $\xi$ , and including measure  $|\gamma|$  in this integral. We write

$$(A.6) \quad \langle Rf, F \rangle_{\mathcal{L}} = \int_{-\infty}^{\infty} \int_{-\infty}^{\infty} f(x, y) \times \left[ \frac{1}{\pi} \int_0^{\pi} F(p, \xi) \frac{d\xi}{|\gamma(P, \xi)|} \right] dx dy.$$

Recognizing that the braced term is the result of acting adjoint operator  $R^*$  on function  $F$ , we rewrite equation (??) accordingly:

$$(A.7) \quad \langle Rf, F \rangle_{\mathcal{L}} = \int_{-\infty}^{\infty} \int_{-\infty}^{\infty} R^*(F)(x, y) f(x, y) dx dy.$$

By the definition of the scalar product on  $\mathcal{M}$ , equation (A.7) can be expressed as

$$\langle Rf, F \rangle_{\mathcal{L}} = \langle f, R^*F \rangle_{\mathcal{M}}.$$

Hence, we have shown that  $R^*$  is adjoint to  $R$  by Definition (A.3.1).  $\square$

## APPENDIX B

### Analytical Solutions

In this appendix, we present analytical solutions for rays and traveltimes of signals in three types of media: homogeneous media, layered media, and linearly inhomogeneous media.

#### B.1. Rays and traveltimes: Homogeneous media

A homogeneous medium is a medium whose properties are constant at every point within it. The properties of a signal travelling within a homogeneous medium is independent of its position or direction of propagation. Mathematically, we can describe a homogeneous medium by a function

$$v(x, z) = v_0,$$

where  $v_0$  is a positive constant.

**B.1.1. Travelttime.** Let  $z = z(x)$  be the path of a signal propagating in a homogeneous medium with velocity  $v_0$ . The travelttime  $T(S, R)$  of the signal travelling between points  $S = (x_S, z_S)$  and  $R = (x_R, z_R)$  is given by

$$T(S, R) = \int_S^R \frac{ds}{v_0}.$$

By linearity of the integral operator, we take  $1/v_0$  outside of the integral and write

$$(B.1) \quad T(S, R) = \frac{1}{v_0} \int_S^R ds.$$

The integral in expression (B.1) is the distance traveled along a path whose arclength element is  $ds$ . Hence, expression (B.1) says that the traveltime of a signal travelling within a homogeneous medium is the length of the path divided by its velocity. Expression (B.1) makes no assumptions about the path of the signal.

We let the ray connecting  $S$  and  $R$  be parameterized by coordinate  $x$ . Hence, the solution to this problem is expressed by function  $z = z(x)$ . In view of this, we rewrite arclength parameter  $ds$  in terms of displacement element  $dx$  by

$$ds = \sqrt{1 + (z'(x))^2} dx,$$

where  $z'(x) = dz/dx$ . In view of expression (B.1), we express traveltime of the signal along  $z(x)$  as

$$(B.2) \quad T(S, R) = \frac{1}{v_0} \int_{x_S}^{x_R} \sqrt{1 + (z'(x))^2} dx.$$

**B.1.2. Rays.** To solve for rays in homogeneous media, we invoke the Euler-Lagrange equations of motion; Theorem 2.3.3. Recall that the solutions to these differential equations are rays, which are solutions to variational equation (2.1). Let  $f$  be the integrand of expression (B.1);  $f(z, z'; x) = \sqrt{1 + (z'(x))^2}$ . The Euler-Lagrange equations of

motion for function  $z(x)$  are

$$(B.3) \quad \frac{\partial f}{\partial z} - \frac{d}{dx} \left( \frac{\partial f}{\partial z'} \right) = 0.$$

Since function  $f$  is independent of  $z(x)$ , we simplify equation (B.3) to

$$(B.4) \quad \frac{d}{dx} \left( \frac{\partial f}{\partial z'} \right) = 0.$$

Equation (B.4) says that the derivative of  $\partial f / \partial z'$  with respect to variable  $x$  is zero; hence, its value is constant. We express this result by

$$(B.5) \quad \frac{\partial f}{\partial z'} = c,$$

where  $c \in \mathbb{R}$  is a constant of integration.

Function  $f$  depends only on  $z'$ . Using properties of differential operators, we rewrite equation (B.5) as a total derivative with respect to  $z'$ ;

$$(B.6) \quad \frac{df}{dz'} = c.$$

Evaluating the total derivative in equation (B.5) we obtain

$$\frac{z'}{\sqrt{1 + (z')^2}} = c.$$

Bringing the radicand to the right-hand side, squaring both sides, and solving for  $z'$  yields the following first-order differential equation:

$$\frac{dz}{dx} = \frac{c}{\sqrt{1 - c^2}}.$$

Letting  $\check{c} = c/\sqrt{1-c^2}$ ,

$$(B.7) \quad \frac{dz}{dx} = \check{c}.$$

We solve differential equation (B.5) by separation of variables. We bring  $dx$  to the right-hand side of equation (B.5);

$$d\bar{z} = \check{c} d\bar{x},$$

where  $dx = d\bar{x}$  and  $dz = d\bar{z}$ . Integrating  $\bar{x}$  from  $x_S$  to  $x$  and  $\bar{z}$  from  $z_S$  to  $z(x)$  yields the expression

$$z(x) - z_S = \check{c}(x - x_S).$$

Letting  $b = z_S - \check{c}x_S$ , we write  $z(x)$  as

$$(B.8) \quad z(x) = \check{c}x + b.$$

We recognize equation (B.8) as the equation of a line  $z$  parameterized by  $x$  with slope  $\check{c}$  and  $z$ -intercept  $b$ . Hence, we have shown that rays in homogeneous media are straight lines.

Traveltime expression (B.1) says that the traveltime of a signal propagating from point  $S$  to point  $R$  is equal to the length of the ray divided by its velocity. In view of equation (B.8) we express this length by the rectangular Euclidean distance between two points on a line; let  $s$  be the length of this path. Then

$$s = \sqrt{(x_R - x_S)^2 + (z_R - z_S)^2}.$$

We write the traveltime of a signal propagating with velocity  $v_0$  along a path of length  $s$  by

$$\begin{aligned} T(S, R) &= \frac{s}{v_0} \\ &= \frac{\sqrt{(x_R - x_S)^2 + (z_R - z_S)^2}}{v_0}. \end{aligned}$$

By using the Lagrange equations of motion and variational principles, we have solved for closed-form expressions of rays and traveltimes of signals in homogeneous media.

## B.2. Rays and traveltimes: Layered inhomogeneous media

In this section, we derive expressions for rays and traveltimes of signals propagating in layered inhomogeneous media; specifically, for a velocity model of the form of equation (5.1). We consider the cases of transmitted and reflected signals.

**B.2.1. Transmitted Signals.** Consider equation (2.2). Let  $S = (x_S, z_S)$  be the coordinate of the source,  $R = (x_R, z_R)$  be the coordinate of the receiver, and  $P_I = (x_I, z_I)$  be the coordinate of the intersection of the ray with the interface. Without loss of generality, let  $z_S < z_I < z_R$ . In view of equation (5.1) we write the traveltime of a signal propagating between points  $(x_S, z_S)$  and  $(x_R, z_R)$  as

$$(B.9) \quad \int_S^R \frac{ds}{v(x, z)} = \int_S^{P_I} \frac{ds}{v_1} + \int_{P_I}^R \frac{ds}{v_2}.$$

Since velocities  $v_1$  and  $v_2$  are constant, they can be brought outside the integral, and

$$\int_S^{P_I} \frac{ds}{v_1} + \int_{P_I}^R \frac{ds}{v_2} = \frac{1}{v_1} \int_S^{P_I} ds + \frac{1}{v_2} \int_{P_I}^R ds.$$

We rewrite equation (B.9) as

$$(B.10) \quad \int_S^R \frac{ds}{v(x, z)} = \frac{1}{v_1} \int_S^{P_I} ds + \frac{1}{v_2} \int_{P_I}^R ds.$$

Equation (B.10) says, for a medium described by velocity function (5.1), the traveltime of a signal passing through an interface is equal to the sum of the traveltimes of the signal through each layer. Hence, the ray can be viewed as the union of a ray passing through the upper layer with a ray passing through the lower layer meeting at  $P_I$ , and each integral can then be viewed as the traveltime of a signal passing through a homogeneous medium described by constant velocity.

As shown in Appendix B.1, the shape of a ray within a homogeneous medium is a straight line. Hence, we express the traveltime of a signal passing through the interface by

$$(B.11) \quad \int_{P_S}^{P_R} \frac{ds}{v(x, z)} = \frac{\sqrt{(x_S - x_I)^2 - (z_S - z_I)^2}}{v_1} + \frac{\sqrt{(x_I - x_R)^2 - (z_I - z_R)^2}}{v_2}.$$

Note that in equation (B.11) the value of traveltime depends only on the value of  $x_I$ , since all other parameters are known. Hence, traveltime

of signals in layered media is a function of  $x_I$  only; we write

$$(B.12) \quad T(x_I) = \frac{\sqrt{(x_S - x_I)^2 - (z_S - z_I)^2}}{v_1} + \frac{\sqrt{(x_I - x_R)^2 - (z_I - z_R)^2}}{v_2}.$$

We have an expression that gives traveltime of a signal propagating through an interface in a horizontally-layered medium as a function of a single parameter,  $x_I$ . However, to obtain the exact traveltime of the signal, we need to find  $x_I$ .

We wish to solve expression (B.12) for  $x_I$  that minimizes traveltime  $T(x_I)$ . Taking the derivative of expression (B.12) with respect to  $x_I$  and setting it equal to zero results in the following equation:

$$\begin{aligned} \frac{dT(x_I)}{dx_I} &= \frac{-2(x_S - x_I)}{v_1 \sqrt{(x_S - x_I)^2 - (z_S - z_I)^2}} + \frac{2(x_I - x_R)}{v_2 \sqrt{(x_I - x_R)^2 - (z_I - z_R)^2}} \\ &= 0. \end{aligned}$$

Bringing the  $(x_S - x_I)$  term to the right hand side and squaring both sides, we obtain

$$\frac{(x_I - x_R)^2}{v_2^2((x_I - x_R)^2 - (z_I - z_R)^2)} = \frac{(x_S - x_I)^2}{v_1^2((x_S - x_I)^2 - (z_S - z_I)^2)}.$$

We manipulate this expression to obtain a polynomial equation of degree 4 in  $x_I$ :

$$(B.13) \quad 0 = (x_S - x_I)^2((x_I - x_R)^2 - (z_I - z_R)^2) + \frac{v_1^2}{v_2^2}(x_I - x_R)^2((x_S - x_I)^2 - (z_S - z_I)^2)$$

We solve this polynomial numerically for its four roots  $\{x_I^j\}_{j=1}^4$  and take the root  $x_I^j \in [x_S, x_R]$  as the  $x$ -coordinate of the point on the interface

through which the signal passes. We solve for the traveltime of the signal by substituting  $x_I$  into expression (B.12), and we construct the ray by joining line segments extending from the source and receiver to  $x_I$ .

**B.2.2. Reflected signals: Reflection at an interface.** Consider a signal arriving at an interface at angle  $\theta_i$  and reflecting at an angle  $\theta_r$ ; the law of reflection says that

$$(B.14) \quad \sin \theta_i = -\sin \theta_r,$$

that is, the angle of incidence and the angle of reflection as measured from the normal to the interface are equal.

Let  $(x_I, z_I)$  be the point on the interface at which the signal is reflected. The length of the segment connecting the source to this point,  $\gamma_{SI}$ , is  $|\gamma_{SI}| = \sqrt{(x_I - x_S)^2 + (z_I - z_S)^2}$ , and the length of the segment connecting the point on the interface to the receiver,  $\gamma_{IR}$ , is  $|\gamma_{IR}| = \sqrt{(x_R - x_I)^2 + (z_R - z_I)^2}$ . In this calculation, the source and receiver are contained within the same layer, which we assume to be homogeneous; without loss of generality, we denote the signal velocity within this layer by  $v(\mathbf{x}) = v_0$ .

Since  $z_I$  is known, we need only calculate  $x_I$  to determine the shape of the ray and the traveltime of the signal along the ray, which is

$$T(x_I) = \frac{\sqrt{(x_I - x_S)^2 + (z_I - z_S)^2} + \sqrt{(x_R - x_I)^2 + (z_R - z_I)^2}}{v_0}.$$

Equation (B.14) states that the angle of incidence and the angle of reflection are equal to each other up to a minus sign. In view of this,

we say

$$\cos \theta_i = \cos \theta_r,$$

from which it follows that

$$\tan \theta_i = -\tan \theta_r.$$

The definition of the tangent function allows us to write

$$(B.15) \quad \frac{z_S - z_I}{x_S - x_I} = -\frac{z_I - z_R}{x_I - x_R}.$$

We obtain the following expression by solving equation (B.15) for  $x_I$ :

$$(B.16) \quad x_I = \frac{x_S - x_R \left( \frac{z_I - z_S}{z_R - z_I} \right)}{1 - \frac{z_I - z_S}{z_R - z_I}}.$$

Expression (B.16) allows us to directly calculate the path of a reflected signal and its traveltime.

**B.2.3. Reflected signals: Total internal reflection.** Let  $\gamma_S$  be a segment extending from the source to the interface and  $\gamma_R$  be a segment extending from the interface to the receiver; the resulting ray is  $\gamma = \gamma_S \cup \gamma_R$ . Furthermore, let  $\theta_I$  be the angle of  $\gamma_S$  with respect to the  $z$ -axis and  $\theta_T$  be the angle of  $\gamma_R$  with respect to the  $z$ -axis. Angle  $\theta_I$  is referred to as the angle of incidence and  $\theta_T$  is referred to as the angle of transmission; these angles are related by Snell's law:

$$(B.17) \quad \frac{\sin \theta_T}{\sin \theta_I} = \frac{v_2}{v_1}.$$

Snell's law predicts an impossible angle of transmission in the case when  $v_2 < v_1$  and  $\theta_{SI} > \arcsin(v_2/v_1)$ . Signals whose angles of incidence satisfy this inequality undergo total internal reflection at the interface. To calculate the path and traveltime of a signal corresponding to total internal reflection, we note that the angle of reflection,  $\theta_R$ , is equal to the angle of incidence,  $\theta_I$ . Let  $\gamma_S$  be the segment of the ray extending from the source to the interface,  $\gamma_I$  be the segment of the ray along the interface, and  $\gamma_R$  be the segment extending from the interface to the receiver; let  $\gamma = \gamma_S \cup \gamma_I \cup \gamma_R$ . Note that  $|\gamma_I|$  is generally nonzero, since the wave is reflected along the interface.

Let  $(x_1, z_I)$  and  $(x_2, z_I)$  be the endpoints of segment  $\gamma_I$ . The traveltime of the signal along ray  $\gamma$  is

$$(B.18) \quad T(x_1, x_2) = \frac{\sqrt{(x_1 - x_S)^2 + (z_1 - z_S)^2}}{v_1} + \sqrt{(x_R - x_2)^2 + (z_R - z_I)^2} + \frac{|x_2 - x_1|}{v_2}.$$

We wish to minimize  $T$  with respect to variables  $x_1$  and  $x_2$  – the points along the interface where the signal is incident and reflected respectively. Invoking the condition that the angle of incidence is equal to the angle of reflection – that is,  $\theta_I = \theta_R$  – we obtain

$$\frac{z_I - z_S}{x_1 - x_S} = \frac{z_R - z_I}{x_2 - x_R}.$$

Solving for  $x_2$ , we obtain

$$(B.19) \quad x_2 = \kappa_1 x_1 + \kappa_2,$$

where  $\kappa_1 = -(z_R - z_I)/(z_I - z_S)$  and  $\kappa_2 = x_R - \kappa_1 x_S$ . Expression (B.19) allows us to rewrite expression (B.18) as

$$\begin{aligned}
 T(x_1) = & \frac{\sqrt{(x_1 - x_S)^2 + (z_1 - z_S)^2}}{v_1} \\
 & + \frac{\sqrt{(x_R - (\kappa_1 x_1 + \kappa_2))^2 + (z_R - z_I)^2}}{v_1} \\
 & + \frac{|x_1(\kappa_1 - 1) + \kappa_2|}{v_2}.
 \end{aligned}
 \tag{B.20}$$

Expression (B.20) expresses traveltime as a function of variable  $x_1$ . Following the method of Section B.2.1, we solve equation  $dT(x_1)/dx_1 = 0$  numerically for  $x_1$ , and substitute this value into  $T$  to obtain the minimum value of traveltime. We then use  $x_1$  to obtain  $x_2$ , which is then used to construct  $\gamma$ .

### B.3. Rays and traveltimes: Linearly inhomogeneous media

To discuss the accuracy of the shapes of generated rays with analytical results, we will follow the method presented in the paper of Epstein and Slawinski in [15]. To test the accuracy of the traveltimes of signals along these rays, we use analytical results presented by Slawinski and Slawinski in [14].

In linearly inhomogeneous media, rays are circular arcs [16]. Noting that the centre of the circle from which these arcs are produced lies at a height  $a/b$  above the surface [15, p.1]; its coordinate is  $z_c = -a/b$ . We need only to solve for the  $x$ -coordinate of the centre of the circle,  $x_c$ . To do so, we invoke the geometric properties of a circle.

Consider source  $S$  at  $(x_S, z_S)$  and receiver  $R$  at  $(x_R, z_R)$ , and let  $\rho$  denote the radius of circle  $\Sigma$  on which  $S$  and  $R$  lie. The midpoint between  $S$  and  $R$  is  $((x_S + x_R)/2, (z_S + z_R)/2) = (x_m, z_m)$ ; let  $SR$  denote the line connecting  $S$  and  $R$ . By properties of circles, radial arm  $OA$  extending from the centre of  $\Sigma$  through  $SR$  at its midpoint intersects  $SR$  at a right angle. Let  $m = (z_R - z_S)/(x_R - x_S)$  be the slope of  $SR$ ; the slope of line  $OA$  is the negative reciprocal of  $m$ . It follows that the equation of line  $OA$  is

$$(B.21) \quad z_{OA}(x) = -\frac{x}{m} + z_{OA}^0,$$

where

$$z_{OA}^0 = z_m + \frac{x_m}{m}.$$

Setting  $z_{OA}(x) = z_C$  in equation (B.21), we solve for  $x_C$ :

$$x_C = -m(z_C - z_{OA}^0).$$

We can parameterize the circular arcs joining  $S$  and  $R$  by parameter  $\vartheta$ . Consider the following change of coordinates:

$$(B.22) \quad \begin{aligned} x(\vartheta) &= \rho \sin(\vartheta) + x_C \\ z(\vartheta) &= \rho \cos(\vartheta) + z_C \end{aligned}.$$

Equations (B.22) allow us to express coordinates  $(x, z)$  in terms of angular coordinate  $\vartheta$ . We can trace out the ray from initial angle  $\vartheta_S$

to final angle  $\vartheta_R$ , where

$$\vartheta_I = \arctan \left( \frac{x_I - x_C}{z_I - z_C} \right),$$

and  $I = S$  or  $R$ .

To calculate the predicted traveltime along this ray we invoke the following expression for traveltime, derived in [14, p.25]:<sup>1</sup>

$$T(S, R; v(z)) = \frac{1}{b} \times \left| \ln \left[ \left( \frac{v(z_S)}{v(z_R)} \right) \left( \frac{1 - \sqrt{1 - (\mathbf{p} v(z_R))^2}}{1 - \sqrt{1 - (\mathbf{p} v(z_S))^2}} \right) \right] \right|.$$

Parameter  $\mathbf{p}$  is the standard ray parameter, which can be expressed in terms of the locations of the source and receiver and the velocity at these points by

$$\mathbf{p}(S, R) = \frac{2bX}{\sqrt{[(bX)^2 + v(z_S)^2 + v(z_R)^2]^2 - [2v(z_S)v(z_R)]^2}},$$

where  $X = x_R - x_S$  is the horizontal offset between source and receiver. The physical significance of ray parameter  $\mathbf{p}$  and its role in raytracing is discussed in [3, Ch. 14].

---

<sup>1</sup>These results were derived by invoking Fermat's principle of least traveltime and by requiring the satisfaction of Snell's Law within the medium. This derivation is done out in detail in the paper cited.

## APPENDIX C

### Code

In this appendix, the code used to implement the methods of simulated annealing raytracing and backprojection are presented. This code is found on the supplied compact disc.



